# EFFECT OF ROLLING PARAMETERS ON THE NO-RECRYSTALLIZATION TEMPERATURE ($T_{nr}$) IN Nb-BEARING STEELS

by

Deng Qi Bai

A Thesis Submitted to the Faculty of Graduate Studies and Research in Partial Fulfillment of the Requirements for the Degree of Master of Engineering

Department of Mining and Metallurgical Engineering
McGill University
Montreal, Canada

January 1993

# EFFECT OF ROLLING PARAMETERS ON THE $T_{nr}$ IN Nb-BEARING STEELS

by

Deng Qi Bai

A Thesis Submitted to the Faculty of Graduate Studies and Research in Partial Fulfillment of the Requirements for the Degree of Master of Engineering

Department of Mining and Metallurgical Engineering
McGill University
Montreal, Canada

January 1993

# ABSTRACT

The recrystallization behavior of three Nb-bearing HSLA steels was investigated during multipass deformation under continuous cooling conditions. The niobium concentrations of these steels varied from 0.05 to 0.09 wt%. The specimens were tested on a computerized torsion machine using a simulation schedule of 17 passes. Deformation temperatures of 1180 °C to 700 °C were employed, together with pass strains of 0.1 to 0.7, strain rates of 0.2 to 10 $s^{-1}$, and interpass times of 2 to 200 seconds. By means of mean flow stress vs. 1000/T diagrams, the effect of reheating temperature, initial grain size, and chemical composition on the $T_{nr}$ (temperature at which recrystallization is no longer complete) was determined. Reheating temperature and microalloying elements have significant influence on the $T_{nr}$, while inicial grain size has no effect on the $T_{nr}$ during multipass deformation.

Furthermore, the effect of deformation parameters such as the pass strain, strain rate, and interpass time on the $T_{nr}$ during multipass deformation was investigated in this way. The $T_{nr}$ decreases with increasing strain and also decreases slightly with increasing strain rate. There is a $T_{nr}$ minimum at times of about 12~15 seconds and both increases and decreases from this value raise this characteristic temperature. When the interpass times are short, solute atoms control the rate of recrystallization, the extent of which decreases as the time is decreased. When the interpass times are long, precipitation takes place and retards recrystallization, so that the extent of softening decreases as the time is extended instead.

The evolution of Nb(C,N) precipitation during simulated rolling was studied with the aid of carbon extraction replication and electron microscopy. Finally, by applying the additivity rule to the isothermal model of Dutta and Sellars, continuous cooling $T_{nr}$'s were predicted from recrystallization-precipitation-temperature-time (RPTT) diagrams; these are shown to be in good agreement with the experimental observations.

# RESUME

Le comportement au cours de la recristallisation a été étudié pour trois aciers HSLA au niobium au moyen de déformations à passes multiples dans des conditions de refroidissement continu. Les teneurs en niobium de ces trois aciers variaient entre 0,05 et 0,09% en masse. Les tests ont été éffectués à l'aide d'une machine de torsion pilotée par ordinateur en utilisant un schéma de déformation de 17 passes. On a utilisé des températures de déformation comprises entre 1180°C et 700°C. Les déformations au cours d'une passe variaient entre 0,1 et 0,7, pour des vitesses de déformation comprises entre 0,2 et 10 $s^{-1}$, et des intervalles de temps entre les passes compris entre 2 et 200 secondes. A l'aide de graphes représentant la contrainte d'écoulement moyenne en fonction de 1000/T, l'effet sur la $T_{nr}$ (température à laquelle la recristallisation n'est plus complète) de la température de réchauffage, de la taille de grain initiale et de la composition chimique a été déterminé. La température de réchauffage et les éléments de microalliage ont une influence significative sur $T_{nr}$, alors que la taille de grain initiale n'a pas d'effet sur $T_{nr}$ au cours d'une déformation multipasse.

De plus, l'effet des paramètres de déformation tels que la déformation au cours d'une passe, la vitesse de déformation et le temps interpasse sur $T_{nr}$ a été étudié. $T_{nr}$ décroit lorsque la déformation et/ou la vitesse de déformation augmentent. $T_{nr}$ présente un minimum pour des temps de 12 à 15 secondes. Pour des temps interpasse courts, ce sont les atomes en solution solide qui contrôlent la vitesse de recristallisation, dont l'amplitude décroit avec les temps décroissants. Pour les temps interpasse longs, de la précipitation a lieu, qui retarde la recristallisation, réduisant du même coup l'adoucissement à mesure que le temps interpasse augmente.

L'évolution de la précipitation des Nb(C,N) au cours d'une simulation de laminage a été étudié au moyen de répliques par extraction et de microscopie électronique. Finalement, en appliquant la règle d'additivité au modèle isotherme de Dutta et Sellars, on a pu prédire les $T_{nr}$ pour un refroidissement continu à partir des diagrammes recristallisation-précipitation-temps-température (RPTT); ces résultats ont été trouvés en bon accord avec les observations expérimentales.

# ACKNOWLEDGEMENTS

The author is grateful to his thesis supervisors, Professors J.J. Jonas and S. Yue, for their guidance, encouragement and support through the whole course of this work.

The author also appreciates the fruitful suggestions received from Dr. P.R. Cetlin of the UFMG, Belo Horizonte, Brazil. Many thanks are due to Dr. W.P. Sun for his stimulating discussions and for the assistance with the preparation of carbon extraction replicas. He expresses similar gratitude to Drs. C. Roucoules and T. Maccagno for their help in carrying out the hot torsion testing.

The pleasant and friendly international environment created by his fellow graduate students along with their knowledge and skills are deeply appreciated. Special thanks are extended to E. Fernandez and L. Mello for their continuous help in various forms.

The author is deeply grateful to the Ministry of the Aerospace Industry, China for providing a visiting fellowship. The financial support received from the Natural Sciences and Engineering Research Council of Canada (NSERC), and the Canadian Steel Industry Research Association (CSIRA) is acknowledged with gratitude.

Finally, the author would like to express his sincere gratitude to his wife and to all his family and friends for their continuous support and encouragement.

# TABLE OF CONTENTS

# LIST OF FIGURES

Figure | Page

Figure | Page

# LIST OF TABLES

CHAPTER 1

# INTRODUCTION

The development of high-strength low-alloy (HSLA) steels constitutes a successful metallurgical innovation in which alloying additions and thermomechanical processing methods have been brought together to produce improved combinations of engineering properties. This practice is relatively inexpensive because the alloying elements are only needed in small concentrations as carbide- or carbonitride-formers and the associated thermomechanical processing precludes the need for further heat treatment.

During the last two decades, much attention has been paid to Nb-bearing steels, and these have been subject to more detailed scientific investigation than any other kind of steel. Their unique combination of properties arises from the precipitation of carbides, nitrides or carbonitrides and from the interaction of these precipitates with the processes of recrystallization and grain growth. A clear understanding of the thermomechanical processing of these materials is therefore essential if the optimum benefit is to be obtained from these interactions.

Much research has recently been focussed on the effects of reheating, roughing, finish rolling, and cooling after rolling on the resulting microstructure and properties. Quantitative relationships have also been established describing the effects of the process variables on the recrystallization kinetics, recrystallized austenite grain sizes and final ferrite microstructures. Furthermore, computer modeling has become an accepted tool for examining the effects of changing the thermomechanical processing variables on the properties produced.

In the literature, many results have been reported describing the effects of single pass deformations; however, only limited data are available regarding the influence of multipass deformations. Under industrial conditions, the situation becomes still more complicated because as many as twenty-two passes can be applied, and deformation is completed under continuous cooling conditions. It is therefore quite difficult for a designer of rolling schedules to predict the effect of the processing variables on the metallurgical phenomena mentioned above. As a result, the optimum form of the relationships linking the microstructure to the processing variables has not yet been achieved. The present study was concerned with clarifying some of these issues; its aims were:

i) To determine the effects of processing variables such as the reheating temperature, strain, strain rate and interpass time on the no-recrystallization temperature, namely, the $T_{nr}$.

ii) To investigate the effects of these processing variables on strain accumulation and on dynamic recrystallization.

iii) To evaluate processing parameter dependence of the microstructural changes that take place under static and dynamic conditions.

To fulfill the above objectives, the present investigation is described as follows:

In Chapter 2, a brief review of HSLA steel technology is presented. Both controlled rolling and microalloying factors are considered. In Chapter 3, the experimental materials and procedures are described, and the methods employed to determine the no-recrystallization temperature are summarized. In Chapter 4, the effects of the deformation parameters on the no-recrystallization temperature are presented and discussed. The method employed to predict the $T_{nr}$ under continuous cooling condition in the case of multipass deformations is also presented. In Chapter 5, the effects of deformation temperature, strain rate, initial grain size, and delay time on the peak strain and peak stress are presented. Finally, in Chapter 6, the general conclusions of this research are summarized.

CHAPTER 2

# LITERATURE REVIEW

## 2.1 THERMOMECHANICAL PROCESSING OF STEELS

In the past hot rolling was traditionally concerned simply with shape changes, and was not used in the production of desirable microstructures. In order to achieve the required strength, and hence microstructure, the major approach utilized before World War II was alloying, e.g. increasing the levels of carbon and manganese[1,2], increasing the levels of elements such as silicon and phosphorus, or adding chromium, nickel or copper[3]. This approach generally gave steels poor toughness, weldability and formability, and increased their cost.

By the early 1950's, it was realized that hot rolling also changed the properties of hot-rolled steel. One of the pioneers of this approach was Domnanfvets Jernverk[4] in Sweden in 1940, which employed finish rolling temperatures substantially lower than used conventionally, to refine the ferrite structure and to improve the properties. The advantage of such processing lies in energy savings by minimizing, or even eliminating, heat

treatment after hot rolling. Such processing was termed 'controlled rolling' in 1958 by Vanderback[4].

During the past twenty years, based on a better understanding of many metallurgical phenomena (such as static and dynamic recrystallization and precipitation), conventional controlled rolling (CCR), recrystallization controlled rolling (RCR) and dynamic recrystallization controlled rolling (DRCR) have been developed[5].

At the same time, controlled rolling has been increasingly utilized to produce high strength low alloy (HSLA) steels which contain alloying additions, such as Nb,Ti and V. The result has been improved combinations of engineering properties through microstructural control.

### 2.1.1 CONVENTIONAL CONTROLLED ROLLING (CCR)

Historically, this was the first type of controlled rolling to come into regular commercial use. This processing generally involves control of all four stages of rolling, i.e.: i) reheating, ii) roughing, iii) finishing, and iv) cooling[6]. An illustration of these four stages is shown in Fig. 2.1.

#### 2.1.1.1 Reheating

In a conventional controlled rolling schedule, the material is usually reheated to a relatively high temperature, ranging from 1050 °C to 1300 °C. The reheating temperature not only controls the amount of microalloying elements dissolved prior to rolling, but also influences the austenite grain size. On the one hand, it is advantageous to maximize dissolution of the microalloy carbonitrides on reheating, to ensure that the desired austenitic microstructure is developed during rolling. On the other hand, it is also essential to avoid austenitic grain growth as much as possible. A fine, uniform as-reheated austenitic grain size helps minimize the development of a duplex austenitic structure after rolling, thereby leading to improved toughness[7].

#### 2.1.1.2 Roughing

In order to refine the relatively coarse, as-reheated austenitic microstructure, a series of high-temperature rolling/recrystallization steps are carried out at temperatures above the no-recrystallization temperature ($T_{nr}$). Recrystallization at this stage is very rapid and can be followed by some grain growth. If the strain and strain rate of the deformation are properly chosen, complete static recrystallization will take place, and small austenite grains will result. If the conditions are not well chosen, then static recrystallization will be incomplete. This will lead to duplex structures after transformation, which are undesirable.

#### 2.1.1.3 Finishing

Finishing operations are usually conducted at temperatures ranging from $T_{nr}$ to the start of the austenite transformation ($A_{r3}$). Recrystallization is no longer possible and the austenite structure is progressively flattened, in an operation known as "pancaking"[8, 9]. The ratio of grain surface to grain volume ($S_v$) increases, although the grain volume remains constant. This provides more potential nucleation sites for the austenite-to-ferrite transformation[10]. Other important nucleation sites are deformation bands inside the austenite grains, which are formed during finishing when more than 50% deformation is applied[11]. When such pancaked austenite grains transform, a very fine ferrite grain size is produced because of the large number of nucleation sites available at the surfaces of the pancaked austenite grains and in the deformation bands. This fine ferrite is responsible for the attractive combination of good toughness properties and high yield strengths[12,13].

#### 2.1.1.4 Cooling

Cooling is a natural and integral part of the thermomechanical process. Its control can yield excellent results in terms of economy, productivity and material properties. Rapid cooling rates during rolling can lower the

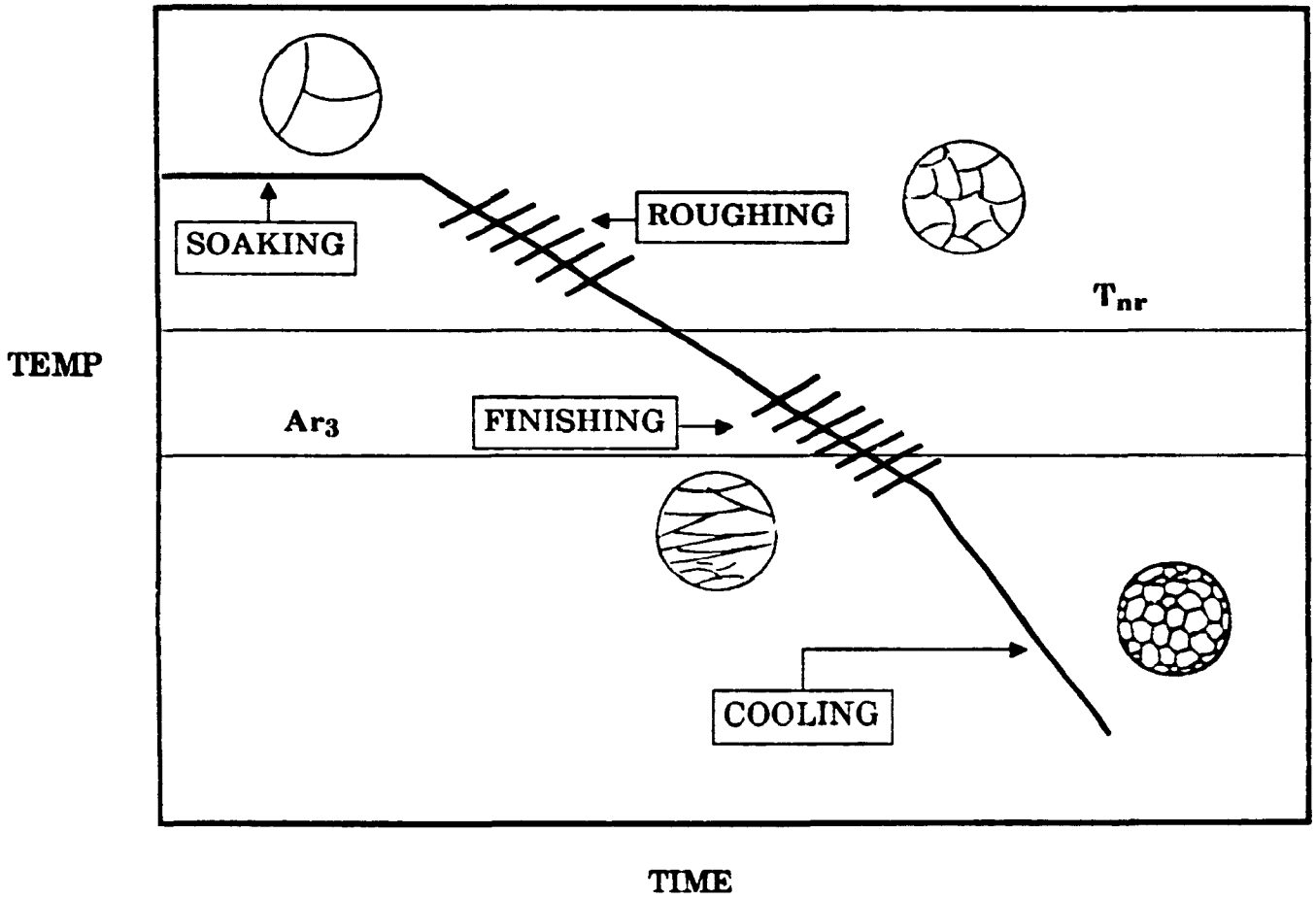


Fig. 2.1 Schematic illustration of controlled rolling and the resulting microstructures
$T_{nr}$ – no-recrystallization temperature;
$A_{r3}$ – start temperature of the austenite-to-ferrite transformation.

transformation temperature ($A_{r3}$), prevent austenite recrystallization prior to transformation, and reduce the extent of carbonitride precipitation in the austenite[1]. Lower $A_{r3}$ temperatures increase the no-recrystallization zone and also decrease the ferrite grain size because, at lower temperatures, ferrite grain growth is more limited. The limitation of precipitation in the austenite region leaves a large proportion of microalloying elements in solution and, as a result, enhanced precipitation in the ferrite region occurs. This is both a source of ferrite grain refinement and improved precipitation strengthening, due to finer precipitate formation at lower temperatures.

Accelerated cooling after rolling can also be used to produce fine ferrite grains. In this way, strength and toughness are improved simultaneously. Nevertheless, when the cooling rate is too high, the toughness may be reduced as a result of bainite formation. Therefore, cooling rates are limited by the hardenability of the steel.

### 2.1.2 RECRYSTALLIZATION CONTROLLED ROLLING (RCR)

Controlled rolling, as described above, is generally based on the use of low finishing temperatures, with the result that fine ferrite grain sizes appear after transformation. Thus, such a style of finishing is inappropriate for certain products, such as heavy plates and thick-walled seamless tubes, which cannot be finished at relatively low temperatures, due to excessive rolling loads. In such cases, it is possible to produce the fine microstructures required by carefully controlling the recrystallization of austenite and arranging for it to occur at successively lower temperatures during finish rolling[15]. These temperatures are, nevertheless, above 900 °C and thus higher than those employed in conventional controlled rolling (CCR).

There are two requirements for the operation of recrystallization controlled rolling to be successful. One is that the recrystallization not be sluggish, so that the times required are not too long. This is achieved by employing V rather than Nb as an alloying element. The second requirement is the prevention of grain growth after each cycle of recrystallization, the occurrence of which can negate the refining effect of recrystallization. For this

purpose, Ti is added to form fine particles of TiN during cooling after continuous casting[15]. When these particles have an appropriate size and frequency distribution, they can completely prevent grain growth of the austenite after each cycle of recrystallization. The fine austenite grains in turn transform into relatively fine grained ferrite, leading to mechanical properties of the hot rolled product which are acceptable for many purposes.

### 2.1.3 DYNAMIC RECRYSTALLIZATION CONTROLLED ROLLING (DRCR)

When the interpass time is short, as is the case in rod and bar, hot strip, and certain other types of rolling processes, there is insufficient time for conventional recrystallization to take place during the interpass delay. For the same reason, the amount of carbonitride precipitation that can take place is also severely limited. As a result, an alternative form of recrystallization can be initiated, known as dynamic recrystallization, which involves the nucleation and growth of new grains *during* deformation[16, 17]. This also requires the accumulation of appreciable strain to enable the recrystallization process to spread completely through the microstructure inherited from the roughing process. In this way, an austenite grain size as fine as 10 μm can be achieved[18].

It is important to note that, under industrial conditions of rolling, CCR, RCR and DRCR can all occur to different degrees during a given operation if the processing parameters have not been optimized so as to favor either: i) strain-induced precipitation and austenite pancaking, ii) conventional recrystallization, or iii) dynamic recrystallization, respectively.

To utilize these different thermomechanical processing routes for the production of commercial HSLA steels, it is necessary to have a clear understanding of the basic metallurgical phenomena associated with the controlled rolling of HSLA steels. These are reviewed in the following sections.

## 2.2 BASIC METALLURGICAL PHENOMENA IN THE CONTROLLED ROLLING OF HSLA STEELS

The success of thermomechanical processing is largely dependent on the control of the softening and/or hardening processes. The types of softening during or after hot deformation can be divided into five distinct categories: i) static recovery, ii) static recrystallization, iii) dynamic recovery, iv) dynamic recrystallization, and v) metadynamic recrystallization.

### 2.2.1 STATIC RECOVERY

After plastic deformation, the strain energy which is stored within the deformed material will be released by the annihilation and rearrangement of dislocations in individual events. During the process, no motion of grain boundaries occurs. The subboundaries, however, become sharper and the dislocation density within the subgrains is reduced with relatively little change in size or shape of the grains. Temperature, strain, strain rate and the addition of alloying elements are the main factors affecting the recovery rate. An increase in temperature results in an increase in the rate of recovery because of enhanced thermal activation. Increasing the strain or strain rate also increases the rate of recovery due to dislocation density increases.

### 2.2.2 STATIC RECRYSTALLIZATION

Usually, static recovery only leads to 25% softening, while static recrystallization can cause 75% softening. Therefore, static recrystallization is the more important softening mechanism involved in controlled rolling. During static recrystallization, the strained grains are gradually replaced by new, strain-free ones by means of nucleation and growth. A large number of dislocations is consumed by the grain boundaries as they migrate through the metal. The rate of static recrystallization is influenced by the strain, strain rate, temperature and grain size. Smaller initial grain sizes and higher strain rates increase the rate of recrystallization. Higher temperatures increase the rate of recrystallization. Strain is a very important factor. For the onset of

static recrystallization, a critical strain (~8%) must be exceeded before recrystallization can begin. The rate of static recrystallization increases with increasing strain, as shown in Fig. 2.2. It can been seen that the time for 50% recrystallization decreases with increasing amount of deformation[19].

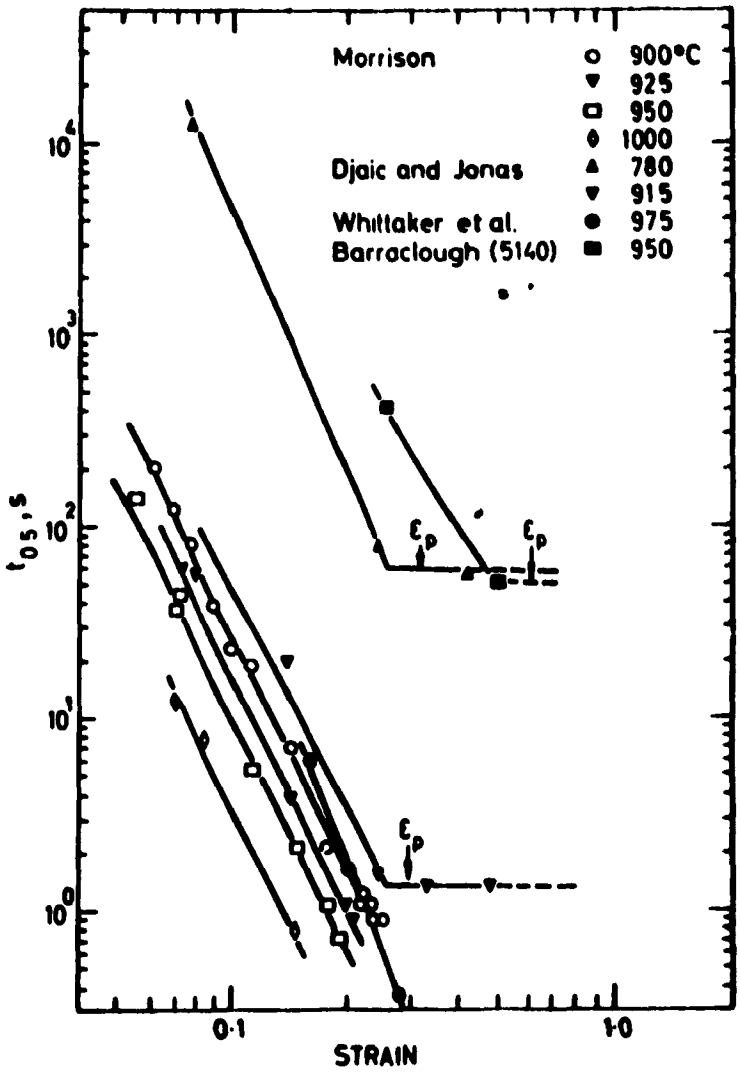


Fig. 2.2 Strain dependence of time for 50% recrystallization in C-Mn and low alloy steels [19].

### 2.2.3 DYNAMIC RECOVERY

In the early stages of hot deformation, the dislocation density increases with strain, but some rearrangement and annihilation of dislocations takes place at the same time. Further straining can lead to one of the following: i) In high stacking fault energy materials, as deformation proceeds, the work hardening rate gradually decreases due to an increase in the annihilation rate of dislocations. When the rate of annihilation of dislocations is equal to the rate of generation of dislocations, a steady state regime is reached. The steady state in hot working is thus characterized by a constant flow stress, as shown in Fig. 2.3a. Under these conditions, the grains are somewhat elongated, but the subgrains maintain constant size and shape. ii) In metals and alloys of medium or low stacking fault energy, e.g. austenite, the subgrains formed develop very tangled boundaries and are of a smaller size. The rate of dislocation annihilation is less than that of dislocation generation and, therefore, the dislocation density increases rapidly during deformation. When the dislocation density reaches a critical value, dynamic recrystallization occurs[20].

### 2.2.4 DYNAMIC RECRYSTALLIZATION

This important concept was originally proposed from the detailed experimental work of Rossard and Blain in 1959[21,22]. Ten years later, it was modeled and interpreted in detail by Luton and Sellars[23]. More recently, Sakui and co-workers[24] and Sakai and Jonas[25] correlated the dynamic recrystallization flow curves with the microstructure.

Unlike static recrystallization, dynamic recrystallization takes place during deformation. The flow curves characteristic of dynamic recrystallization display well-developed peak stresses if recrystallization is complete, as shown in Fig. 2.3b. The predominant nucleation sites for dynamic recrystallization are grain boundaries with high dislocation densities[26]. However, deformation bands within the grains and subgrains can also act as nucleation sites[25]. During deformation, when strains exceed the critical strain

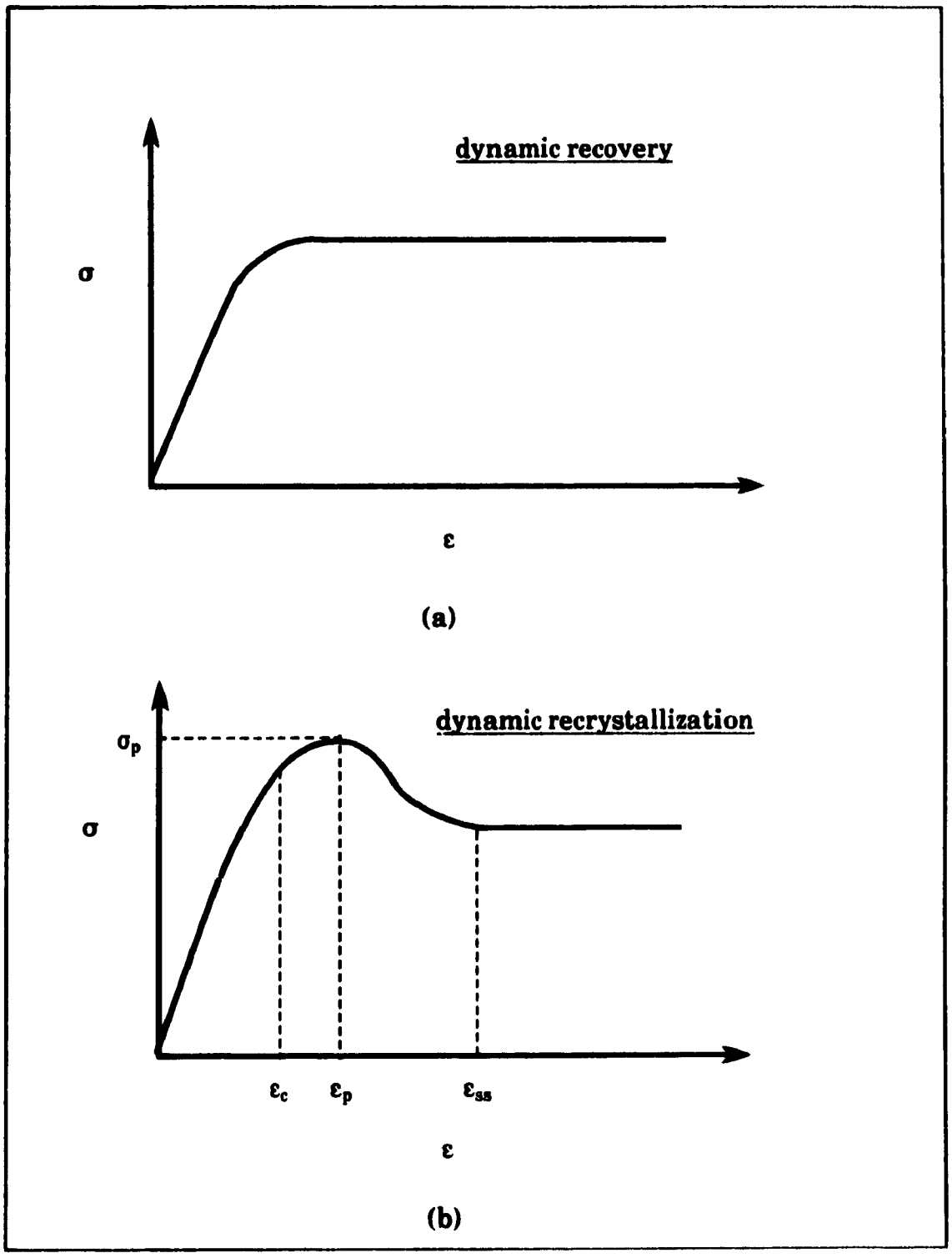


**Fig. 2.3** Schematic illustration of the two types of true-stress-true-strain curves accompanying steady-state deformation at elevated temperatures.

$\varepsilon_c$ ($\varepsilon_c \approx 0.8\ \varepsilon_p$, the peak strain), recrystallization is initiated at the austenite grain boundaries and is propagated into the grain interiors by a mechanism known as 'necklacing'[18,27]. This will progress with continuing deformation until the deformed austenite is entirely replaced by a fine grain size.

Although there has been some controversy concerning the possibility of dynamic recrystallization under industrial rolling conditions, Samuel et al. reported that dynamic recrystallization could take place under strip rolling conditions[28]. Pussegoda et al. also reported that dynamic recrystallization can be initiated at relatively high temperatures, as in billet piercing during the manufacture of seamless tubes[29]. In their investigation, strains as high as 1.5 were applied in a single pass, which was large enough to initiate dynamic recrystallization. It is generally impossible to reach $\varepsilon_p$ during single pass deformation for most industrial practices, except in the case of large reduction 'single step' operations, such as extrusion and planetary hot rolling. However, when the interpass time is short, such as in rod rolling and hot strip rolling, there is insufficient time for static recrystallization to take place between multiple passes. Under these conditions, the work hardening or 'strain' is accumulated from pass to pass, until it exceeds the critical strain for the initiation of dynamic recrystallization. Short interpass times will also limit the occurrence of strain-induced precipitation, thus permitting dynamic recrystallization to take place.

### 2.2.5 METADYNAMIC RECRYSTALLIZATION

When high temperature deformation is halted during dynamic recrystallization (i.e. beyond $\varepsilon_c$), many nuclei are already present within the material, and grow via grain boundary migration. These boundaries can continue to migrate in the absence of a load. The softening process due to the continued growth of these nuclei is known as metadynamic recrystallization. As this type of recrystallization does not require nucleation, it proceeds very rapidly upon the termination of deformation[9,30].

## 2.3 ROLE OF MICROALLOYING ADDITIONS DURING CONTROLLED ROLLING

At present, HSLA steels are predominantly low in carbon (0.05 to 0.15 pct) and are alloyed with small quantities of strong carbonitride-forming elements, such as niobium, vanadium or titanium[31, 32]. This microalloying is intended to contribute to enhanced mechanical properties, primarily through ferritic grain refinement, often supplemented by precipitation and/or substructural (dislocation) strengthening.

It is well known that additions of Mo, Nb, Ti, Al, and/or V to a plain carbon steel are effective in retarding recovery and recrystallization[33, 34]. In the past, most attention was paid to the role of niobium in retarding austenite recrystallization in HSLA steels[35-37]. Previous research suggests that the retardation of austenite recrystallization in Nb-steels results from the pinning of austenite grain boundaries and subboundaries by either: i) niobium carbonitride precipitates; or ii) niobium atoms in solution in the austenite. It appears that the dramatic retardation of austenite recrystallization, which occurs during commercial controlled rolling, results from the strain-induced precipitation of carbonitrides on the austenite substructure. Some investigators have suggested that solute-drag effects on austenite recrystallization in Nb-steels are small compared to the effects of strain-induced carbonitride precipitation[38, 39]. Nevertheless, other workers have argued strongly that solute-drag controls the recrystallization kinetics[40]. Akben et al. suggest that the recrystallization kinetics are controlled by both solute-drag and precipitation[41, 42].

### 2.3.1 INTERACTION BETWEEN CARBONITRIDE PRECIPITATION AND RECRYSTALLIZATION

#### 2.3.1.1 Driving Force for Recrystallization

The strain induced boundary migration model has been widely accepted as the mechanism for the nucleation of recrystallization[43 49]. This model was

originally put forth by Beck and Sperry[46, 47] and was subsequently advanced through the work of Bailey and Hirsch[48].

Under this model, the driving force for recrystallization results from the difference in dislocation density between adjacent austenite subgrains[44]. To balance strain energy, the grain boundaries will "bulge" into grains of high dislocation density[45]. Quantitatively, the driving force, $F_{RXN}$, has been described by[45-48]:

$$F_{RXN} = \frac{\mu b^2 \Delta\rho}{2} \tag{2.1}$$

where $\mu$ is the shear modulus, b is the Burgers vector, and $\Delta\rho$ is the change in dislocation density as the recrystallization front moves.

#### 2.3.1.2 Drag Force for Recrystallization

Zener originally pointed out that, in the presence of a second phase, grain boundary migration may be inhibited because the second phase particles replace part of the grain boundary, and this increment of grain boundary area must be created if the boundary is to move away from the particles[50]. Zener's theory was later quantified by Gladman[51], who assumed that the grain boundaries move rigidly through a regular array of spherical particles. The pinning force for each particle can be expressed as

$$F_{PIN} = 4r\gamma N_s \tag{2.2}$$

where r is the particle radius, $\gamma$ is the interfacial energy per unit area of boundary, and $N_s$ is the number of particles per unit area of boundary.

For the rigid boundary model, $N_S$ is calculated from $N_s^R = 3f_v/2\pi r^2$; For the flexible boundary model proposed by Cuddy[52, 53], $N_S$ can be determined from $N_s^F = 3f_v^{2/3}/4\pi r^2$. The most realistic model was the one proposed by Hansen et al.[42], where $N_S$ is expressed as $N_s^S = 3f_v l/8\pi r^3$. $f_v$ in the above equations is the precipitate volume fraction.

Substitution of the expressions for $N_s^R$, $N_s^F$, and $N_s^S$ into equation 2.2 gives the respective pinning force for each model:

$$F_{PIN}^R = \frac{6\gamma f_v}{\pi r} \tag{2.3}$$

$$F_{PIN}^F = \frac{3\gamma f_v^{2/3}}{\pi r} \tag{2.4}$$

$$F_{PIN}^S = \frac{3\gamma f_v \bar{l}}{2\pi r^2} \tag{2.5}$$

For hot deformed or cold deformed austenite, if $F_{RXN} < F_{PIN}$, the grain boundaries will be completely arrested, whereas if $F_{RXN} \gg F_{PIN}$, the precipitates should not have any significant effect on boundary migration. However, if $F_{RXN} > F_{PIN}$ and the magnitudes are comparable, the boundary may move, but at some reduced velocity.

### 2.3.1.3 RPTT Diagram

Numerous investigations have been undertaken to study the interaction between carbonitride precipitation and recrystallization[54-59]. The recrystallization-precipitation-temperature-time (RPTT) diagram is a convenient tool for analyzing this interaction. Based on their experimental results, Hansen et al. proposed a schematic RPTT diagram[54], as shown in Fig. 2.4. Above $T_0$ (the equilibrium solution temperature for the operative

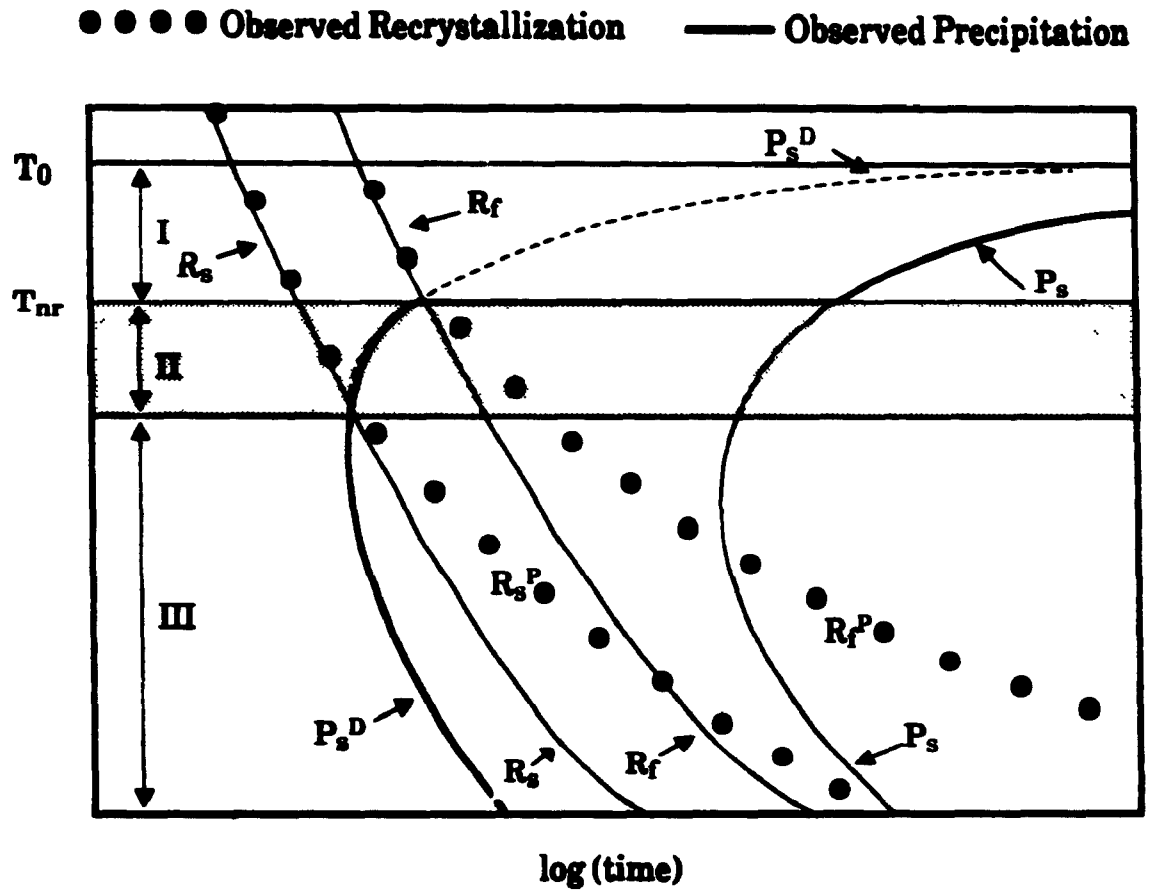


**Fig. 2.4 Schematic recrystallization-precipitation-temperature-time (RPTT) diagram[54].**

precipitation process), precipitation is thermodynamically impossible. Below $T_0$, however, three interaction regions are possible. In region I, recrystallization is complete before precipitation starts (even with the potential accelerating effect of prior plastic deformation) and thus, no interaction occurs. Accordingly, precipitation eventually takes place in the recrystallized austenite along the $P_s$ curve. The recrystallization process, preceding any such precipitation in this case, is defined by the $R_s$ and $R_f$ curves.

In region II, the introduction of new and potent nucleation sites by deformation has the effect of shifting the C-curve to shorter times ($P_s^D$). Precipitation takes place after recrystallization is initiated in this case, but before it is complete. Therefore, recrystallization starts along the $R_s$ curve, but ends along $R_f^P$ curve because of the retardation of precipitation. In region III, precipitation takes place before recrystallization (i.e., along the $P_s^D$ curve), and now both the start and finish of recrystallization are delayed (to the $R_s^P$ and $R_f^P$ curves).

The precipitation/recrystallization interactions and, in fact, the actual temperature ranges over which the various regions are operative, are sensitive to the degree of supersaturation or to the temperature interval between $T_0$ and the post-rolling holding temperature. Sufficient supercooling is necessary for any interaction to occur. But, if $T_0$ is too low, regions III and even II may be cut off by austenite decomposition into ferritic transformation products. Strain is another very important factor influencing this kind of interaction because both the recrystallization and precipitation kinetics change significantly with strain. Therefore, it is always considered as a critical parameter in the modeling and simulation of hot deformation.

#### 2.3.1.4 Effect of Microalloying Elements

At very high temperatures above the precipitate solution temperature, the precipitation of a second phase is impossible, and the recrystallization kinetics are rapid enough to complete recrystallization in a very short time. Below the precipitate solution temperature, but above the nose temperature of

the PTT curve, the recrystallization kinetics are retarded, while precipitation is promoted because both the rate of precipitation and the volume fraction of precipitates increase with decreasing temperature. Under industrial rolling conditions, whether or not recrystallization or precipitation controls the processing, depends upon which one takes place first. Accordingly, the no-recrystallization temperature (or the $T_{nr}$) is often used as a criterion to design the thermomechanical processing schedules of microalloyed steels. Deformation above the $T_{nr}$ leads to fully recrystallized austenite grains, whereas, below this temperature, partially or fully unrecrystallized grains may be the result.

It has been reported that the $T_{nr}$ is closely related to the amount and type of microalloying elements dissolved in the austenite during reheating. Based on their experimental results and the results from the literature, Boratto et al. have derived an empirical equation for predicting the $T_{nr}$ as follows[60, 61]:

$$T_{nr} = 887 + 464C + (6445Nb - 644\sqrt{Nb}) + (732V - 230\sqrt{V}) + 890Ti + 363Al - 357Si \qquad (2.6)$$

As expected, Nb has the strongest influence on the $T_{nr}$. Mn increases the effectiveness of Nb by increasing the solubility of NbC. Thus, more Nb is released into solution and the solute drag effect of Nb is enhanced in this way. This is, however, a weak effect. Akben et al.[41] reported that increasing the Mn level from 1.25 to 1.9% decreases the NbC solution temperature from 996 to 991 °C (i.e. by only 5 °C) in a 0.05% C, 0.03% Nb base composition. Hence, any increases in Mn level above 1% will have little influence on recrystallization retardation, causing little increase in the $T_{nr}$.

Apart from the small effect of V at low concentrations, Si is the only element in the correlation which decreases the $T_{nr}$. This may be because Si decreases the solubility of NbC in austenite[62], thus reducing the amount of Nb in solid solution, and hence decreasing the Nb solute drag effect on the $T_{nr}$. In

other words, as in the case of Mn, it appears that Si affects the $T_{nr}$ indirectly via its effect on the solubility of NbC.

Dutta and Sellars defined the $T_{nr}$ as the recrystallization limit temperature (RLT), which represents the lowest temperature at which complete recrystallization might be expected to occur[63]. Cuddy introduced the concept of the $T_{RS}$, and defined it as the temperature at which partial recrystallization is first observed[52, 64]. He also found that this critical temperature increased by increasing the initial solute level. The rate of increase, however, varied greatly with the type of solute. Nb, through the formation of Nb(C,N), is the most effective in raising the $T_{RS}$; V, which forms VN in austenite, is the least effective, as shown in Fig. 2.5.

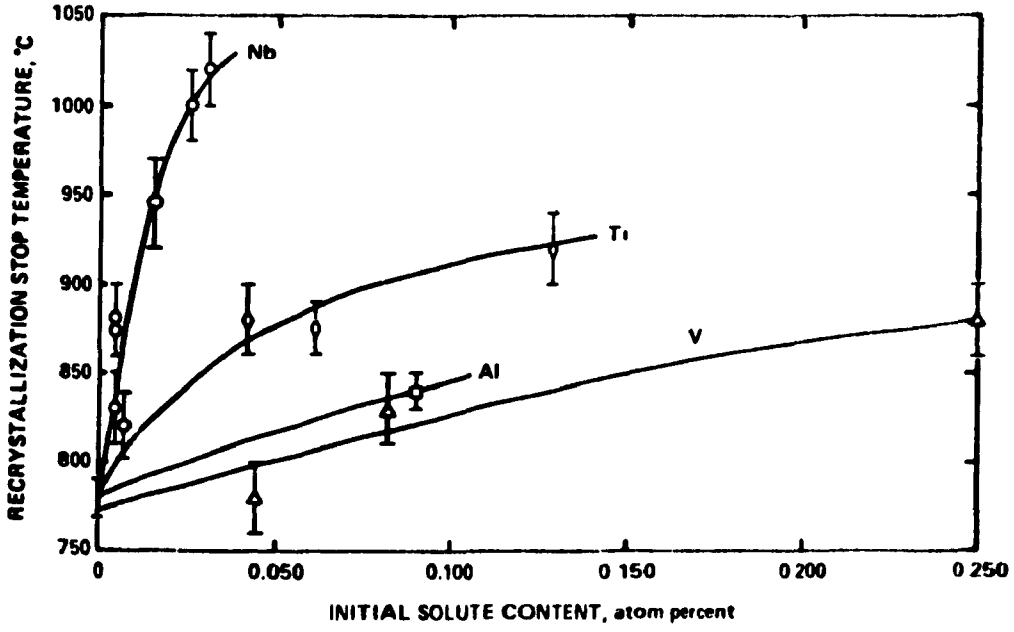


**Fig. 2.5** The increase in recrystallization-stop temperature with increase in the level of microalloy solutes in a 0.07C, 1.40Mn, 0.25Si base steel [52].

The data in Fig. 2.5 indicate that the increase in the $T_{RS}$ over that of the base steel (plain carbon steel) $\Delta T = (T_{RS} - 780)$ is related to the atomic percent of solute X according to:

$$\Delta T_{RS} = \alpha X^{1/2} \tag{2.7}$$

where α is a measure of the strength of the solute's effect on the $T_{RS}$. From the data in Fig. 2.5, α values were determined and are presented in Table 2.1.

Table 2.1 α factor related to solute

| solute | α<br>°C/(at. %)$^{1/2}$ |
|---|---|
| Nb | 1350 |
| Ti | 410 |
| Al | 200 |
| V | 200 |

Yamamoto et al. pointed out that the effect of solute atoms on static recrystallization may be explained by the degree of lattice distortion; furthermore, the degree of lattice distortion can be indirectly detected by the change in the lattice constant[38]. The result shown in Fig. 2.6 seems to give a consistent correlation between the retarding rate and the lattice constant change per atomic %. Alloying elements yielding large changes in lattice constant lead to relatively high retarding rates.

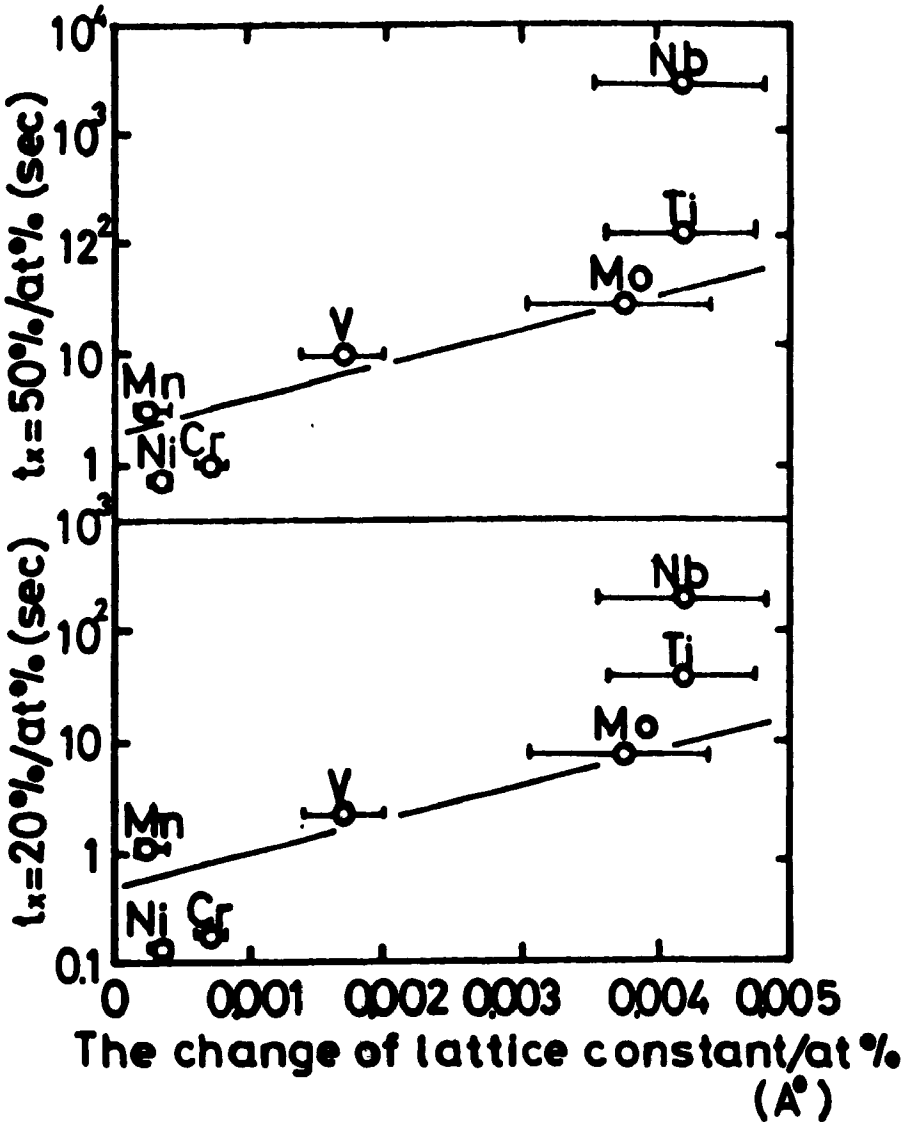


**Fig. 2.6** The correlation between $t_{x=20\%}$, $t_{x=50\%}$ and the change of lattice constant [38].

### 2.3.2 MODELLING OF RECRYSTALLIZATION AND PRECIPITATION

Much attention has been paid to modelling the recrystallization of austenite. Sellars originally found that the kinetics of static recrystallization in hot working can be described by the Avrami equation[65]:

$$X = 1 - exp[-0.693(t/t_{0.5})^k] \qquad (2.8)$$

where X is the volume fraction recrystallized after time t, and $t_{0.5}$ is the time to 50% recrystallization. The exponent k, typically 1 to 2, is not very sensitive to deformation parameters, whereas $t_{0.5}$ changes by orders of magnitude over the range of conditions encountered during hot rolling. It is therefore essential to have a quantitative description of $t_{0.5}$, in terms of the process variables. Some relations have been proposed for C-Mn steels by various investigators[63, 66-71], and are summarized in Table 2.2.

It can be seen that the recrystallization kinetics of plain carbon steels have been extensively investigated, but much less information is available for microalloyed steels. It is clear that microalloyed steels exhibit a discontinuity in the typical Avrami behavior[38, 42,72]. This is probably because of precipitation, which makes it more difficult to model recrystallization kinetics during the hot deformation of microalloyed steels. A quantitative model for the prediction of strain induced Nb(C,N) precipitation was developed by Dutta and Sellars in 1987[63]. In 1989, Liu and Jonas developed another model for titanium carbonitride[73]. Later, in 1991, Sun and Jonas developed a model for MnS precipitation[74]. These models are summarized in Table 2.3. Based on the Liu-Jonas model, Park and Jonas modelled Nb(C,N) precipitation under continuous cooling conditions using the additivity rule[75].

Based on the above review, it seems that there are limited data concerning the effect of deformation parameters, such as strain, strain rate and interpass interval, on the no-recrystallization temperature, under

conditions of continuous cooling. The present work focuses on a systematic investigation of the effect of processing parameters on the no-recrystallization temperature, $T_{nr}$.

**Table 2.2 Recrystallization models reported in the literature**

| Investigator | Static recrystallization |
|---|---|
| Sellars et al.[63, 65] | C-Mn Steel $X = 1 - \exp\{k(t/t_{0.5})^2\}$ $k = \ln 0.5$<br>$\varepsilon_p = 4.9\times10^{-4} d_0^{1/2} Z^{0.15}$ $Z = \dot{\varepsilon}\exp(312000/RT)$<br>when $\varepsilon > 0.8\varepsilon_p$: $t_{0.5} = 2.5\times10^{-19}\varepsilon^{-4} d_0^2 \times \exp(300\,000/RT)$<br>when $\varepsilon < 0.8\varepsilon_p$: $t_{0.5} = 1.06\times10^{-5} Z^{0.6} \times \exp(300\,000/RT)$<br>Nb Steel $X = 1 - \exp\{k(t/t_{0.05})^2\}$ $k = \ln 0.95$<br>$t_{0.05} = A d_0^2 \varepsilon^{-4} \times \exp(300\,000/RT)\exp\{[(275\,000/RT) - B\|\mathrm{Nb}\|\}$<br>$A = 6.75\times10^{-20}$ $B = 185$ |
| Esaka et al.[66] | C-Mn Steel $X_s = (1 - X_p)\{1 - \exp(-t/\tau)1/3\}$<br>$X_p = 1 - \exp\{-[(\varepsilon - \varepsilon_c)/(\varepsilon_s - \varepsilon)]^m\}$ $m = 0.026\exp(4600/T)$<br>$\varepsilon_s = 2.25\{1 - \exp(-d_0/K)\}$ $K = 472\dot{\varepsilon}^{-0.0723}\exp(-2600/T)$<br>$\tau_s = 9.11\times10^{-15}\dot{\varepsilon}^{-2.36}\exp(67670/RT)$ |
| Yada et al.[71] | C-Mn Steel $X = 1 - \exp\{-0.693[(t - t_0)/t_{0.5}]^2\}$<br>$t_{0.5} = 2.2\times10^{-12}\varepsilon^{-2}\dot{\varepsilon}^{-2} S_v^{-0.5} \times \exp(30\,000/T)$<br>$S_v = (24/\pi d_0)\{0.491\exp(\varepsilon) + 0.155\exp(-\varepsilon) + 0.1433\exp(-3\varepsilon)\}$ |

## Table 2.2 (Cont.)

| Investigator | Static recrystallization |
|---|---|
| Kwon et al.[68] | C-Mn Steel $X = 1 - \exp\{-0.693(t/t_{0.5})^2\}$<br>$t_{0.5} = A d_0^{1.4145} \varepsilon^{-3.144} Z^{-0.121} \exp(-Q_R/RT)$<br>$A = 3.32 \times 10^{-15}$ $Q_R = 285\,000$<br>Nb Steel $X = 1 - \exp\{k(t/t_{0.05})^2\}$ $k = -0.0513$<br>$t_{0.5} = A d_0^2 \varepsilon^{-4} \exp(Q_A/RT) \exp\{[(Q_B/\mathrm{RT}) - 185][\mathrm{Nb}]\}$<br>$\times \exp\{[(Q_C/T) - (C/r)][[\mathrm{NbC}]/r]\}$<br>$A = 6.75 \times 10^{-8}$ $B = 185$ $C = 2.063 \times 10^5$<br>$Q_A = 300\,000$ $Q_B = 2.75 \times 10^5$ $Q_C = 1.534 \times 10^7$ |
| Choquet et al.[67] | HSLA Steel $X = 1 - \exp\{-0.693(t/t_{0.5})^2\}$<br>$t_{0.5} = \nu_V d_\gamma^{0.878} \varepsilon^{-0.28} \varepsilon^P \exp(Q_R/RT)$<br>$Q_R/R = 39\,660 - 6025.8[\mathrm{C}]^{0.4} + 755[\mathrm{C}]^{0.65} + 2.848 \times 10^{-3}[\mathrm{Mn}]^2$<br>$+ 4423[\mathrm{Mo}]^{0.2} + (466.45 + 5.57 \times 10^5 (T_C - T) 4[\mathrm{Nb}]^{0.68}$<br>$P = d_\gamma^{-0.115}\{-3.89 + f_p[\mathrm{Nb}]\}$ $\nu_V = f_R(\mathrm{C}, \mathrm{Mn}, \mathrm{Mo}, \mathrm{Nb})$ |
| Roberts et al.[70] | C-Mn Steel $X = 1 - \exp\{-0.693(t/t_{0.5})^2\}$<br>$t_{0.5} = 5 \times 10 - 21 d_0^2 \varepsilon^{-4} \exp(Q_R/RT)$<br>$Q_R = 330\,000$ J/mol<br>Ti-V Steel $X = 1 - \exp\{-0.693(t/t_{0.5})^2\}$<br>$t_{0.5} = 5 \times 10 - 18 d_0^2 (\varepsilon - 0.058)^{-3.5} \exp(Q_R/RT)$<br>$Q_R = 280\,000$ J/mol |
| Hodgson et al.[69] | C-Mn Steel $X = 1 - \exp\{-0.693(t/t_{0.5})^{1.5}\}$<br>$t_{0.5} = 0.53 Z^{-0.6} \exp(240\,000/RT)$ |

## Table 2.3 Precipitation models reported in the literature

| Investigator | Strain-induced precipitation |
|---|---|
| Dutta-Sellars [63] | Nb(C,N) $t_{0.05} = A[\mathrm{Nb}]^{-1}\varepsilon^{-1}Z^{-0.5}\exp(270\,000/RT) \times \exp\{B/T^3(\ln k_s)^2\}$ <br> $A = 3\times10^{-6} \quad B = 2.5\times10^{10}$ |
| Liu-Jonas [73] | Ti(C,N) $P_s = H(\rho X_{Ti})^{-1}\exp(Q/RT)\exp(\Delta G/kT)$ <br> $H = 0.0156$ <br> $\Delta G = 16\pi(0.25\gamma)^3/3(\Delta G_{chem} + \Delta G_\varepsilon)^2$ |
| Sun-Jonas [74] | MnS $P_s = (\Gamma/ND_{Mn}^{\text{eff}}X_{Mn}^{\text{so}})\exp(\Delta G^*/kT)$ <br> $\Gamma = \Theta^* a_{\alpha\text{-}Fe}^2$ <br> $\Delta G^* = 16\pi(\xi\gamma)^3/3(\Delta G_{chem} + \Delta G_\varepsilon^* + \Delta G_{vac})^2$ |

CHAPTER 3

# EXPERIMENTAL MATERIALS AND PROCEDURE

## 3.1 EXPERIMENTAL MATERIALS

For the purpose of investigating the effect of processing parameters on the critical temperatures, $T_{nr}$ and $A_{r3}$, three Nb-bearing HSLA steels were used in the present work. The chemical compositions of these steels are shown in Table 3.1. Steels A and B both have low carbon contents and relatively high niobium contents. The main difference between these two steels is that the titanium level in steel B is higher than in steel A. The niobium concentration in steel C is in the medium range, while the carbon content is higher than in either steel A or steel B. The range of Nb concentration, from 0.05 wt% to 0.09 wt%, makes it possible to investigate the effect of solute drag on the recrystallization of austenite. Furthermore, the different combinations of niobium and carbon concentration lead to different supersaturations at different reheating temperatures, which makes it possible to investigate the effect of reheating temperature on the recrystallization of austenite during subsequent deformation. To compare the effect of various microalloying elements on the recrystallization of austenite, a titanium-vanadium steel was

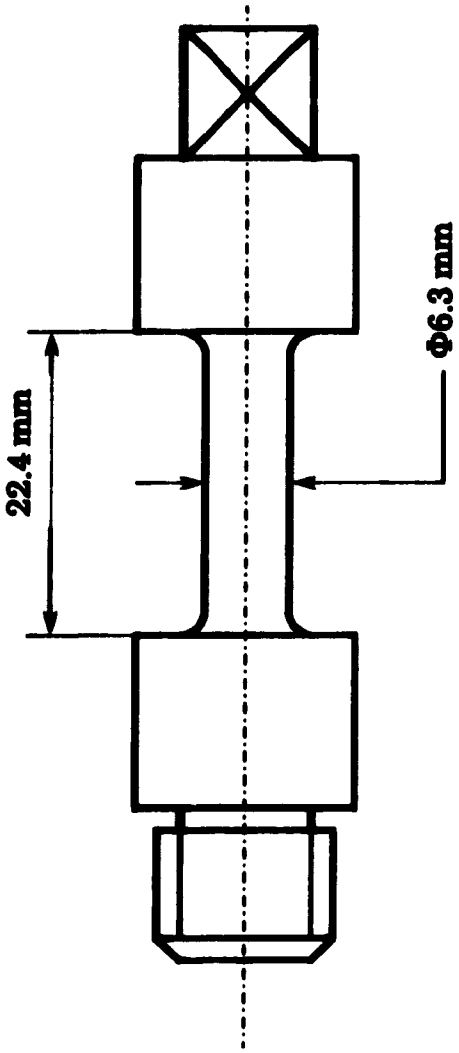


Fig. 3.1 Geometry of the torsion specimen.

used, and a plain carbon steel was also used as a base steel for comparison purposes.

## 3.2 SPECIMEN GEOMETRY

The as-received plates were cut into bars 15 mm×15 mm×80 mm with their axes in the rolling direction. Before machining, all of them were heat treated at 1000 °C for two hours and then air cooled in order to eliminate the rolling texture present in the as-received plates. Then, the bars were machined into torsion specimens with gauge lengths of 22.4 mm and diameters of 6.3 mm (see Fig. 3.1). This specimen size was selected to allow rapid cooling after the completion of a test, and also to allow relatively high strain rates to be reached.

## 3.3 EXPERIMENTAL EQUIPMENT

### 3.3.1 HOT TORSION MACHINE

Experiments were carried out on a servo-hydraulic, computer controlled MTS machine equipped with a Research Incorporated radiant furnace controlled by a Leeds and Northrup system. Details of the apparatus are shown in Fig. 3.2. A lathe bed was used as the frame of the torsion machine on which the motor-furnace-torque cell system was mounted longitudinally[76]. This motor is driven by an MTS hydraulic power supply and can develop a maximum torque of 100 N.m and a maximum speed of 628 rpm. The speed and direction of rotation of the motor are controlled by a servo valve that proportions the hydraulic fluid flow to the motor in relation to the magnitude of an electrical signal.

The specimen is held by means of nickel-based superalloy loading bars, which are connected to the motor and torque cell; the latter is mounted on the lathe saddle so that it can be moved axially. In the present study, a 1000 in-lbf (112.98 N-m) capacity cell was used to measure the load transmitted by the test specimen and its associated electronics were calibrated for four ranges

**Table 3.1 Chemical compositions of the steels investigated in weight %**

| STEEL | C | Si | V | Mn | Mo | Ti | Al | Nb | N |
|---|---|---|---|---|---|---|---|---|---|
| PC | 0.09 | 0.28 | --- | 1.44 | --- | --- | 0.02 | --- | 0.007 |
| V-Ti | 0.048 | 0.22 | 0.1 | 1.3 | --- | 0.02 | 0.032 | --- | 0.005 |
| High Ti | 0.055 | 0.24 | --- | 1.3 | --- | 0.16 | 0.036 | --- | 0.004 |
| A(0.09Nb) | 0.04 | 0.27 | --- | 1.53 | 0.14 | 0.007 | --- | 0.09 | 0.008 |
| B(0.07Nb) | 0.04 | 0.31 | 0.003 | 1.67 | 0.197 | 0.026 | 0.038 | 0.07 | 0.01 |
| C(0.05Nb) | 0.125 | 0.33 | 0.155 | 0.43 | 0.168 | --- | --- | 0.05 | 0.005 |

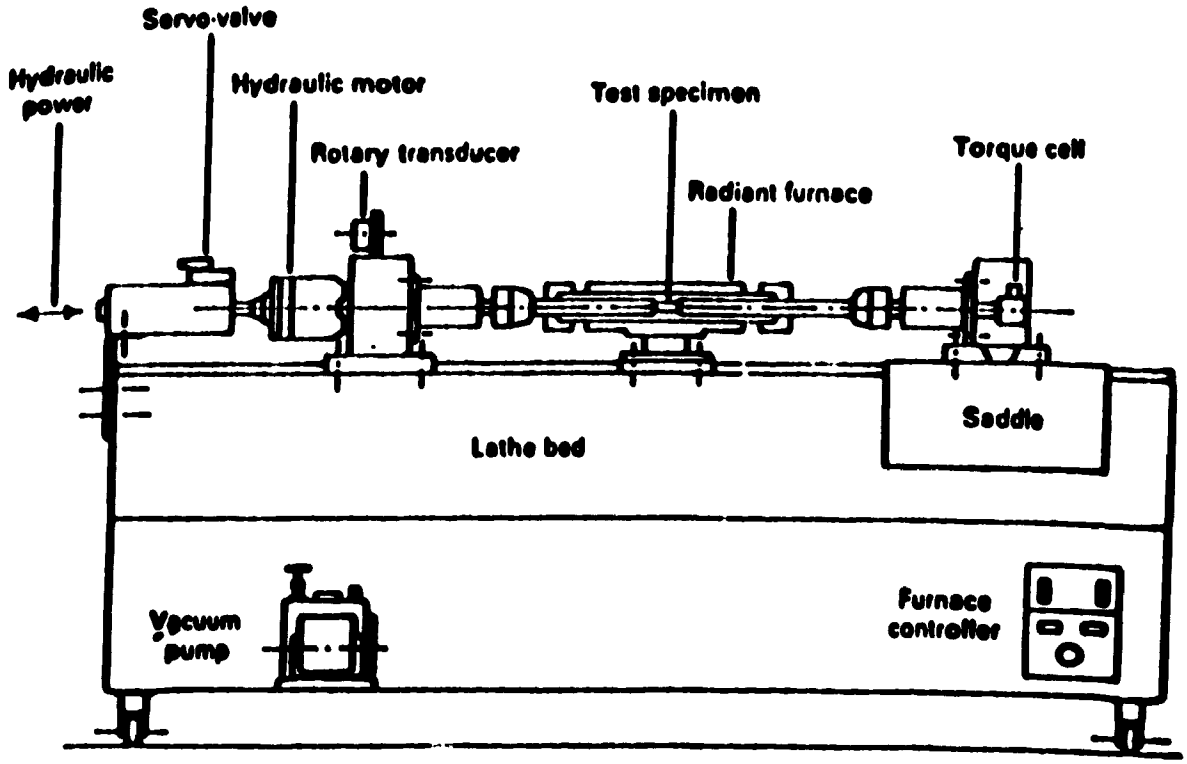


**Fig. 3.2 The servo-hydraulic hot torsion machine used in these experiments. It is mounted on a lathe bed[76].**

(1000, 500, 200, and 100 in-lbf), which correspond to 112.98, 56.49, 22.60, and 11.30 N-m. This relatively low capacity was selected to ensure adequate resolution of the torque measurements obtained from the small samples. The displacements, i.e. the angle of twist of the sample, were measured by the rotary transducer connected to the motor shaft.

The test specimens were heated by means of a water-cooled radiant furnace, model E4-10PA, which allows transient specimen temperatures of up to 1650 °C (3000 °F) to be reached. The furnace temperature was controlled by a Leeds and Northrup system. A digital industrial temperature controller was used with this system, which is linked to the programmer and the furnace through a thermocouple and a power supply, respectively. The temperature was also read on the computer screen, and could be written onto the hard disk together with the other data. To get good reproducibility of the temperature readings, an open-ended thermocouple was fixed to the gage length by a thin wire. The temperature of the specimen was controlled in this way, and any deformation heating was compensated by the temperature controller, which reduced the current to the furnace via the power supply. As shown in Fig. 3.3, cooling from a high temperature down to 800 °C, and cooling rates of up to 2 °C/s could be accurately controlled by adjusting the power supply automatically. Higher cooling rates were obtained by blowing compressed air into the furnace or by shutting down the power.

Oxidation of the specimens at high temperatures was prevented by passing a constant flow of high purity argon through the furnace.

### 3.3.2 COMPUTERIZED TESTING SYSTEM

The torsion machine was linked to a COMPAQ 386 computer which has a core memory of 10Mb RAM. In this computer, OS/2 is employed for the operating system, together with Windows. TestStar is used to control the test procedure. Lotus 1-2-3/G was put on the hard disk for data processing. A minimum interpass time of 10 ms can be obtained with this system. Fig. 3.4 shows an angular displacement-time curve taken from an actual test; here the requested interpass time was 18 ms, and the attained interpass time was 20 ms. Strain rates of 0.02/s~2/s could be obtained using the regular specimen, while the higher strain rates of 5/s~10/s were produced using a shorter specimen. As shown in Fig. 3.5, the delay in reinitiating straining somehow is related to the P value of the gain; the higher the P value, the sooner is

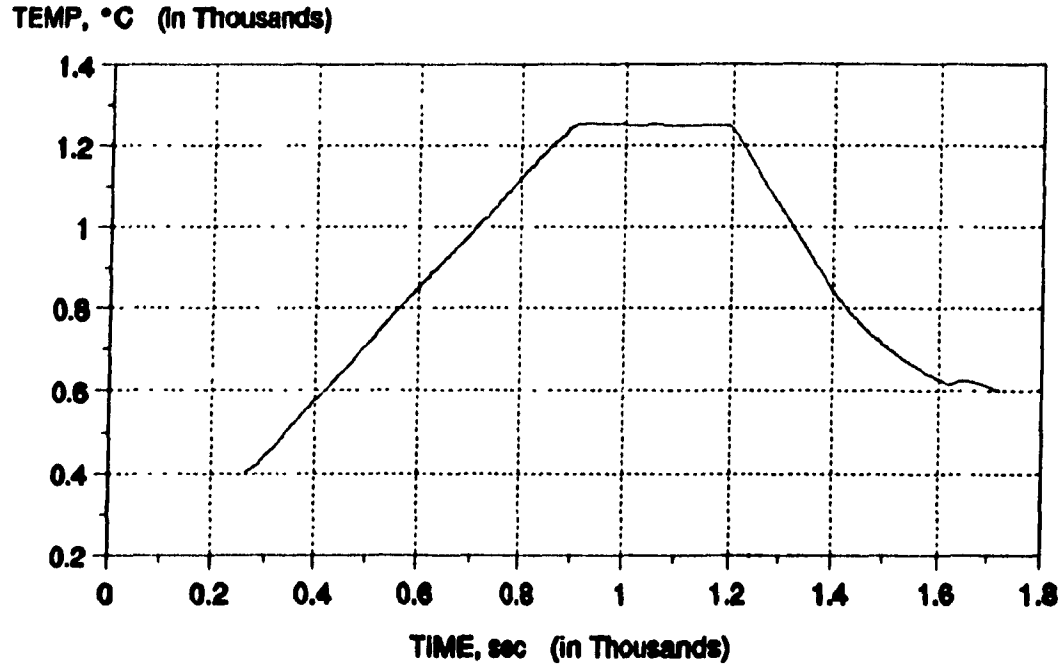


(a) Cooling rate = 2 °C/s

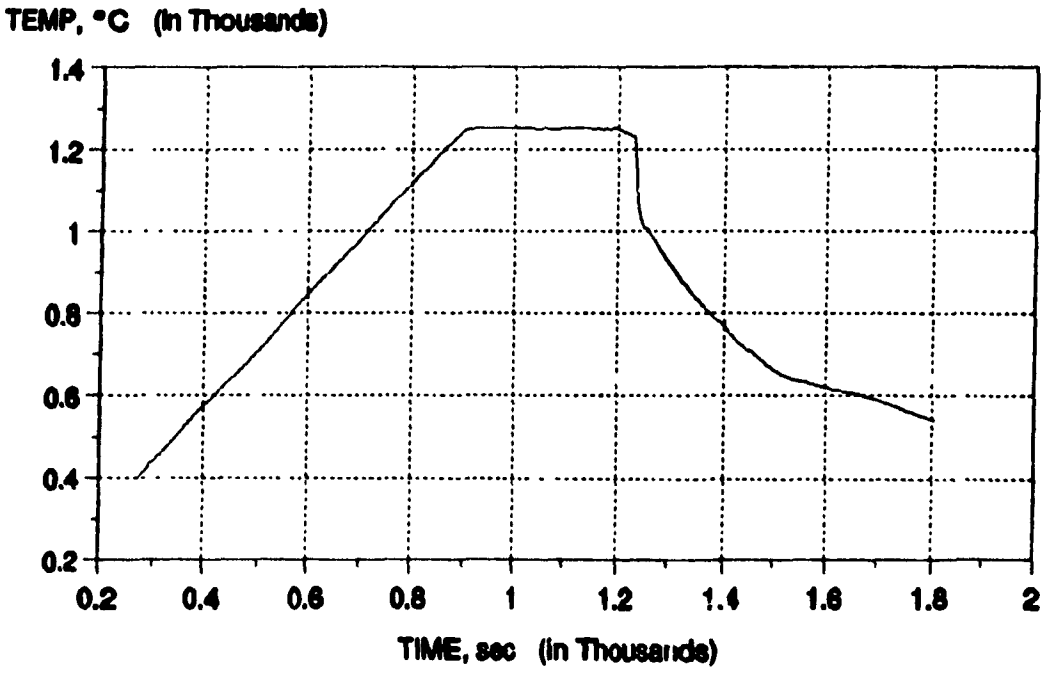


(b) Cooling rate after shutdown of power

Fig. 3.3 Cooling rate curves.

straining reintroduced. When the P value is too high, on the other hand, other problems arise, such as hunting and vibration of the rotation bar. A schematic diagram of the operations involved in running a test is shown in Fig. 3.6.

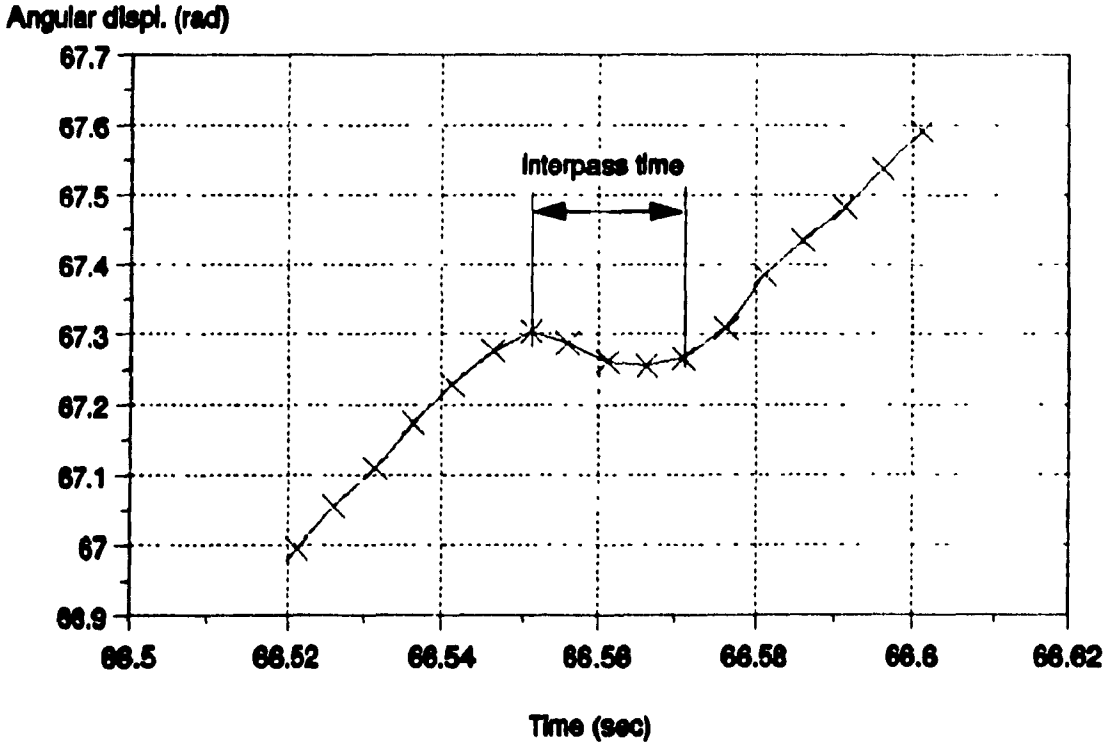


Fig. 3.4 Interpass time between passes.

## 3.4 AUSTENITIZATION TEMPERATURE

The equilibrium solution temperatures of the Nb(C,N) in the various alloys were evaluated from the following equation given by Irvine et al.[32]

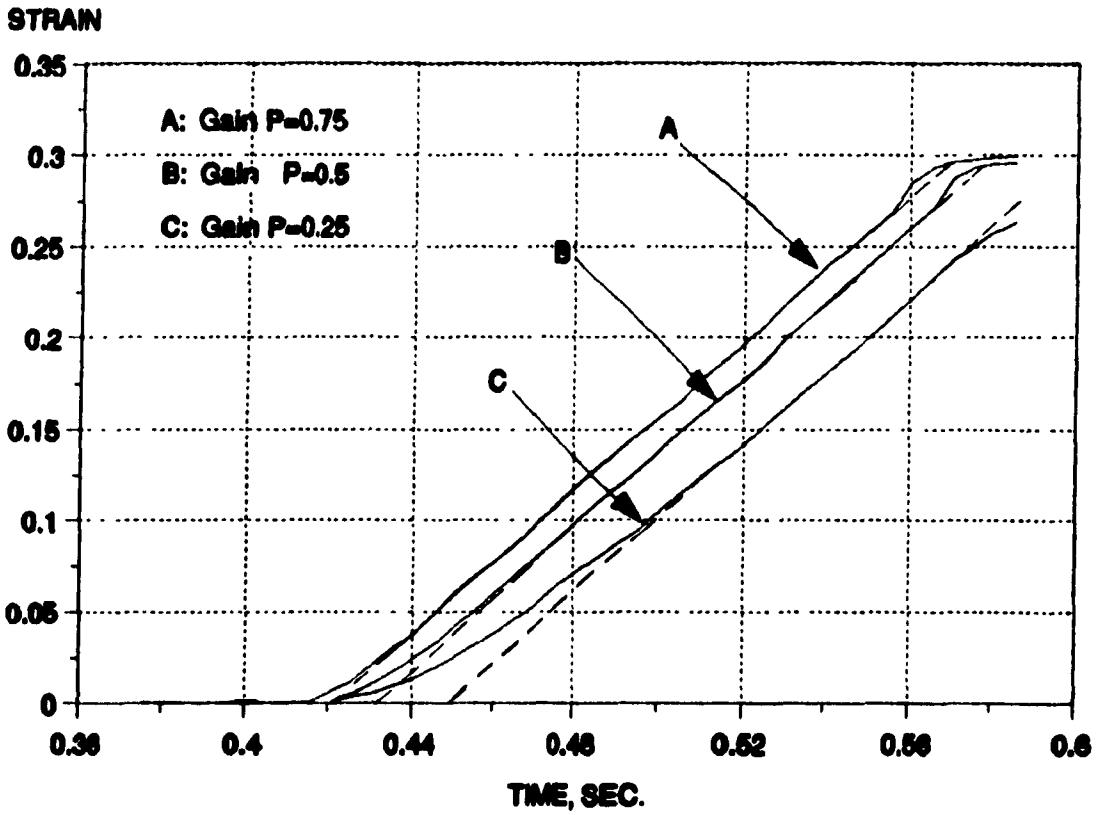


Fig. 3.5 Dependence of response time on the P value of the gain.

$$\log[Nb][C+\frac{12}{14}N]=2.26-\frac{6770}{T} \qquad (3.1)$$

The solution temperatures for the present steels were estimated to be approximately 1187 °C for steel A, 1153 °C for steel B (assuming that the formation of Nb(C,N) is dominant), and 1240 °C for steel C. When the reheating temperatures are chosen to be above these temperatures, the total niobium, carbon, and nitrogen contents of the steels should be in solution; conversely, when the reheating temperature is lower than these temperatures, the amounts to be expected in solution are lower. In the present work, reheating temperatures of 1250 °C, 1150 °C, and 1050 °C were used to give different degrees of Nb(C,N) supersaturation during subsequent deformation.

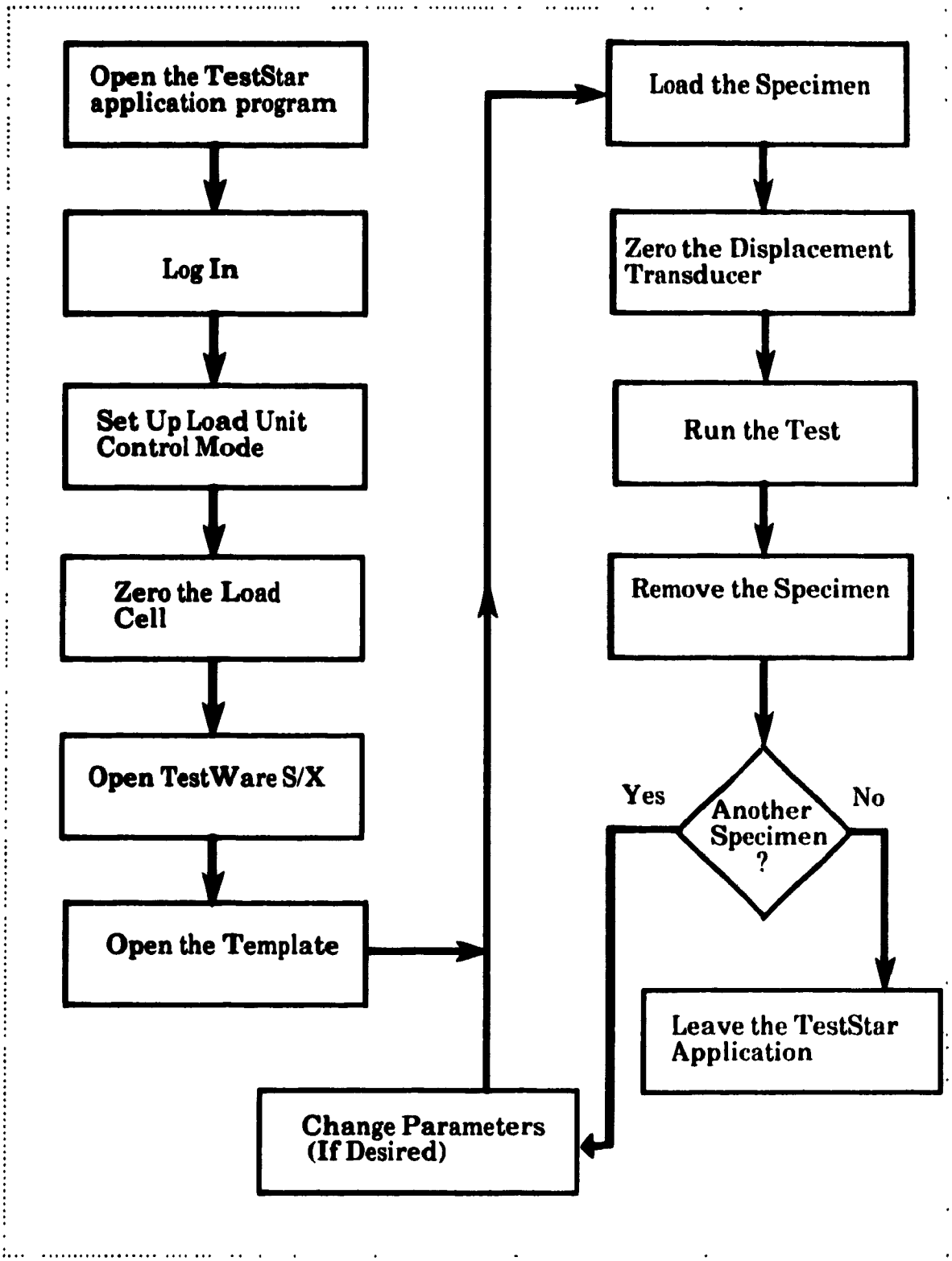


Fig. 3.6 A schematic diagram of the test procedure.

## 3.5 DETERMINATION OF THE $T_{nr}$ AND $A_{r3}$

Various methods have been used to determine the $T_{nr}$ in the laboratory. These have generally involved some form of compression testing or laboratory scale hot rolling. Single or multipass deformation schedules are performed to simulate rolling conditions and the $T_{nr}$ is evaluated from the resulting metallographic or flow stress data. In general, these tests are designed to generate a detailed picture of the recrystallization behaviour. In order to obtain an interrelationship between time, strain and temperature, many tests are required. A new technique developed by Boratto et al.[60] permits the $T_{nr}$ and $A_{r3}$ to be determined in a single test. This technique includes: i) evaluation of the equivalent stresses and strains; ii) calculation of the mean flow stresses; and iii) evaluation of the $T_{nr}$ and $A_{r3}$.

### 3.5.1 EVALUATING THE EQUIVALENT STRESSES AND STRAINS

The torque and twist data from the experiments were used to calculate the equivalent stresses and equivalent strains. The equivalent stress at the surface of the specimen is evaluated from the torque T via the relation proposed by Fields and Backofen[77],

$$\sigma_{eq} = \frac{\sqrt{3}T(3+m+n)}{2\pi r^3} \qquad (3.2)$$

and the equivalent strain at the surface is proportional to the measured angle of twist $\Theta$, as given by:

$$\varepsilon_{eq} = \frac{r\Theta}{\sqrt{3}L} \qquad (3.3)$$

Here, r and L are the specimen radius and length, respectively, m is the rate sensitivity and n is the work hardening coefficient derived from the torque. These coefficients are defined as follows:

$$m = \partial lnT / \partial ln\dot{\Theta} \tag{3.4}$$

$$n = \partial lnT / \partial ln\Theta \tag{3.5}$$

Although both m and n vary with strain, for the sake of simplicity, constant values of $m = 0.17$, and $n = 0.13$ were employed. The variations in m and n are much smaller than the mean value of the multiplier $(3 + m + n) = 3.3$, and the approximations, therefore, do not introduce a large error.

### 3.5.2 CALCULATING THE MEAN FLOW STRESSES

According to the definition of Fig. 3.7, the mean flow stress of each pass can be calculated using the numerical integral given by

$$\bar{\sigma}_{eq} = \frac{1}{\varepsilon_b - \varepsilon_a} \sum_{i=a}^{b} \frac{\sigma_{i+1} + \sigma_i}{2} \times (\varepsilon_{i+1} - \varepsilon_i) \tag{3.6}$$

$$\bar{\sigma}_{eq} = \frac{1}{\varepsilon_b - \varepsilon_a} \int_{\varepsilon_a}^{\varepsilon_b} \sigma_{eq} d\varepsilon_{eq} \tag{3.7}$$

where $\bar{\sigma}_{eq}$ is the mean flow stress, $\sigma_{eq}$ is the equivalent flow stress and $(\varepsilon_b - \varepsilon_a)$ is the equivalent strain of the pass of interest.

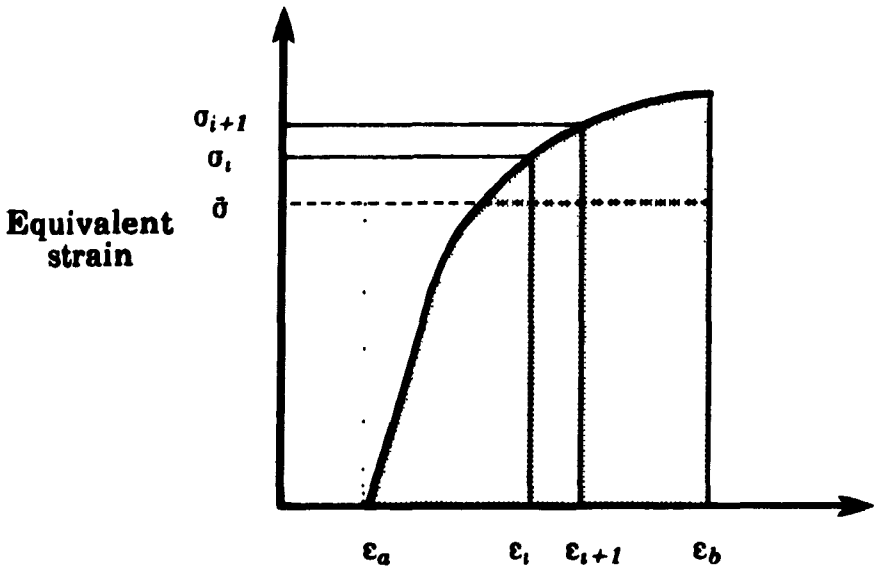


**Fig. 3.7 Equivalent stress-equivalent strain curve.**

### 3.5.3 EVALUATING THE $T_{nr}$ AND $A_{r3}$

The dependence of the mean flow stress on inverse absolute temperature for microalloyed steels is shown in Fig. 3.8. Based on the slope changes that can be seen, processing can be divided approximately into four regions. In region I (high temperature region), recrystallization takes place fairly rapidly, so that there is no strain accumulation and no work hardening; in this case, the mean flow stress depends only on the temperature. The mean flow stress increases slowly with decreasing temperature. In region II (intermediate temperature region), only partial recrystallization takes place or no recrystallization at all, so the strain is accumulated from pass to pass and continued work hardening is displayed. In this case, the mean flow stress increases more rapidly with decreasing temperature. The cessation of full recrystallization is responsible for a slope change at the intersecting point of

regions I and II. According to Boratto et al.[60], the temperature that corresponds to this point can be defined as the no-recrystallization temperature ($T_{nr}$) for plate rolling.

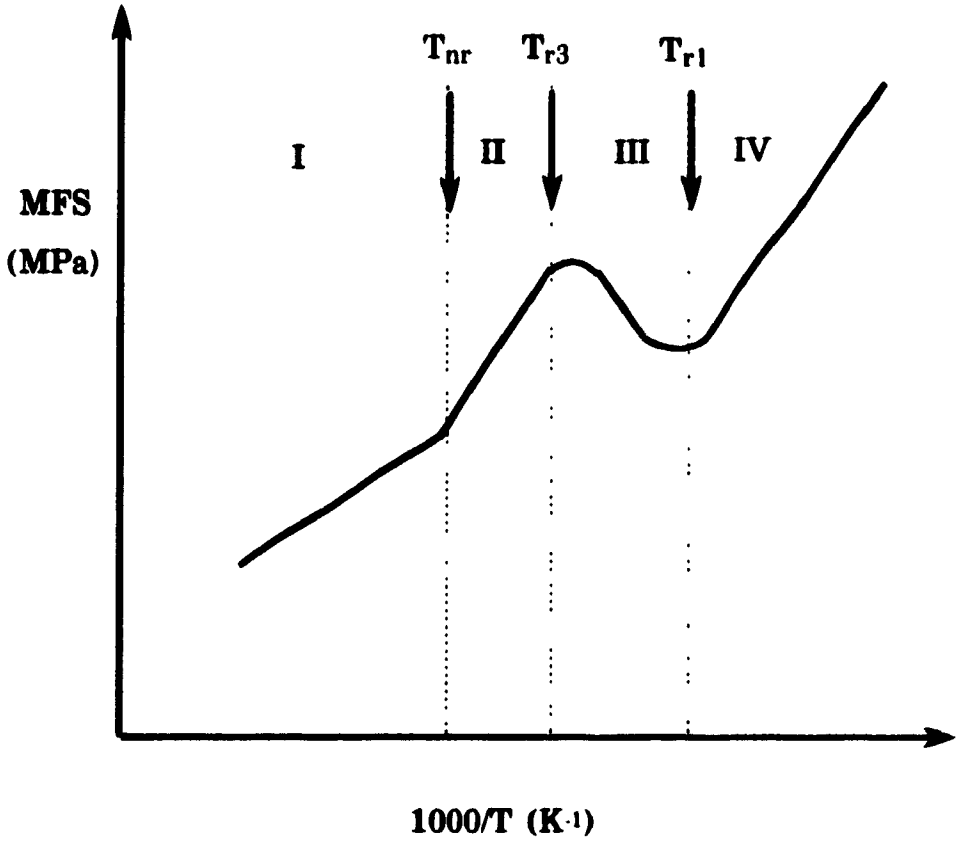


**Fig. 3.8 The dependence of the mean flow stress on the inverse absolute pass temperature.**

When processing is carried out to lower temperatures, the austenite-to-ferrite transformation takes place; this leads to the mean flow stress dropping because ferrite is softer than austenite. With a further continuous increase in the ferrite fraction, the mean flow stress decreases continuously until the transformation is finished; then the mean flow stress increases again. The

temperatures that correspond to these two points of further intersection can be defined as the start ($A_{r3}$) and finish ($A_{r1}$) temperatures of the austenite-to-ferrite transformation.

These critical temperatures can be determined by assuming a linear dependence of $\bar{\sigma}_{eq}$ on 1000/T in regions I, II and IV, i.e.[60];

$$\bar{\sigma}_{eq} = (A + B \times 1000/T) \qquad for\ T \geq T_{nr} \tag{3.8}$$

and

$$\bar{\sigma}_{eq} = (A' + B' \times 1000/T)(1 - V_f) + (C + D \times 1000/T)V_f \qquad for\ T < T_{nr} \tag{3.9}$$

Here, $V_f$ is the volume fraction of ferrite at temperature T; it is calculated using the following empirical equation:

$$V_f = E(1000/T)F/[1 + E(1000/T)F] \tag{3.10}$$

A is the intercept and B is the slope of the line in region I. Similarly, A'and B', C and D are the equivalent constants for regions II and IV, respectively. E and F are coefficients related to the transition curve in region III. The critical temperatures themselves are given by:

$$T_{nr} = 1000(B - B')/(A' - A) \tag{3.11}$$

$$A_{r3} = 1000(32.32E)^{1/F} \tag{3.12}$$

$$A_{r1} = 1000(E/32.32)^{1/F} \tag{3.13}$$

Here, $A_{r3}$ is the temperature at $V_f=3\%$ and $A_{r1}$ is the temperature at $V_f=97\%$. The constants A, B, A', B' C, D, E and F were calculated using a nonlinear least squares optimization method.

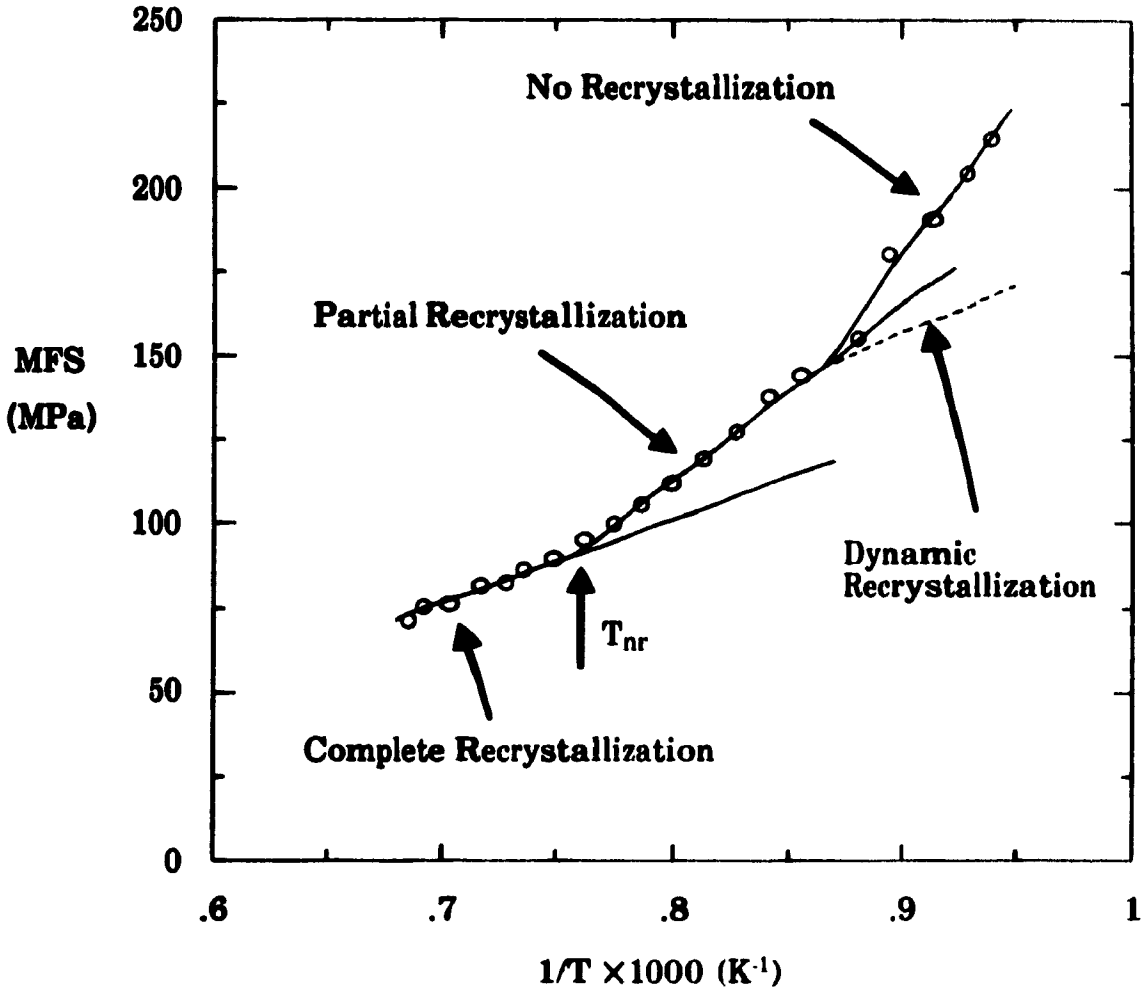


**Fig. 3.9** Dependence of the mean flow stress (MFS) on the inverse absolute pass temperature for samples of steel A deformed according to schedule A; $\varepsilon=0.3$, $\dot{\varepsilon}=2/s$, $t=10$ s.

Actually, in the austenite range, there are two changes in the slope of the mean flow stress curve, as shown in Fig. 3.9. The temperature corresponding to the first change was defined above. The temperature corresponding to the second change is where recrystallization ceases

completely. The changes in mean flow stress can be understood in terms of the retardation of recrystallization by the precipitation of Nb(C,N). According to Dutta and Sellars[63], the first slope change corresponds to the point of intersection of the $t_{0.05p}$ (time for 5% precipitation) and $t_{0.95x}$ (time for 95% recrystallization) curves in an RTT-PTT diagram. The second change is related to the point of intersection of $t_{0.05p}$ and $t_{0.05x}$ (time for 5% recrystallization). For microalloyed steels, the first change can always be seen, whereas in many cases, the second change does not appear.

There are two possible values of the slope change at temperatures below this point. If strain accumulation cannot initiate dynamic recrystallization, the mean flow stress will change along the solid line; this is the case of rolling with long interpass times (for example, 30 seconds), as in reversing mills. The mean flow stress changes along the broken line as long as dynamic recrystallization is initiated. Rolling with short interpass times is coincident with this situation, as in continuous mills.

For a strain/pass of 0.3, strain rate of 2/s, and interpass time of 30 s, the measured $T_{nr}$ for steel B was 960 °C. To demonstrate the accuracy of the $T_{nr}$ measurements, two isothermal tests were executed at temperatures close to the $T_{nr}$ determined by the method described above. Two mean flow stress-total equivalent strain (or pass number) curves are shown in Fig. 3.10. For the lower curve, the isothermal stage was initiated at pass 9, at which the temperature was about 965 °C (> the $T_{nr}$). For the upper curve, the isothermal stage was initiated at pass 11, at which the temperature was 900 °C (< the $T_{nr}$). It can be seen that above the $T_{nr}$, the mean flow stress remained at the same level (about 133 MPa) for all of the passes. This implies that no strain accumulation or work hardening took place, and that full interpass softening occurred under these conditions.

Below the $T_{nr}$, however, the mean flow stress increased with pass number over the first three passes. This phenomenon can be understood in terms of the strain accumulation that takes place during deformation at temperatures below the $T_{nr}$. When the accumulated strain reached the critical value for static or dynamic recrystallization, the stored strain energy was released somewhat, which led to a slightly lower value of the mean flow stress

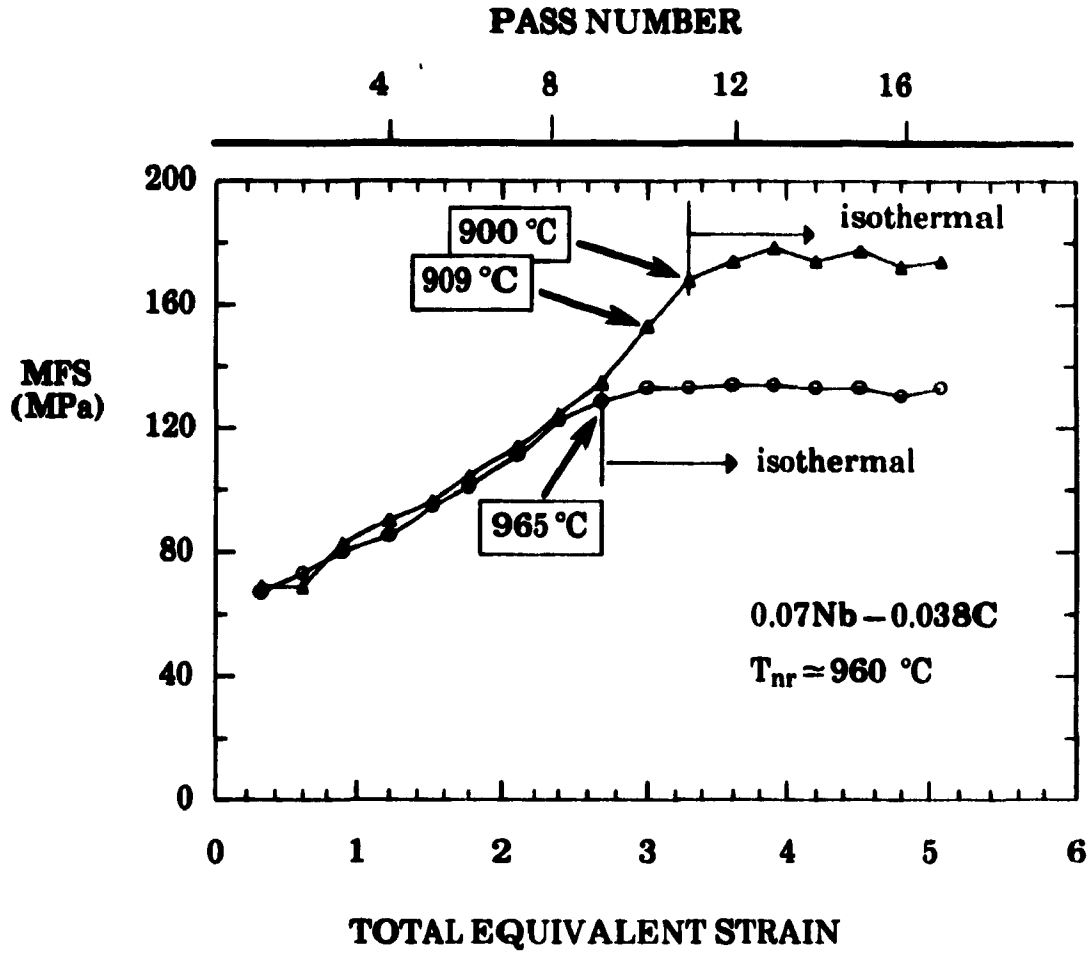


**Fig. 3.10** MFS vs. total equivalent strain (or pass number) under isothermal deformation conditions at temperatures above and below the $T_{nr}$.

in the next pass. The repetition of this process is probably responsible for the oscillations of the mean flow stress evident on the diagram. The degree of interpass softening, X, under the isothermal conditions was calculated from the expression:

$$X = \frac{\sigma_m - \sigma_{yi}}{\sigma_m - \sigma_{y0}} \tag{3.14}$$

where $\sigma_m$ is the flow stress at the end of the previous pass, $\sigma_{y0}$ is the flow (yield) stress of the first pass of the isothermal stage, and $\sigma_{yi}$ is the flow stress of the present pass. Fig. 3.11 illustrates the relevant interpass softening curve. It can be seen that the fractional softening above the $T_{nr}$ is around 95% for all of the passes, but below the $T_{nr}$, the fractional softening ranges from 55% to 75%.

Fig. 3.12 shows the microstructures close to the $T_{nr}$. It can be seen that the quenched structure at temperatures above the $T_{nr}$ is completely recrystallized austenite, while in the case of samples quenched at temperatures below the $T_{nr}$, the structure is only partially recrystallized.

It worth pointing out that the $T_{nr}$ determined by the present method represents the lowest temperature at which complete recrystallization might be expected to occur during a 30 second delay. In the case of a continuous cooling schedule, however, a 30 second delay corresponds to a 30 °C decrease in temperature. This continuous decrease in temperature can slow down the recrystallization process sufficiently that recrystallization is not completed during this interpass time. Because of such considerations, the actual no-recrystallization temperature is probably higher than that determined from the MFS-1/T curve. For the present case, it can be defined as follows:

$$T_{nr}^{*} = T_{nr} + 30\ ^{\circ}C \tag{3.15}$$

where $T_{nr}$ is determined from the MFS-1/T curve, and $T_{nr}^{*}$ is the no-recrystallization temperature corrected for continuous cooling conditions. The correction of 30 °C corresponds to the decrease in temperature from one pass to the next.

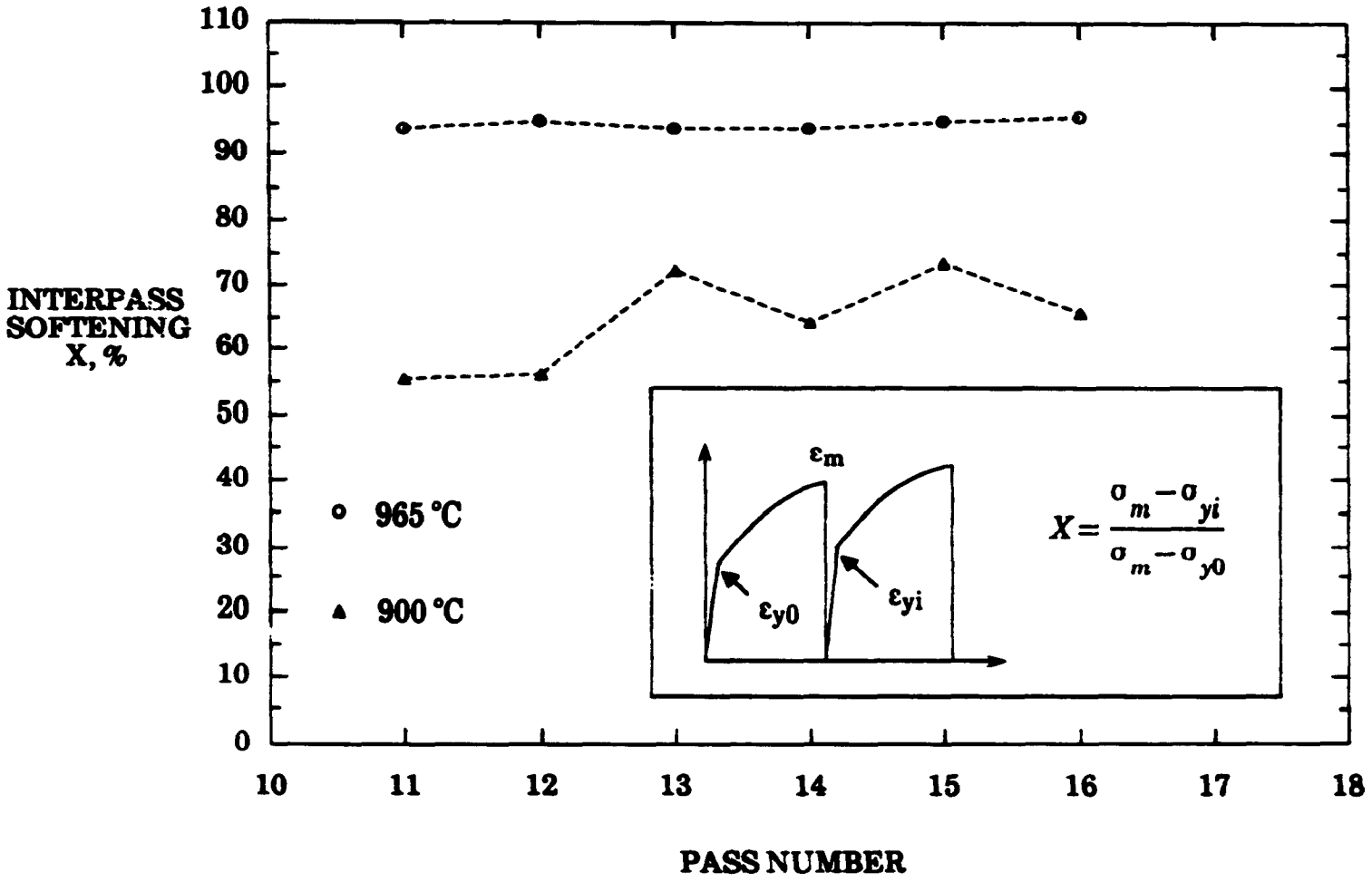


Fig. 3.11 Interpass softening at temperatures above and below the $T_{nr}$ ($T_{nr}$ = 960 °C).

(a)

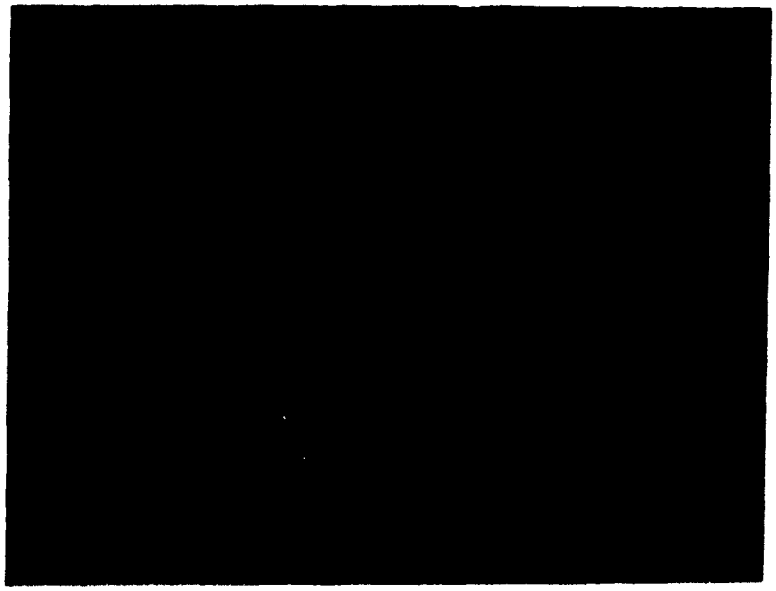

(b)

Fig. 3.12 Microstructures close to the $T_{nr}$ (the $T_{nr}$ = 960 °C)
(a) quenched at 970 °C after a 30 s delay;
(b) quenched at 940 °C after a 30 s delay.

## 3.6 ROLLING SCHEDULES

### 3.6.1 SCHEDULE A

Multipass torsion tests were designed to investigate the effect of deformation parameters, such as the strain per pass, strain rate, and interpass time, on the $T_{nr}$. Table 3.2 lists the test parameters: strain ranges from 0.1 to 0.7, strain rate ranges from 0.2 $s^{-1}$ to 10 $s^{-1}$, and interpass times from 2 s to 200 s. For a particular test, the strain per pass, strain rate and interpass time are

Table 3.2 Test parameters for schedule A

| |
|---|
| Strain/pass |
| $\varepsilon = 0.1, 0.2, 0.3, 0.4, 0.5, 0.7$ |
| Strain rate |
| $\dot{\varepsilon} = 0.2, 2, 5, 10/s$ |
| Interpass time |
| $t = 2, 5, 7.5, 10, 12.5, 15, 20, 30, 50, 80, 100, 150, 200$ s |

identical. A schematic schedule for this investigation is illustrated in Fig. 3.13. First of all, a specimen was reheated to a selected solution temperature and soaked at this temperature for 15 minutes; then it was cooled down at a constant cooling rate. During cooling, 17 passes were applied at a constant strain rate, and there was an interpass delay between the passes. To maintain the same 30 °C interpass decrease in temperature, slower cooling rates were

used for the longer interpass times and faster cooling rates for the shorter interpass times. The cooling rates for different tests are given by:

$$\beta = \frac{30\,^{\circ}C}{t} \qquad (3.16)$$

where $t$ is the interpass time in seconds.

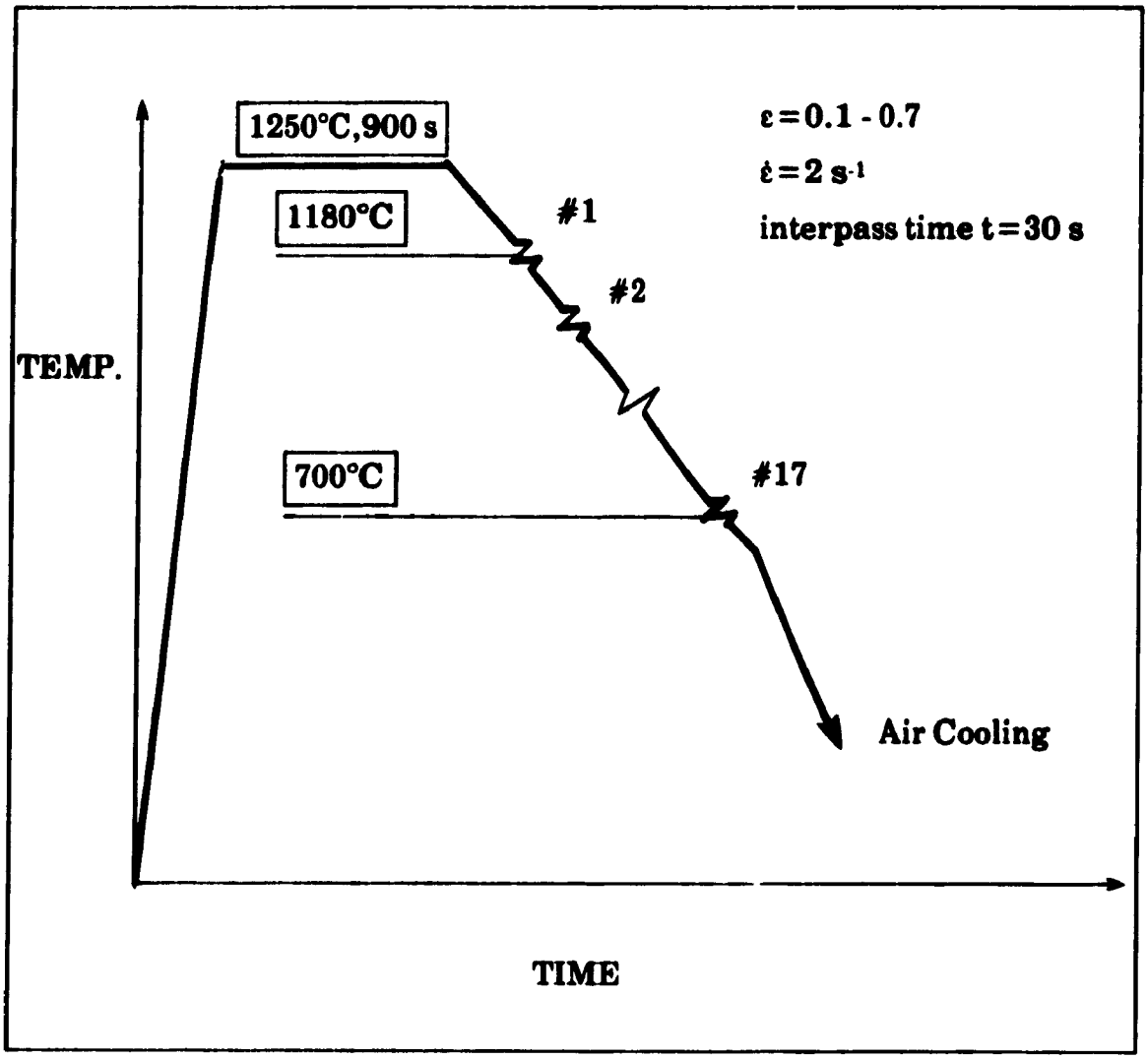


Fig. 3.13 Schedule A employed in the present hot torsion tests.

### 3.6.2 SCHEDULE B

Schedule B was designed to investigate strain accumulation during multipass deformation; it consists of four roughing passes followed by a single finishing pass. The strains and deformation temperatures of the 5th pass ranged from 0.3 to 2.4 and 1060 °C to 850 °C, respectively. The test parameters employed are listed in Table 3.3.

Table 3.3 Test parameters for schedule B

| Pass No | Deformation temperature (°C) | Pass strain | Interpass time (s) |
|---|---|---|---|
| 1 | 1180 | 0.3 | 30 |
| 2 | 1150 | 0.3 | 30 |
| 3 | 1120 | 0.3 | 30 |
| 4 | 1090 | 0.3 | 30 |
| 5 | 1060~850 | 0.3~2.4 | 30~240 |

### 3.6.3 SCHEDULE C

Schedule C (see Fig. 3.14) was designed for investigating the possibility of dynamic recrystallization under isothermal deformation conditions when shorter interpass times were employed.

## 3.7 METALLOGRAPHIC EXAMINATION

The microstructures produced along a radius of the specimen are presented in Fig. 3.15. It can be seen that the as-reheated structure is uniform within the cross section of the specimen, while the structures are not uniform after deformation because of the strain gradient present in the solid bar torsion

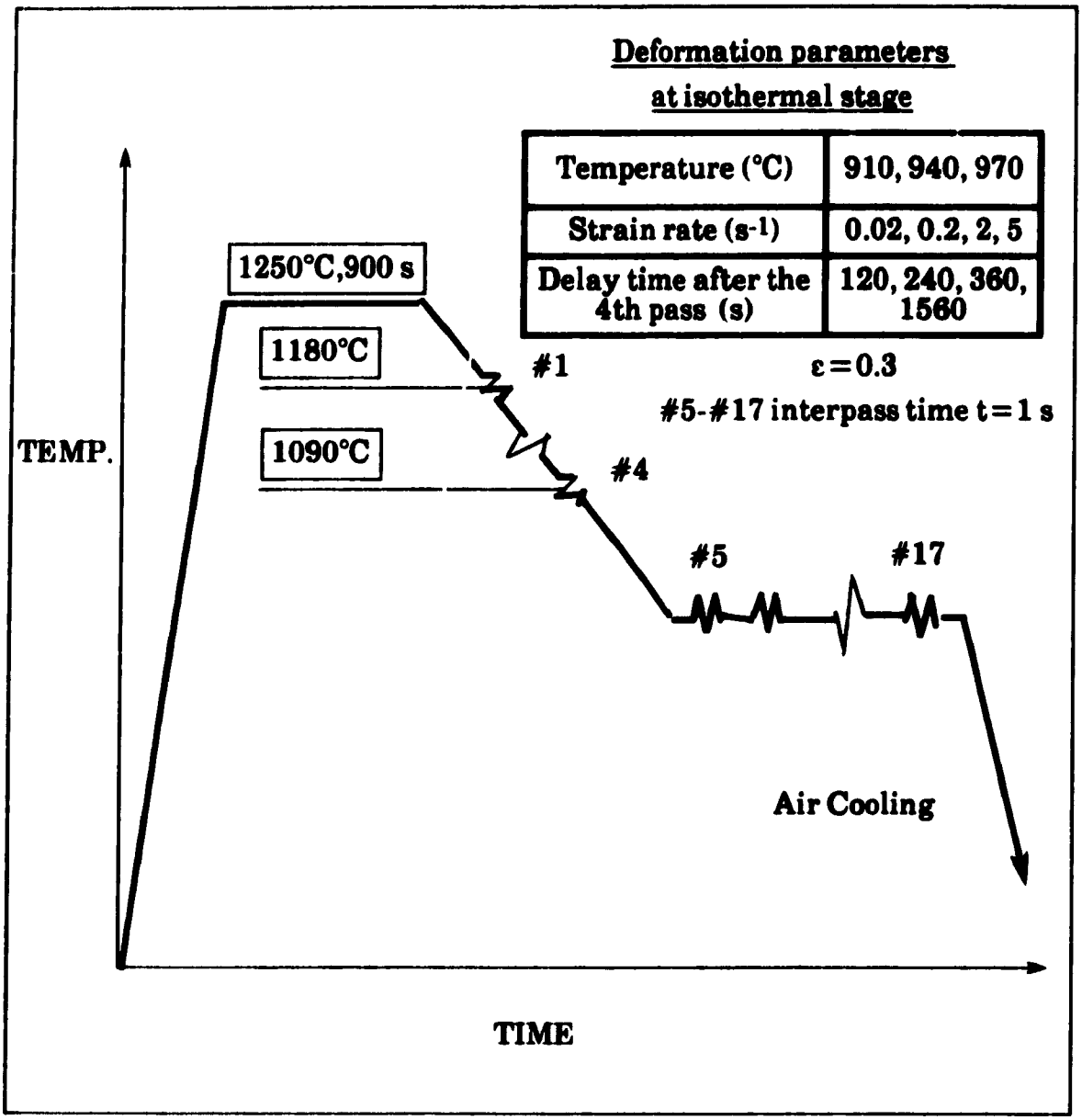


Fig. 3.14 Schedule C employed in the present hot torsion tests.

samples. In the surface layer, the austenite is uniform and refined by recrystallization; in the centre, however, the original grain size is retained although some local grain boundary movement has taken place. It should be noted that there is grain coarsening in a small area around 1/2 R. This is probably because the strains in this region are close to the critical strain which leads to grain coarsening. Based on this knowledge, the stresses and strains

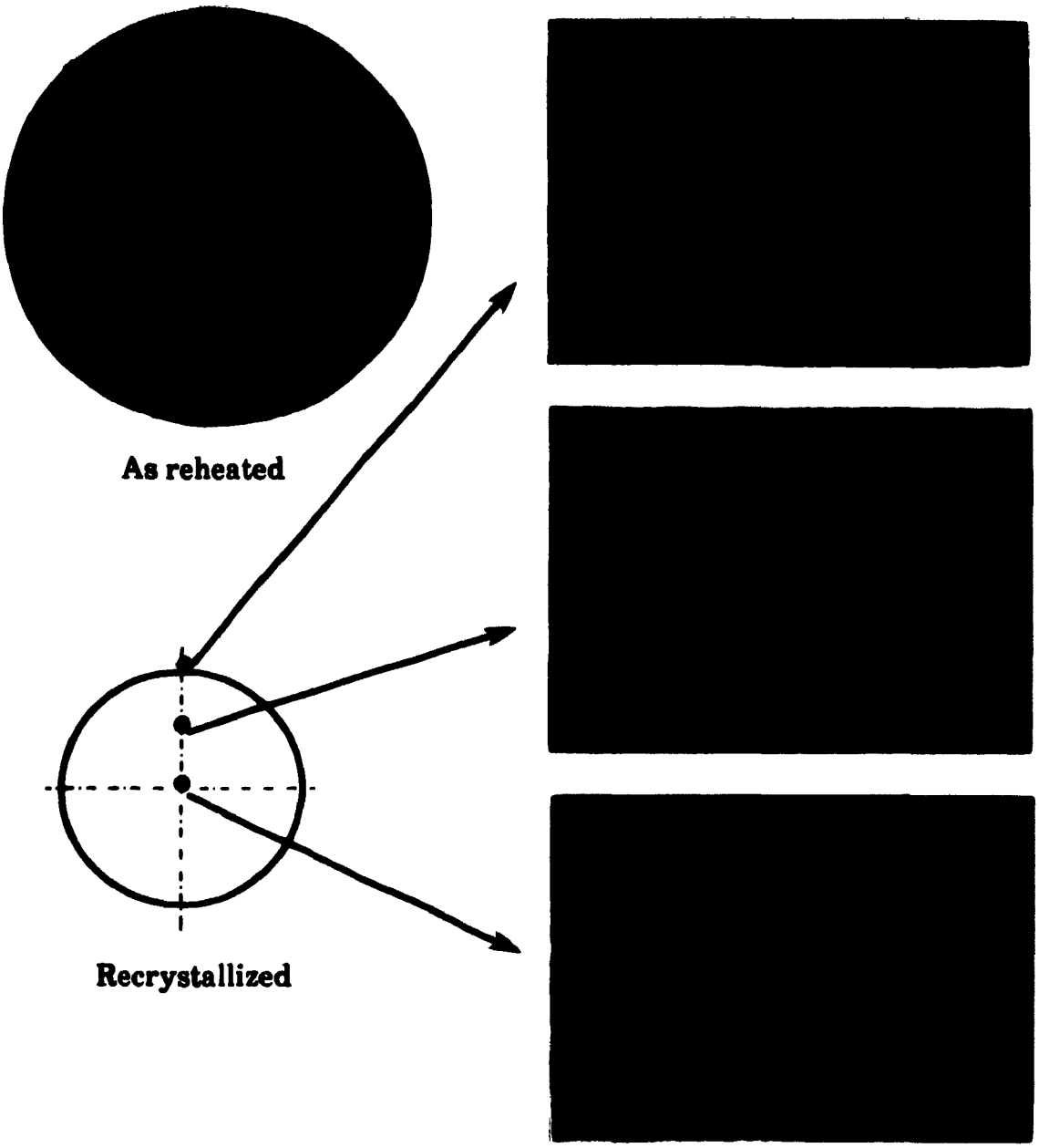


**Fig. 3.15** Distribution of the microstructure along a radius of the specimen before and after deformation followed by recrystallization.

were always calculated using the maximum radius, and the microstructures were always examined at the specimen subsurface.

In order to reveal the prior austenite microstructure, a series of tests was interrupted at selected temperatures, and the specimens were quenched in water. The latter were sectioned and ground using silicon carbide papers and polished with 1 μm diamond paste and 0.05 μm alumina, in sequence. The polished specimens were etched using a solution based on a saturated aqueous picric acid solution, with small additions of HCl. The composition of the etchant and the etching conditions were varied for specimens deformed under different conditions until the prior-austenite grain structure was revealed.

## 3.8 ELECTRON MICROSCOPY

In order to check the effect of interpass time on precipitation during continuous cooling, a set of specimens was tested using schedule A with interpass times of 5, 30, 80, and 200 seconds to the 9th pass. At this point the deformation temperature was 940 °C; it was then cooled to 910 °C and quenched. The specimens were prepared as described above, and then lightly etched with 2% nital for about 5~10 seconds. Carbon was deposited on the etched surfaces using a vacuum evaporator in vacuums better than $5\times10^{-4}$ torr.

Squares approximately 2 mm×2 mm were scribed on the coated surfaces and removed by electropolishing using a solution of 10% nital. During etching, the current was slowly increased until small bubbles began to form. The removed carbon replicas were washed gently in a 50-50 mixture of ethanol and distilled water and then in distilled water. They were finally mounted on TEM copper grids (3 mm, 200 mesh) and dried. The carbon replicas were examined in a JEM-100 CXII scanning transmission electron microscope fitted with a PGT system IV energy dispersive X-ray spectrometer (EDS) for the chemical analysis of individual particles.

CHAPTER 4

# STATIC RECRYSTALLIZATION

The aim of the present work was to investigate the influence of processing parameters such as strain per pass, strain rate, interpass time, and chemical composition on austenite recrystallization and final microstructure. For this purpose, a clear understanding of the essential effect of these parameters on the critical temperatures (i.e. no-recrystallization temperature, and austenite-to-ferrite transformation temperatures) is required. The detailed objectives of this work were the following.

1) To investigate the effect of reheating temperature, initial austenite grain size, and chemical composition on the $T_{nr}$.

2) To investigate the effect of deformation parameters, such as pass strain, strain rate, and interpass time, on the $T_{nr}$.

3) To develop a method of predicting the no-recrystallization temperature, $T_{nr}$.

To accomplish the objectives described above, hot torsion tests were performed according to a variety of schedules. During testing, all experimental data were recorded and stored on the microprocessor. At the end of each test, the stress-strain curve for each pass was plotted and the mean flow stress was computed. Plotting the mean flow stress against the inverse absolute pass temperature, a series of diagrams similar to Fig. 3.7 were obtained. Furthermore, the $T_{nr}$'s were determined by means of the method described in Chapter 3.

## 4.1 REHEATED AUSTENITE GRAIN SIZE

The initial austenite grain size was revealed by water quenching immediately after a selected specimen reached the test temperature. Fig. 4.1 shows the microstructures of steel A, the V-Ti steel and the plain carbon steel after reheating at 1250 °C. It can be seen that the grain size of the plain carbon steel (~400 μm) is much larger than that of steel A (~100 μm), while the grain size of steel A is larger than that of the V-Ti steel. Actually, the reheating temperature of 1250 °C is higher than the coarsening temperature of the plain carbon steel (~1000 °C), which led to the grain coarsening and resulted in the huge initial austenite grain size. Niobium addition in steel causes a marked retardation of grain growth, which led to the smaller initial austenite grain size after reheating. Titanium has the strongest retarding effect on grain growth because the stability of TiN and its slow growth rate[1] enables it to act as a strong grain growth inhibitor at high temperatures. Therefore, a small addition of titanium to steel leads to considerable grain refinement. The as-reheated austenite grain sizes are listed in Table 4.1.

## 4.2 EFFECT OF REHEATING TEMPERATURE AND INITIAL AUSTENITE GRAIN SIZE

### 4.2.1 REHEATING TEMPERATURE

The MFS (mean flow stress)-1000/T diagrams are shown in Fig. 4.2. It can be seen that the $T_{nr}$'s determined from the MFS-1000/T diagrams are

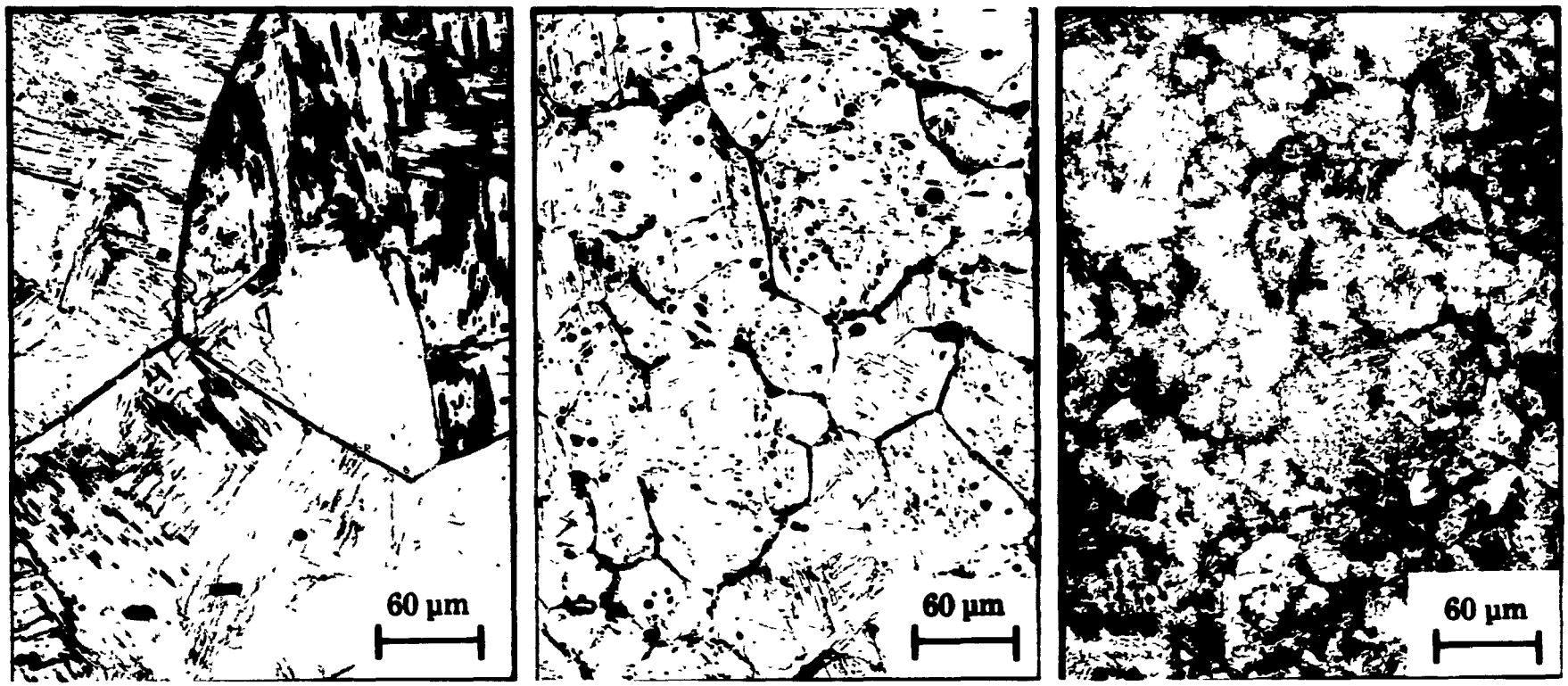


PC steel 0.09Nb steel 0.1V-0.02Ti steel

Fig. 4.1 Reheated austenite microstructures (reheating temperature: 1250 °C; soaking time: 15 min)

almost the same for reheating temperatures of 1280 °C and 1250 °C. For a reheating temperature of 1150 °C, however, the slope change shifts to a lower temperature. Fig. 4.3 shows the dependence of the $T_{nr}$ on reheating temperature. It demonstrates that the $T_{nr}$ increases with increasing reheating temperature; when the reheating temperature reaches 1250 °C, however, the $T_{nr}$ does not change with further increase in reheating temperature.

Table 4.1 Reheated austenite grain sizes

| Steel Type | Austenitization Temperature, °C | γ-Grain size, μm |
|---|---|---|
| A (0.09Nb) | 1250<br>1150 | 100<br>65 |
| B (0.07Nb) | 1250<br>1150<br>1050 | 85<br>55<br>40 |
| C (0.05Nb) | 1250<br>1150<br>1050 | 125<br>65<br>50 |

For steels A and B, the niobium concentration is almost the same, so that the difference in $T_{nr}$ between these two steels is small. An interesting observation here is that the $T_{nr}$ of steel C is higher than that of steels A and B, even though the niobium concentration of steel C is lower. This phenomenon can be explained in terms of the niobium supersaturation, which is a driving force for Nb(C,N) precipitation. This ratio can be calculated in two steps. The first step involves calculating the austenite composition at the solution temperature; in the second step, the supersaturation ratio at the deformation temperature is then calculated. Following Wadsworth et al.[78], the austenite composition at a given solution temperature was calculated as follows:

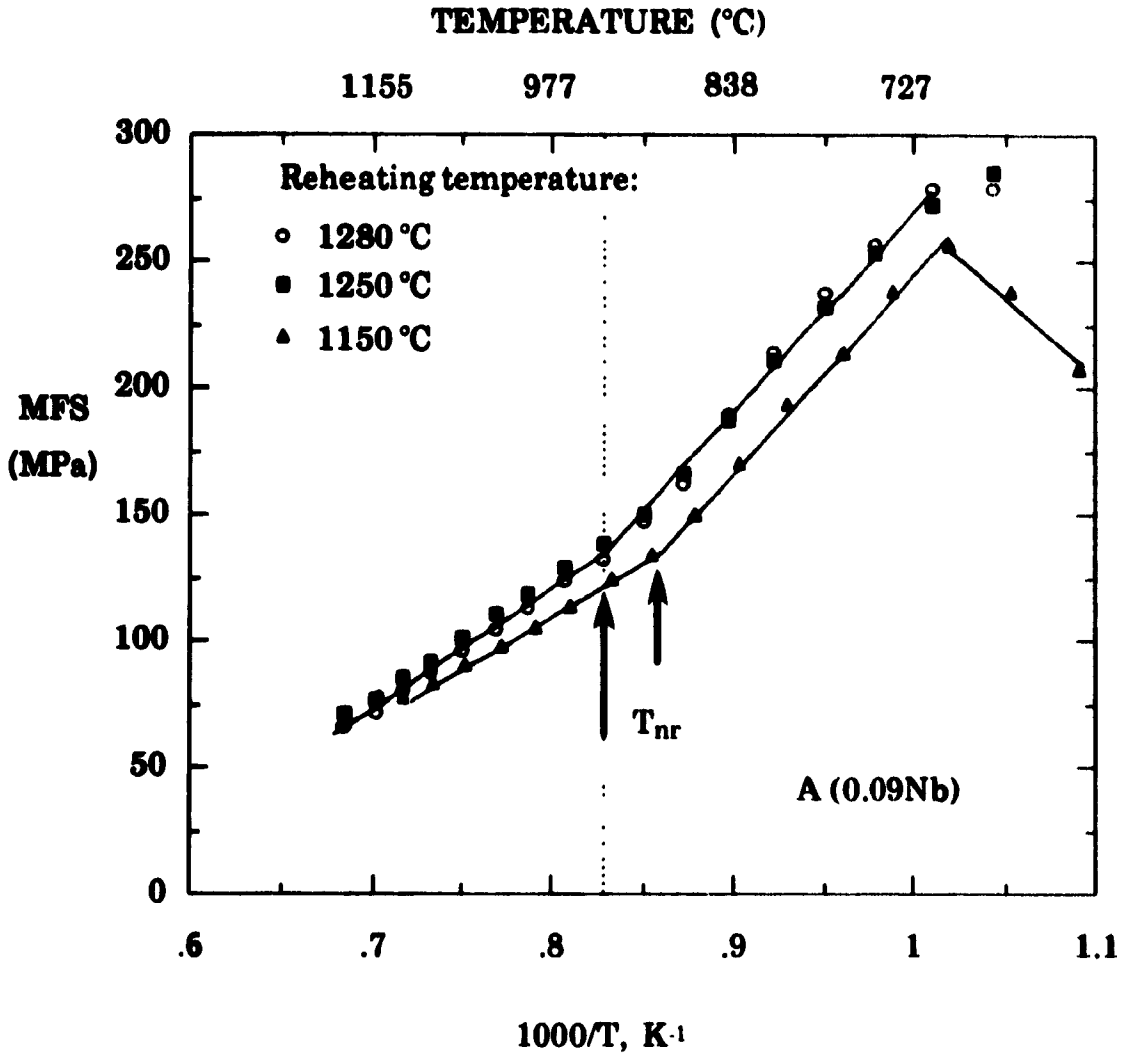


**Fig. 4.2** Dependence of the mean flow stress on inverse absolute pass temperature for samples deformed according to schedule A: pass strain $\varepsilon = 0.3$, strain rate $\dot{\varepsilon} = 2\ s^{-1}$, interpass time $t = 30$ s.

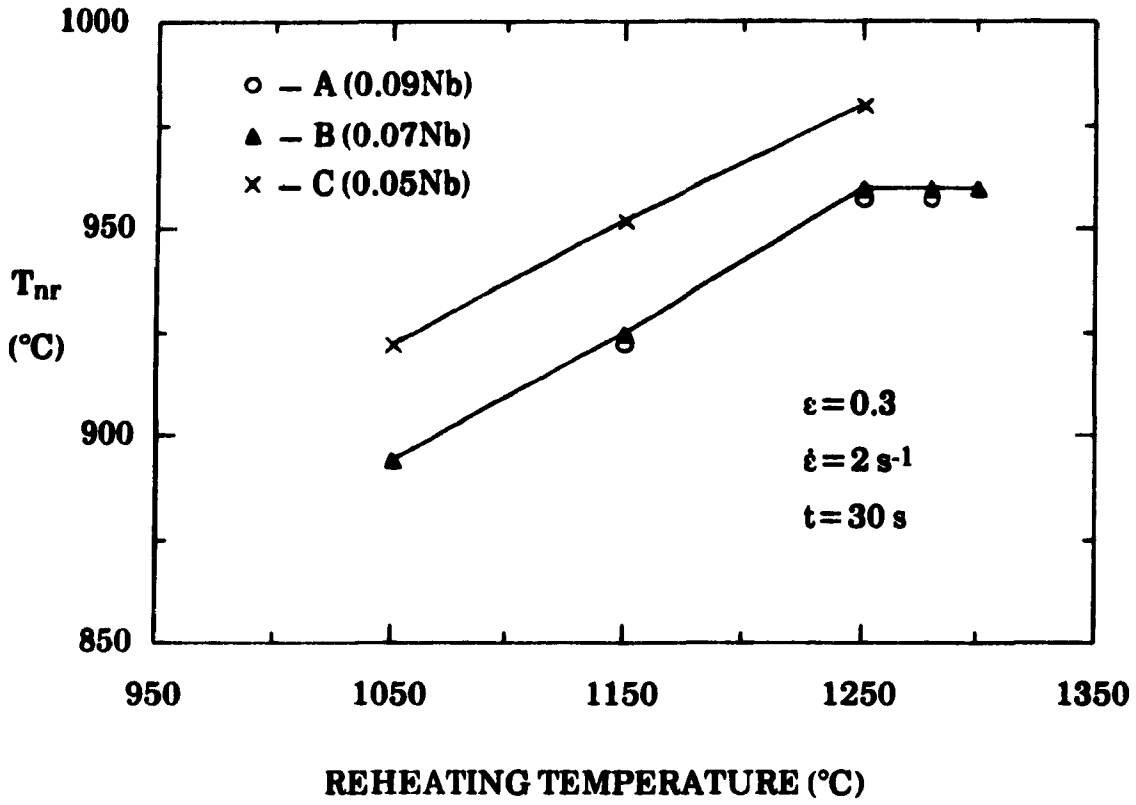


**Fig. 4.3 Dependence of the no-recrystallization temperature, $T_{nr}$ on reheating temperature.**

$$p[B]^{n+1} - r[B]^n - qk = 0 \qquad (4.1)$$

Equation (4.1) is soluble when $n=1$; once $[B]$ has been found, $[A]$ can be derived from the solubility product $k$:

$$[A] = \frac{k}{[B]^n} \qquad (4.2)$$

where $r$ is a constant, and $p$ and $q$ are the mass fractions of $A$ and $B$ in $AB_n$, respectively. The latter can be readily determined from the atomic weights $a_A$ and $a_B$ of elements $A$ and $B$. For a given alloy (p, q, and r fixed) at a given temperature ($k$ fixed), the values of $[A]$ and $[B]$ can be derived. Table 4.2 shows

the austenite compositions calculated using the Wadsworth et al. equations. In the present case, [*A*] and [*B*] in the Wadsworth et al. equations were replaced by [*Nb*] and [*C* + 12/14 *N*], respectively.

As shown in Table 4.2, the reheating temperature of 1250 °C is higher than the solution temperatures ($T_{sol}$) of all the steels; therefore all of the Nb(C,N) precipitates were expected to be dissolved in the austenite after 15 minutes of soaking at this temperature. For reheating temperatures of 1150 °C and 1050 °C, some of the Nb(C,N) remained undissolved, so that the Nb concentrations were lower in these materials. This led to lower niobium supersaturations under these conditions.

Table 4.2 Austenite composition at the reheat temperature

| Steel Type | Calculated Solution Temperature, °C | Austenitization Temperature, °C | Calculated Austenite Composition at Reheat Temperature, wt % | |
|---|---|---|---|---|
| | | | Nb | (C+12/14N) |
| A (0.09Nb) | 1187 | 1250 | 0.090 | 0.047 |
| | | 1150 | 0.071 | 0.045 |
| B (0.07Nb-0.026Ti) | 1153 | 1250 | 0.070 | 0.047 |
| | | 1150 | 0.068 | 0.047 |
| | | 1050 | 0.033 | 0.042 |
| C (0.05Nb) | 1240 | 1250 | 0.049 | 0.125 |
| | | 1150 | 0.027 | 0.119 |
| | | 1050 | 0.012 | 0.117 |

For the various solution temperatures, the solubility products were calculated using the solubility expression of Irvine et al.[32]. As demonstrated in equation 3.1, it is obvious that at a processing temperature of 960 °C, the niobium supersaturation can be maintained at a constant level by keeping the product [Nb][C + 12/14 N] at a constant value, where Nb, C, and N refer to the concentrations of these elements in solution in the austenite. The familiar solubility construction, shown in Fig. 4.4, is due to Wadsworth et al.[82]. The curves are solubility isotherms and represent the loci of possible austenite

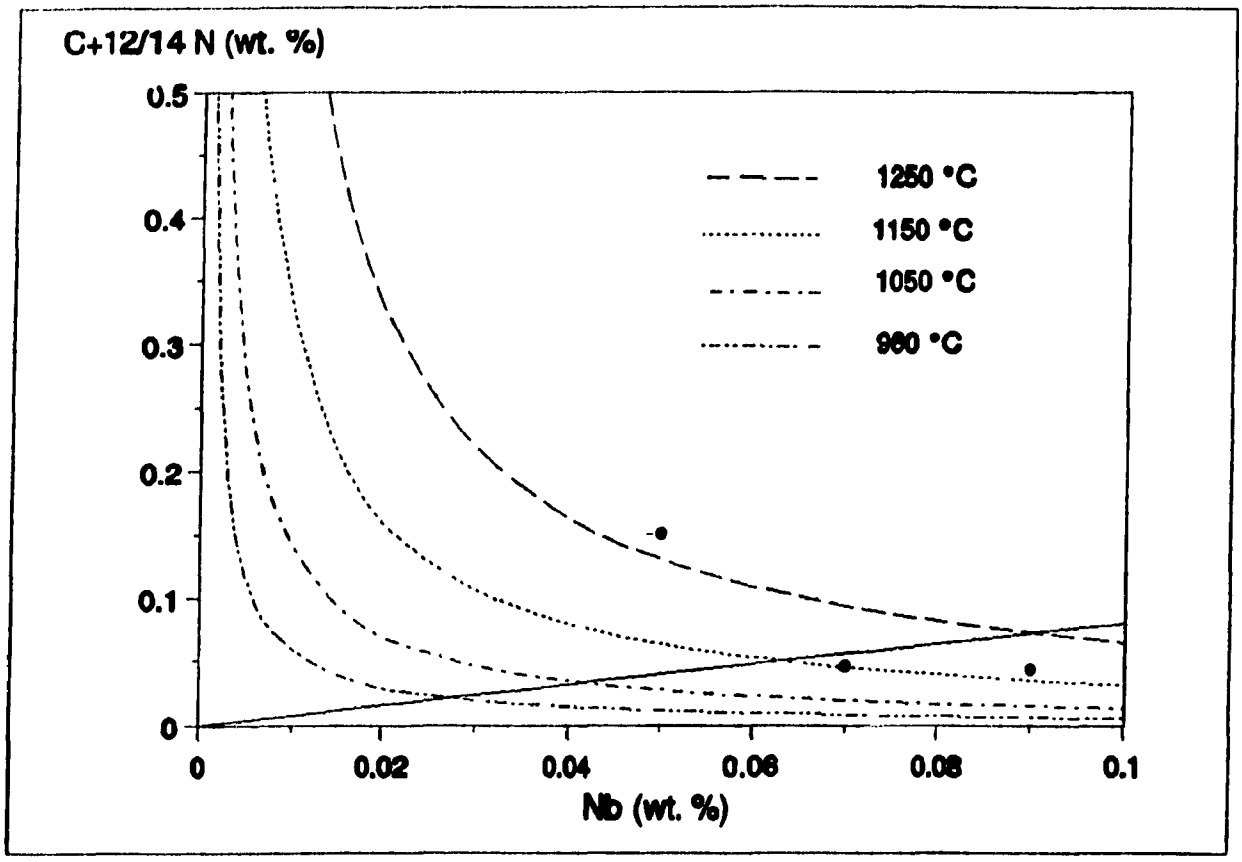


**Fig. 4.4 Nb(C,N) solubility plot. The compositions of the steels tested are shown as darkened circles.**

matrix compositions at various temperatures. The line with a slope of about 1/8 which begins at the origin represents the stoichiometric combinations of Nb and (C + 12/14 N) in the austenite; at all the points on this line, the number of niobium atoms is exactly equal to the total number of carbon and nitrogen atoms. The slope is approximately 1/8, because the atomic weight of Nb is about eight times greater than that of carbon. It can be seen that the product [Nb][C + 12/14 N] can be held at a constant value by lowering the carbon concentration while increasing the Nb concentration, or by increasing the carbon concentration while lowering the Nb concentration. Thus the

supersaturation ratio depends not only on the niobium concentration but also on the carbon concentration in solution.

The steel composition, and the austenite compositions in equilibrium with Nb(C,N) at various temperatures, lie on a common line which is parallel to the stoichiometric line. The graphical construction of Fig. 4.4 allows us to predict, knowing only the steel composition, the equilibrium austenite composition at any temperature (by the intersection of the appropriate solubility isotherm with a line drawn parallel to the stoichiometric line passing through the point representing the overall steel composition). At any temperature, the equilibrium precipitate volume fraction is proportional to the length of the line connecting the point which represents the overall steel composition to the point which represents the equilibrium austenite composition. The key result here is that, for a fixed supersaturation, as the steel composition approaches stoichiometry, there is an increase in the volume fraction of carbonitrides that can form at any temperature. Stoichiometric steel compositions allow the "maximum" amount of precipitation to occur at any temperature below the solution temperature because the correct proportions of Nb and C+N required to form Nb(C,N) are always present. Compositions away from stoichiometry are lacking in either Nb or C+N; this can lead to some Nb or C+N remaining as solute in the austenite.

The Nb and C+N concentrations of the experimental steels are plotted as full circles in Fig. 4.4. In addition, lines are drawn to indicate the amount of precipitation which can occur on going from a reheating temperature to a 960 °C processing temperature. From this diagram, it is evident that the higher the solution temperature, the higher the solubility product, and the higher the supersaturation ratio. The amounts of precipitate available at this temperature (960 °C) in the three Nb-steels are within a factor of 2~3.

The supersaturation ratios can also be calculated using the following equation:

$$k_s = \frac{[Nb][C + \frac{12}{14}N]_{soln}}{10^{2.26-6770/T}} \qquad (4.3)$$

The equilibrium volume fractions of Nb(C,N) available at 960 °C were calculated using the following equation given by Valdes and Sellars[79]

$$V_v \approx \frac{M_{Fe}(V_m)_{Nb(C,N)}}{100 M_{Nb}(V_m)_{Fe}}[Nb](1 - 1/k_s) \qquad (4.4)$$

Here $M_{Fe}$ and $M_{Nb}$ are the molar masses of iron and niobium, and $(V_m)_{Nb(C,N)}$ and $(V_m)_{Fe}$ are the molar volumes of Nb(C,N) and austenite. Following the above authors, $M_{Fe} = 56$, $M_{Nb} = 93$, $(V_m)_{Nb(C,N)} = 1.28 \times 10^{-5}$ and $(V_m)_{Fe} = 7.3 \times 10^{-6}$ $m^3 mol^{-1}$ were employed in the above equation.

The results obtained at 960 °C are listed in Table 4.3. It can be seen that the supersaturation ratios in steels A and B are lower than in steel C, even though the initial niobium concentrations in the former two steels are higher than in the latter one. This is because the supersaturation ratio depends not only on the niobium but also on the carbon content. The carbon content of steel C is much higher than those of steels A and B, which gives steel C a higher supersaturation ratio at a given temperature. Thus, it is expected that steel C will have a higher driving force for Nb(C,N) precipitation during subsequent deformation. Since the effect of solute drag is smaller than that of strain induced precipitation in the range of temperatures where strain induced precipitation can occur, it is understandable that the steel C $T_{nr}$'s are higher than those of steels A and B (see Table 4. 3). This is in agreement with the investigation carried out by Speer and Hansen[39]. In their work, they found that a lower carbon concentration results in faster austenite recrystallization due to a smaller carbonitride supersaturation, and thus a reduced precipitate nucleation rate. In the literature, Luton et al. also reported similar results [80].

**Table 4.3 Supersaturation ratios and volume fractions of Nb(C,N) at 960 °C**

| Steel Type | Austenitization Temperature, °C | Supersaturation Ratio at 960 °C | $V_v$ | $T_{nr}$, °C |
|---|---|---|---|---|
| A (0.09Nb) | 1250 | 7.2 | $0.82\times10^{-3}$ | 957 |
| | 1150 | 5.4 | $0.61\times10^{-3}$ | 922 |
| B (0.07Nb) | 1250 | 5.6 | $0.61\times10^{-3}$ | 960 |
| | 1150 | 5.4 | $0.59\times10^{-3}$ | 925 |
| | 1050 | 2.4 | $0.20\times10^{-3}$ | 894 |
| C (0.05Nb) | 1250 | 10.4 | $0.47\times10^{-3}$ | 980 |
| | 1150 | 5.4 | $0.23\times10^{-3}$ | 952 |
| | 1050 | 2.4 | $0.74\times10^{-4}$ | 922 |

The reheating temperatures of 1150 °C and 1050 °C are lower than the solution temperatures, so that some Nb(C,N) precipitates remain undissolved in the austenite. This weakens the precipitation retarding effect and also accelerates recrystallization because the large undissolved precipitates act as nucleation sites for recrystallization[34, 81-83]. The results in Fig. 4.3 demonstrate that the $T_{nr}$ decreases significantly with decreasing reheating temperature due to the lower supersaturation ratio and the lower volume fraction of precipitate available at the lower reheating temperatures. As listed in Table 4.3, for steel C (0.05Nb-0.125C), when the reheating temperature is decreased from 1250 °C to 1050 °C, the supersaturation ratio decreases from 10.4 to 2.4, and the volume fraction decreases from $0.47\times10^{-3}$ to $0.74\times10^{-4}$. This led to about a 60 °C decrease in the $T_{nr}$.

For a given temperature, the relationship between the time for 5% precipitation ($t_{0.05p}$) and the supersaturation ratio ($k_s$) can be derived from the quantitative model developed by Dutta and Sellars[63].

$$t_{0.05p} = A\, exp(\frac{B}{ln^2 k_s}) \qquad (4.5)$$

Here A and B are constants for a fixed composition, strain and Zener-Hollomon parameter. Fig. 4.5 shows the time for 5% precipitation at 960 °C as a function of the supersaturation ratios pertaining to different reheating temperatures for steel C. The times for 5% recrystallization ($t_{0.05x}$) and 95% recrystallization ($t_{0.95x}$) are also presented in the same figure for comparison. It can be seen that when $k_s$ is equal to 10.4 (for steel C reheated at 1250 °C), the $t_{0.05p}$ is greater than $t_{0.05x}$, but less than $t_{0.95x}$, which suggests that precipitation will take place after recrystallization has started but before recrystallization can be completed. This can shift the completion of recrystallization to longer times, or to higher temperatures. (In fact, the $T_{nr}$ in this case is 980 °C, 20 °C higher than the deformation temperature.) When $k_s$ is equal to 5.4 or 2.4 (for steel C reheated at 1150 and 1050 °C), $t_{0.05p}$ is higher than $t_{0.95x}$, so that recrystallization is complete before precipitation can take place (the relevant $T_{nr}$'s are 951 °C and 922 °C, respectively). It can be seen that for a reheating temperature of 1050 °C , the $t_{0.05p}$ value is about six orders of magnitude higher than the one for a reheating temperature of 1150 °C, even though the $k_s$ only changes from 5.4 to 2.4.

It was observed that in the cases of 1150 °C and 1050 °C, the $T_{nr}$'s of steel C are still higher than those of steels A and B. This behavior cannot be explained in terms of precipitate supersaturation or volume fraction effects. This is because: (1) the supersaturation was approximately the same for these three steels when the same reheating temperatures of 1150 °C and 1050 °C were used; (2) the estimated precipitate volume fractions were slightly higher in steels A and B than in steel C. Here the reason may be related to differences in the precipitate coarsening kinetics. In steels A and B, some Ti is present, especially in steel B, where the concentration of Ti is 0.026%. As reported in the literature, TiN is very stable and can be retained at very high temperatures (at least 1300 °C). The reheating temperatures of 1150 °C and 1050 °C cannot dissolve all of the TiN, so that some TiN particles are expected

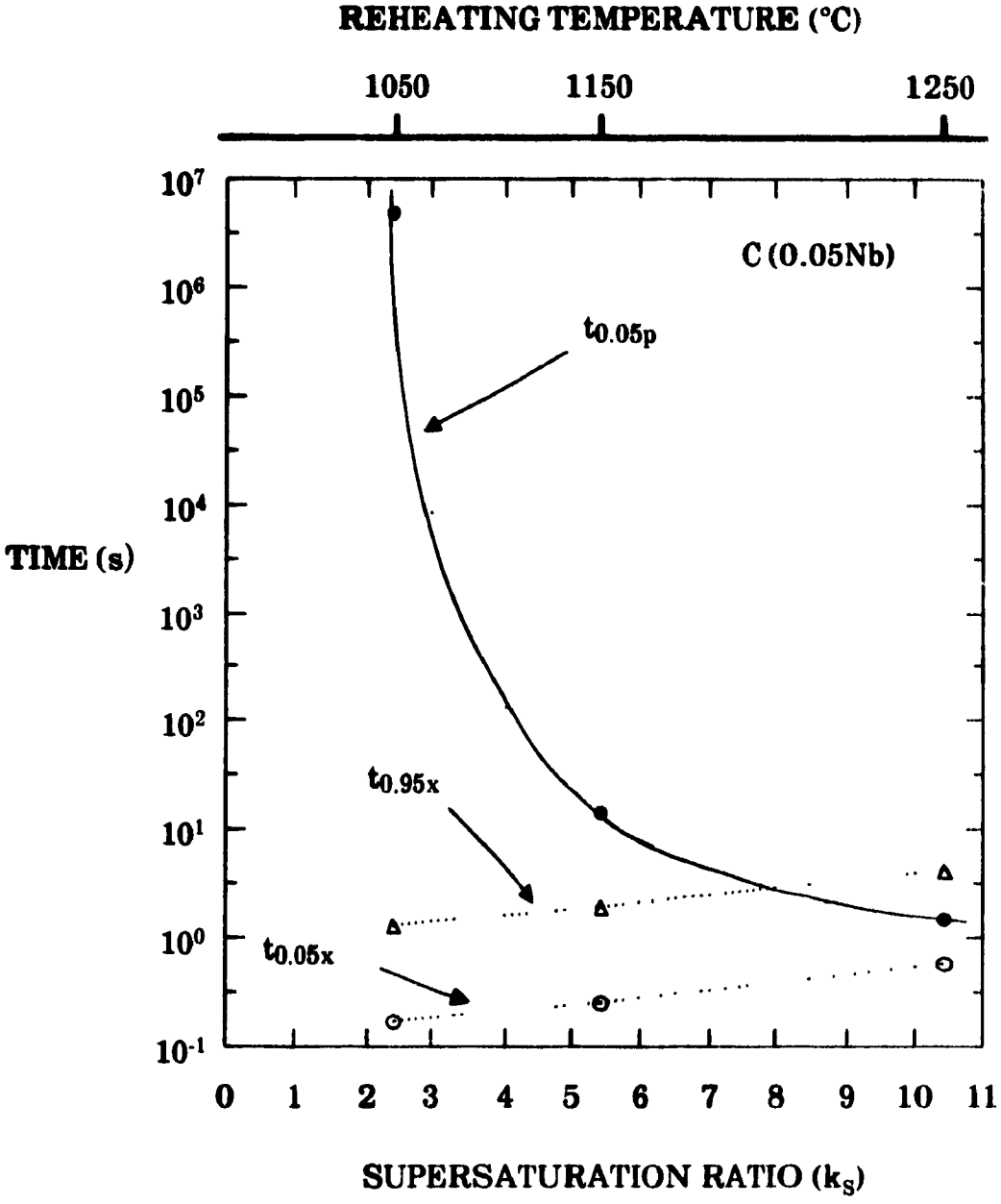


**Fig. 4.5 Dependence of $t_{0.05p}$ on the supersaturation ratio ($k_S$).**

to be undissolved. Two specimens were reheated to 1250 °C and 1050 °C, soaked at these temperatures for 15 minutes, and then quenched. The TEM micrographs of these specimens shown in Fig. 4.6 demonstrate that there are less undissolved particles in the higher temperature than in the lower temperature case. These large undissolved particles can act as nucleation sites

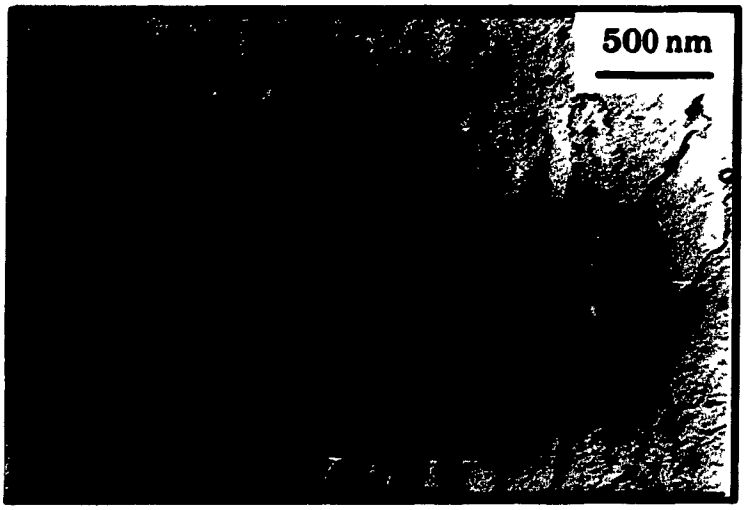


(a) 1250 °C


(b) 1050 °C

Fig. 4.6 Carbon extraction replicas showing the effect of reheating temperature on Nb(C,N) precipitation.

for recrystallization, thereby increasing the recrystallization rate. On the other hand, the large particles can also act as nucleation sites for the subsequent precipitation of Nb(C,N)[84, 85]; this would promote precipitate coarsening instead of the formation of more fine precipitates. This phenomenon therefore also accelerates recrystallization.

### 4.2.2 INITIAL AUSTENITE GRAIN SIZE

Actually, different reheating temperatures lead to different initial austenite grain sizes. The lower the reheating temperature, the smaller the initial grain size will be. One may think that the decrease in $T_{nr}$ associated with lower reheating temperatures not only results from lower supersaturation ratios but also from smaller initial austenite grain sizes. This is not surprising because there is considerable evidence in the literature indicating that the initial grain size has a strong effect on the recrystallization kinetics. It is worthy of note that most of these publications were single pass deformation experiments. For multipass deformation, the situation could be different. To check this out, the following tests were done using steel B.

Prestrains ranging from 0.07 to 1.2 were given prior to executing schedule A. The aim of this treatment was to produce different initial austenite grain sizes. A prestrain of 0.07 at 1250 °C led to grain coarsening and gave a very large initial grain size (~150 μm). Prestrains of 0.3, 0.6, 0.9 and 1.2 were applied at 1210 °C for different tests, and the specimens were then cooled to the regular test temperature (1180 °C). It can be seen that large prestrains led to finer initial grain sizes. Prestrains of 0.3 and 0.6 refined the as-reheated grain size by static recrystallization to 58 μm and 50 μm respectively. Prestrains of 0.9 and 1.2 can initiate dynamic recrystallization, which led to a finer initial grain size of about 40 μm. It can be seen that the initial grain size ranged from 150 μm to 40 μm, which should have led to a significant change in the $T_{nr}$. The results presented in Fig. 4.7, however, show almost the same value of $T_{nr}$ for specimens with different initial grain sizes. This implies that the initial grain size has no effect on the $T_{nr}$. The explanation for this observation can be that, as a result of repeated recrystallization, there is a rapid convergence of initially dissimilar grain sizes

to nearly the same grain size. This will be demonstrated later using a plain carbon steel.

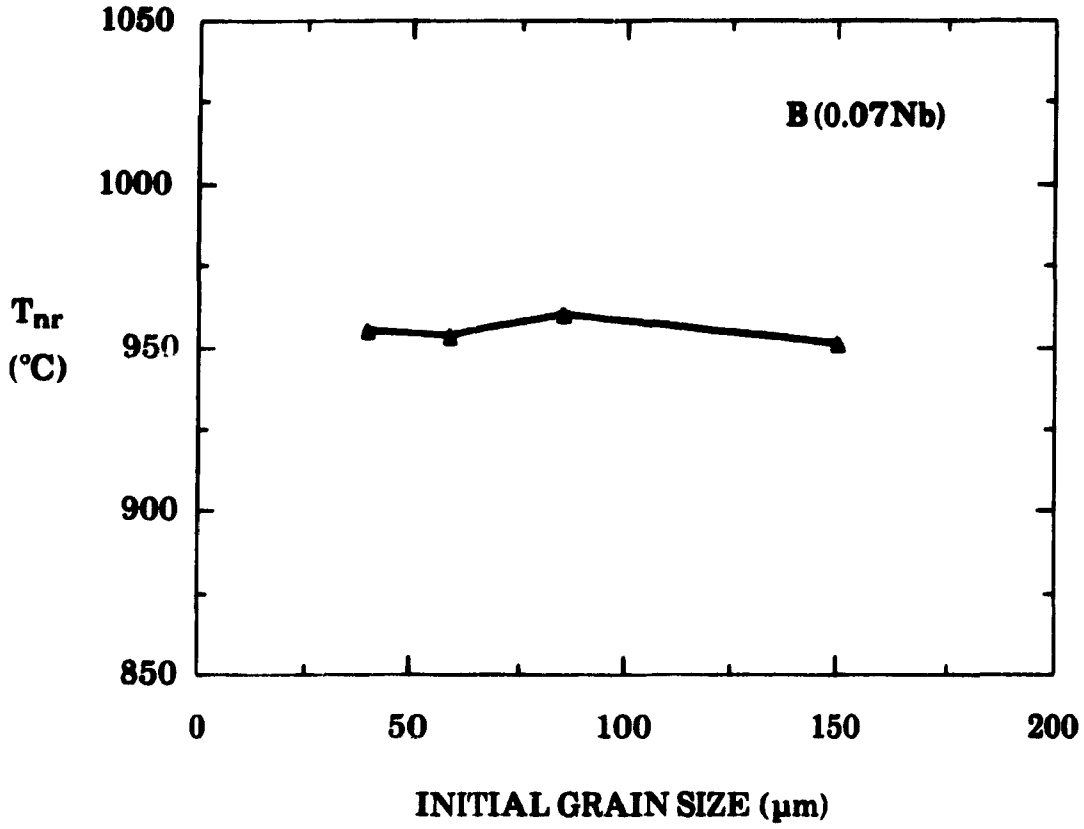


Fig. 4.7 Dependence of the no-recrystallization temperature, $T_{nr}$, on the initial grain size (strain rate $\dot{\varepsilon}=2\ s^{-1}$, interpass time = 30 s).

Fig. 4.8 shows the microstructure evolution predicted using the following equation given by Sellars[19]:

$$d_{rex}=Dd_0^{0.67}\varepsilon^{-0.67} \qquad \varepsilon<\varepsilon^* \qquad (4.6)$$

Here, $d_0$ is the initial grain size of the austenite, $\varepsilon$ is the pass strain, and D is a constant for which the value D = 0.9 was adopted for the present computation. It can be seen that after the 4th pass, the predicted grain sizes for dissimilar initial grain sizes are almost the same. Further deformation no longer

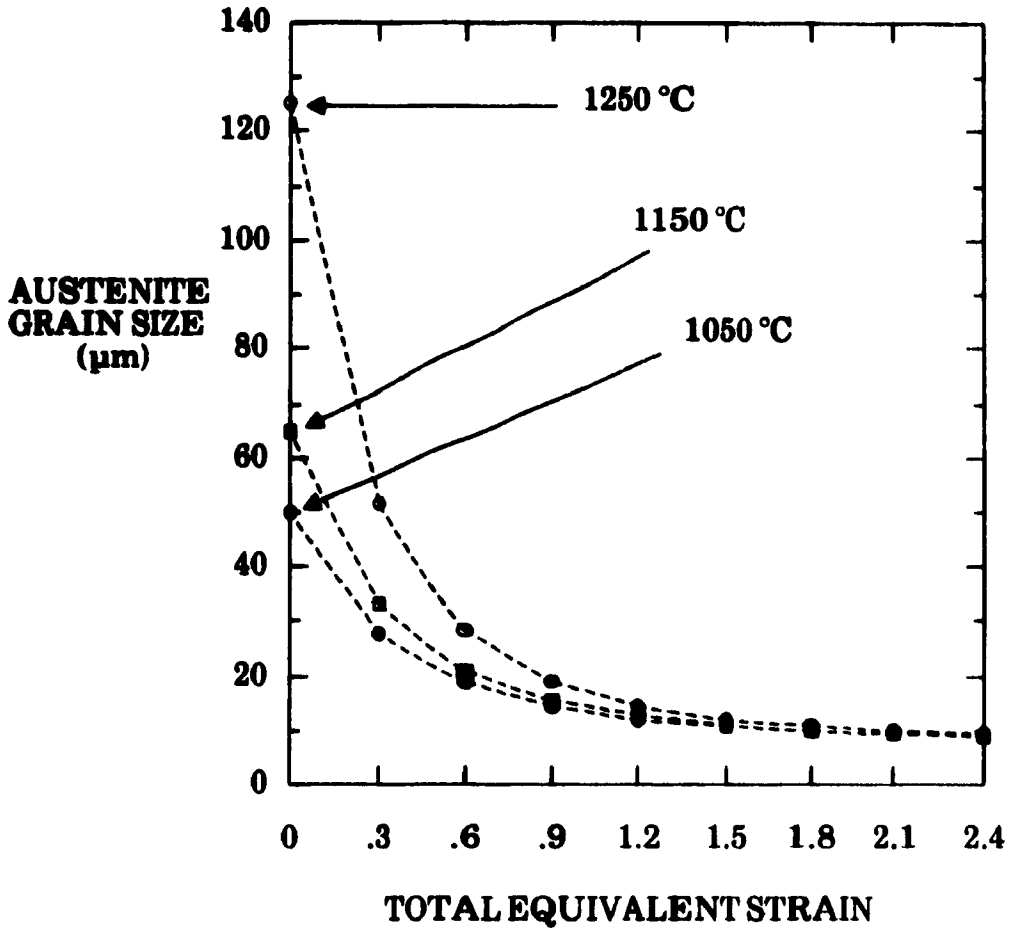


**Fig. 4.8** **Evolution of the recrystallized grain size in the 0.07Nb steel during multipass rolling with pass equivalent strains of 0.3, calculated from the relationship for the recrystallized grain size[19].**

changes the grain size, which means that from the 5th pass (at 1060 °C) to the 7th pass (at 1000 °C), the grain size remains at a constant value. The temperature at which recrystallization can be completed is around 1000 °C for the present steel; therefore, the same final grain sizes were obtained before recrystallization ceased even if the initial grain size was dissimilar. Thus the effects of the initially dissimilar grain sizes were eliminated by the successive recrystallizations. A similar observation was reported by Cuddy[51 52]; in his work, the degree of recrystallization during the interpass delay was

determined by metallography. Roberts also pointed out the rather weak dependence of statically recrystallized grain size ($d_{rex}$) on pre-existing grain size ($d_0$) during multipass deformation[86].

### 4.2.3 GRAIN REFINEMENT OF AUSTENITE DURING MULTIPASS DEFORMATION

In order to further test the explanations provided above, it was necessary to check the metallography. The problem for steels A and B was the low carbon content, which led to low hardenability, and to difficulty in revealing the austenite grain boundaries. Steel C had a higher carbon content, but the number of specimens was limited. A plain carbon steel was therefore used to check the evolution of the microstructure during multipass deformation. A schedule with four passes, strains of 0.4/pass, a strain rate of 2/s, and interpass times of 30 s, was designed for this purpose.

Reheating temperatures of 1200 °C and 950 °C were used to produce dissimilar initial grain sizes. In the first case, specimens were reheated to 1200 °C and soaked at this temperature for 30 minutes, then cooled to test temperature (950 °C) at a cooling rate of about 1 °C/s. This gave an initial grain size of 375 μm. In the second case, a reheat temperature of 950 °C and 10 minutes soaking gave an initial grain size of 30 μm.

Fig. 4.9 shows the evolution of grain size during multipass deformation. It can be seen that 1) the mean grain sizes converge to the same value after the 4th pass, even though the initial grain sizes were quite different (375 μm and 30 μm); 2) in the first case, the grain size was refined significantly after the first two passes, while in the second case, the grain size did not change after the first three passes; however, at the 4th pass, the grain size decreased slightly (from 30 μm to 25 μm). The question raised here is why the grain size decreases more quickly with a large initial grain size than with a small initial grain size. It seems there is a limitation to the effectiveness of grain refinement by static recrystallization. Reportedly, the limit of grain size obtainable by static recrystallization is about 15 μm. Priestner et al. suggested that coarse-grained austenite recrystallizes to finer grain sizes until

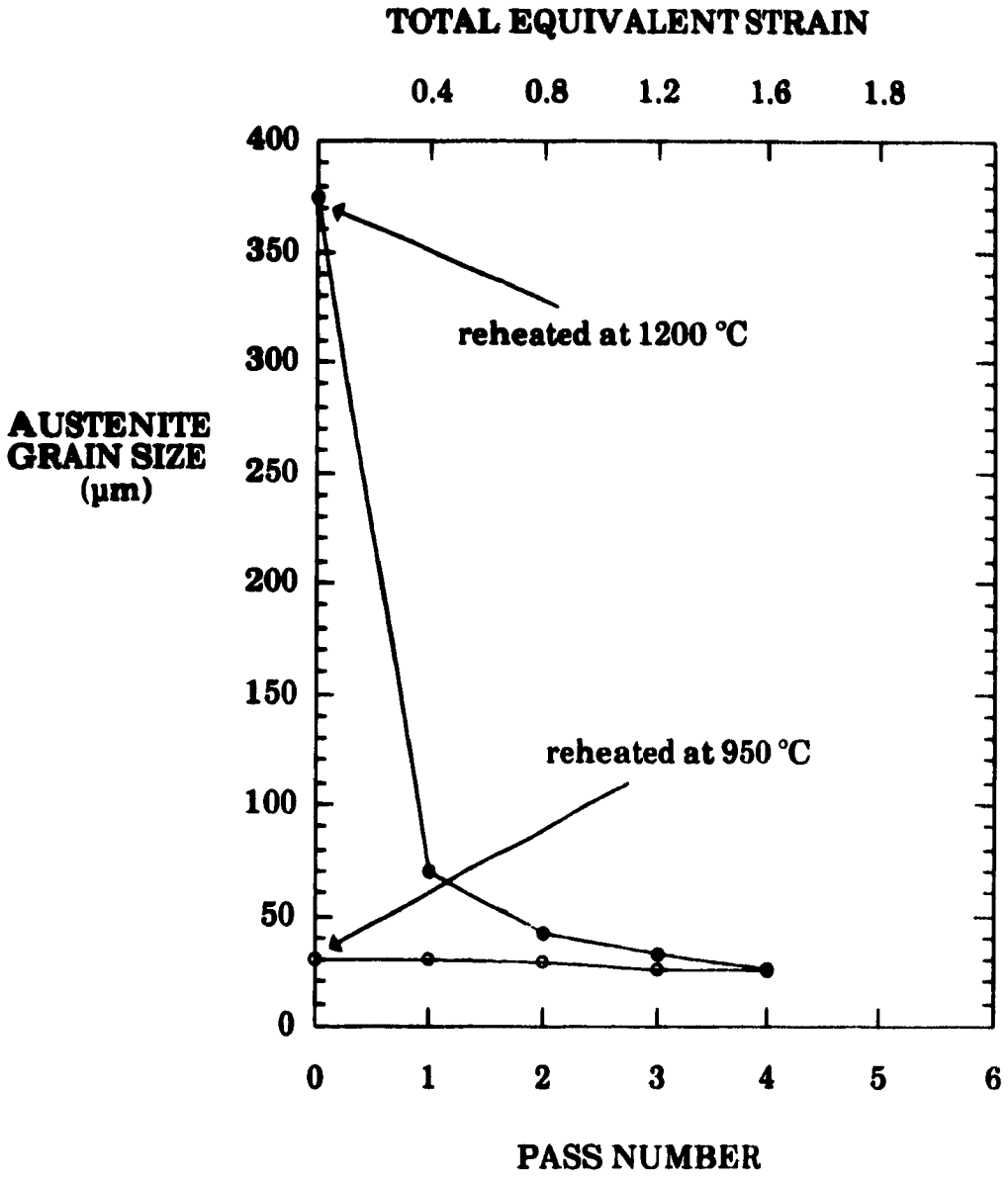


**Fig. 4.9** Evolution of the recrystallized grain size of the PC steel during multipass rolling with pass equivalent strains of 0.4/pass, a strain rate of 2/s, and interpass times of 30 s.

a limiting size is reached, at which it appears that recrystallization produces no further refinement[87]. In the second case, it is difficult to believe that recrystallization is actually stopped, since both the stress-strain curves and the microstructures show that recrystallization takes place after every pass.

Thus recrystallization continues to produce the same (limiting) grain size. Further grain refinement was obtained by dynamic recrystallization.

### 4.2.4 DEFORMATION PATTERNS

As described above, grain refinement is faster with a coarse initial grain size than with a fine initial grain size. This phenomenon cannot be explained using boundary nucleation theory since small grains provide more nucleation sites for recrystallization than large grains. One can consider instead the role of deformation mechanisms such as crystallographic slip, boundary migration, boundary sliding, and recovery. The deformation mechanisms (or deformation patterns) for large grains and small grains are different. To study the recrystallization behavior of deformed austenite, it is important to know the deformation mechanisms pertaining to some extreme situations. The following possible deformation patterns are discussed here to explain the effect of recrystallization on grain refinement.

#### 4.2.4.1 Deformation of Large Grains

In this pattern, crystallographic slip and dislocation multiplication play important roles. The grains are elongated by deformation as long as dynamic recrystallization is not initiated. The elongated grains have a higher density of nucleation sites (both inside the grains and at grain boundaries). Rhines et al. suggested that the ease of deformation of individual grains is in proportion to their volume-to-surface ratios. Where the ratio is high, as in the case of the large grains, the resistance to deformation may be expected to be low[88].

#### 4.2.4.2 Deformation of Mixed Structures

In the case of mixed structures, the large grains have a low resistance to deformation because of their high volume-to-surface ratios, while the small grains have a higher resistance to deformation because of their low volume-to-surface ratios. At the beginning of deformation, the large grains deform more,

while the small grains deform less. There is also intragranular deformation in the large grains and intergranular deformation near the small grains. This kind of inhomogeneous deformation will lead to the retention of the mixed structures.

#### 4.2.4.3 Deformation of Small Grains

For a fine, uniform structure, the resistance to intragranular deformation is expected to be high, so that intergranular deformation, such as boundary sliding, becomes more important. The increase in grain boundary area produced by this mechanism is lower than with straight grain elongation; also there is less chance for nucleation inside the grains, so that the density of nucleation sites for recrystallization is lower. This may explain the above observations for the lower reheat temperature case, in which there is little change of grain size during continuing deformation.

For the Nb-bearing steels, the situation becomes more complicated because of the introduction of Nb(C,N) precipitates. Precipitates in the matrix will strengthen the austenite against crystallographic slip, while precipitates on grain boundaries will retard boundary sliding. That is partly why the $T_{nr}$ for Nb-bearing steels is much higher than for plain carbon steels.

## 4.3 EFFECT OF MICROALLOY ADDITIONS

In the present study, three Nb-bearing steels, one Ti bearing steel, and one V bearing steel were used to investigate the effect of microalloying elements on the no-recrystallization temperature. Fig. 4.10 shows the mean flow stress vs 1000/T curves of Nb steel A, the 0.1V-0.02Ti steel, and the plain carbon steel. It can be seen that the mean flow stress of the plain carbon steel is only a function of temperature, and increases linearly with decreasing temperature over the whole austenite range. This suggests that there was no strain accumulation in this material, and that full recrystallization took place between passes. For the Nb-bearing steel, however, the slope of the mean flow stress curve changed at around 960 °C. As mentioned in Chapter 3, this

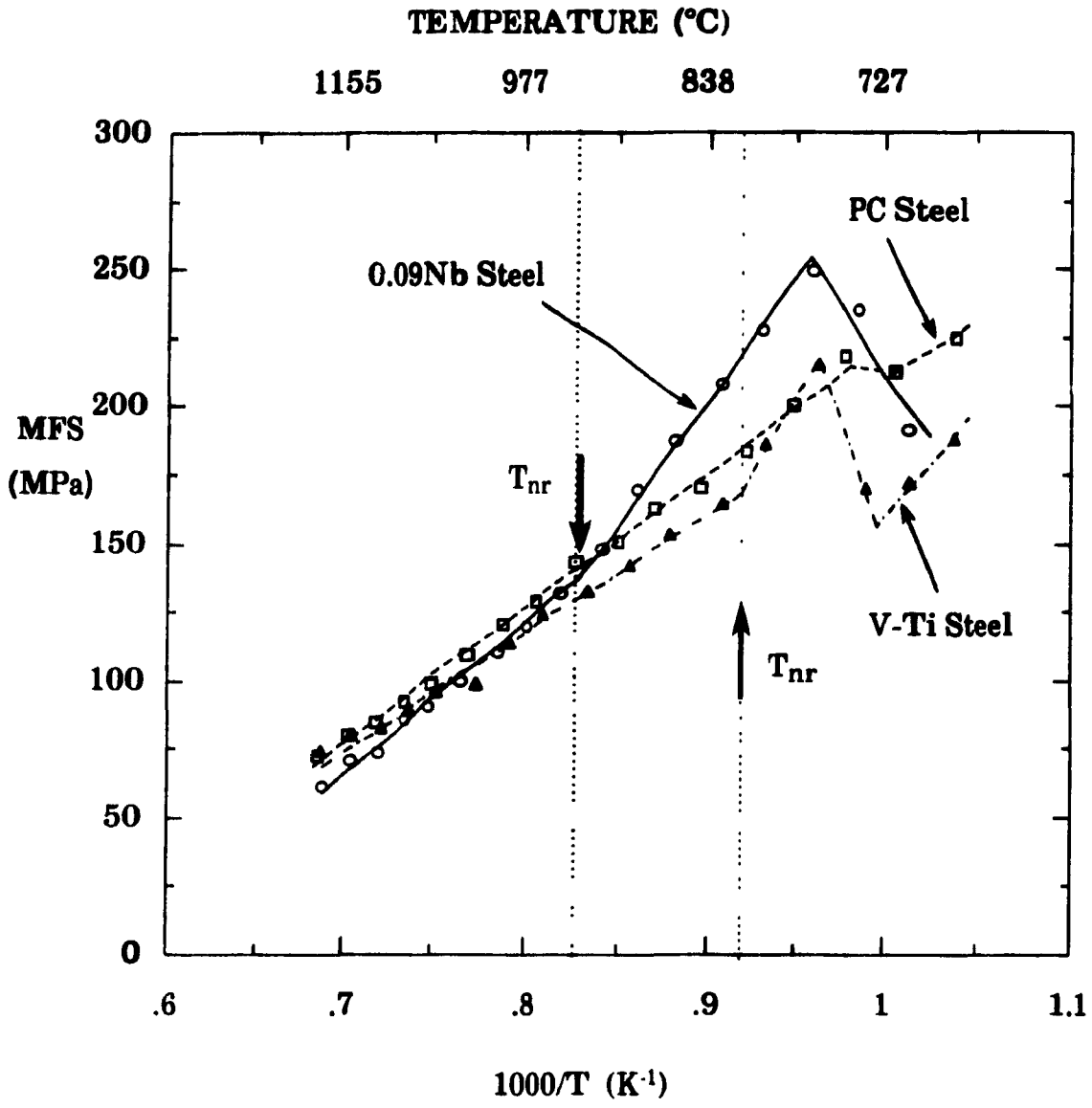


Fig. 4.10 Dependence of the mean flow stress on inverse absolute pass temperature for samples deformed according to schedule A: pass strain $\varepsilon = 0.3$, strain rate $\dot{\varepsilon} = 2\ s^{-1}$, interpass time $t = 30$ s, reheating temperature $T_A = 1250$ °C.

temperature is defined as the no-recrystallization temperature under the present deformation conditions. Compared with the Nb-bearing steel, the Ti-bearing steel has a lower $T_{nr}$, which is about 840 °C.

Fig. 4.11 shows the measured $T_{nr}$ for all of the investigated materials. It can be seen that among these steels, the Nb-bearing grades have the highest $T_{nr}$'s, while the V-bearing one has the lowest $T_{nr}$. The $T_{nr}$ for the Ti-bearing steel is lower than in the Nb-bearing grades, but much higher than in the V-bearing steel, even though the Ti content of 0.16Ti is approximately twice the Nb content of the Nb-bearing steels. As reviewed in Chapter 2, Cuddy summarized the effect of solutes on the $T_{RS}$ (recrystallization stop temperature) in terms of the atomic percent of solute X according to the equation $\Delta T_{RS}=\alpha X^{1/2}$. For the Nb-bearing steel, the $\alpha$ value can be as high as 1350. For the Ti-bearing steel, the $\alpha$ value is around 410; for the V-bearing steel, however, the $\alpha$ value is only 200 [52]. From the Boratto-Yue empirical equation [60, 61], each 0.01 percentage change of Nb concentration will lead to a 50 °C change in the $T_{nr}$, each 0.01 percentage change in the Ti level will lead to a 9 °C change in the $T_{nr}$, while there is only a 4 °C change for each 0.01% V content change. It is obvious that Nb is the most effective element in retarding the recrystallization of austenite, while V is the least effective. The order of effectiveness of the microalloying elements with respect to the retardation of recrystallization is Nb, Ti, and V.

It has been known that a solute in solution has a retarding effect on the recrystallization of austenite, but that the major retardation of recrystallization is attributable to strain induced precipitation. For the Nb-bearing steels, relatively high supersaturations in the lower austenite temperature range lead to rapid niobium carbonitride formation; thus the retarding effect of precipitation is more effective, and the $T_{nr}$ can be higher. The relatively low supersaturation of vanadium, on the other hand, leads to a weaker retarding effect on recrystallization, thus resulting in the lowest $T_{nr}$.

## 4.4 EFFECT OF DEFORMATION PARAMETERS

### 4.4.1 EFFECT OF STRAIN

In order to understand the effect of deformation on the $T_{nr}$, the MFS (mean flow stress) vs. 1000/T curves are presented in Fig. 4.12 for specimens tested with pass strains of 0.1, 0.3, 0.4 and 0.5. For these tests, the strain rate

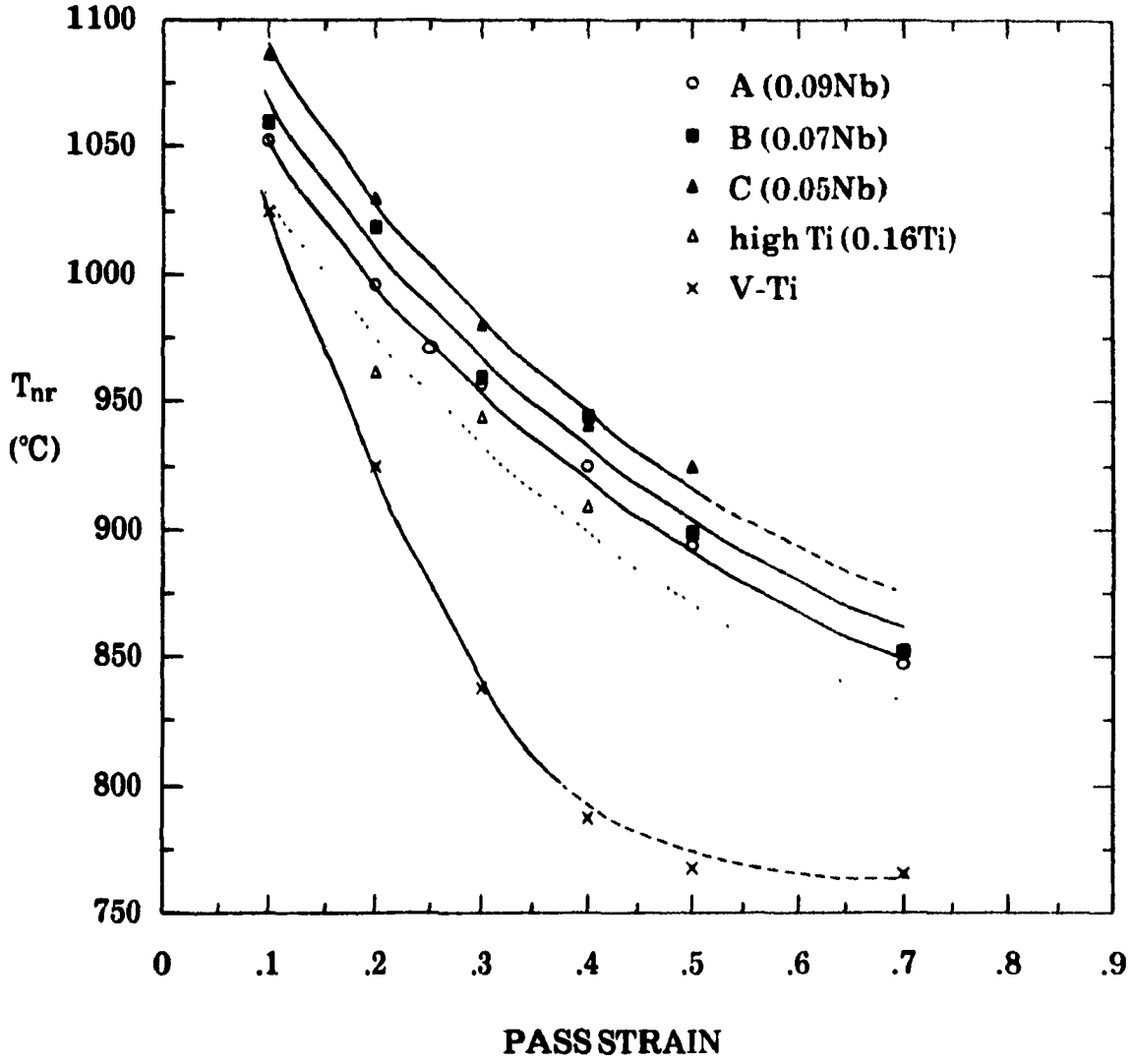


**Fig. 4.11 Dependence of the $T_{nr}$ on pass strain ($\dot{\varepsilon}=2\ s^{-1}$, $t=30$ s).**

and interpass time were held constant at $\dot{\varepsilon}=2\ s^{-1}$ and $t=30$ s. It can be seen from the figure that the mean flow stress increases with increasing pass strain, and that the mean flow stress slope change occurs at higher temperatures when the pass strain is reduced. This indicates that the $T_{nr}$ decreases with increasing pass strain. Fig. 4.13 demonstrates the dependence of the $T_{nr}$ on pass strain for the three Nb-bearing steels. This dependence can be described by the following relationship:

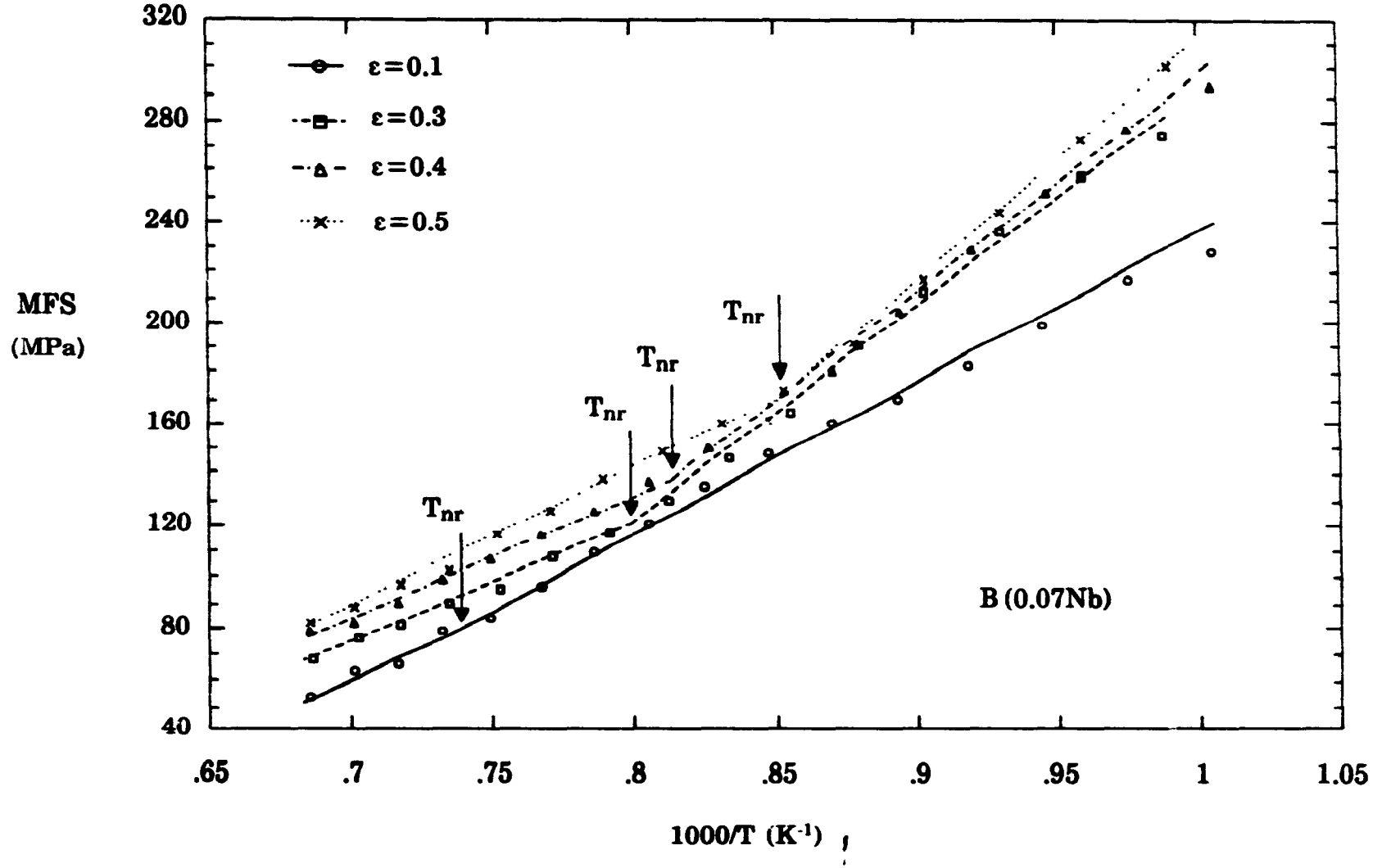


Fig. 4.12 **Dependence of the mean flow stress (MFS) on inverse absolute pass temperature for samples deformed according to schedule A; $\dot{\varepsilon} = 2\ s^{-1}$, $t = 30\ s$.**

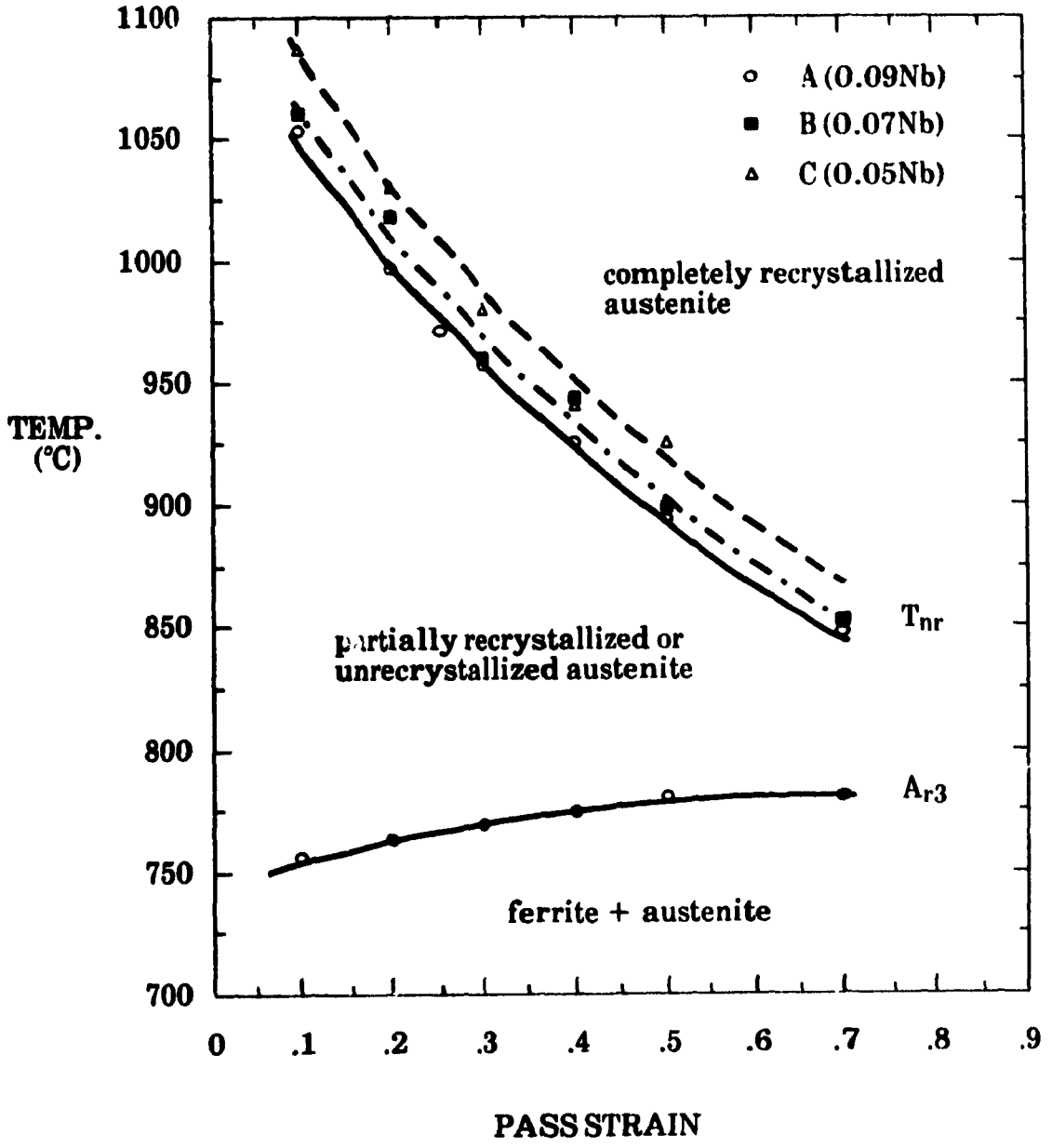


**Fig. 4.13** Dependence of the $T_{nr}$ and $A_{r3}$ on pass strain (strain rate $\dot{\varepsilon} = 2$ $s^{-1}$, interpass time = 30 s).

$$T_{nr}=\zeta exp(-0.36\varepsilon) \qquad (4.7)$$

where $\zeta$ is 1078, 1088 and 1103 for steels A, B and C, respectively. It can be seen that even a small change in pass strain leads to a significant change in the $T_{nr}$. When the strain is increased from 0.1 to 0.7, for instance, the $T_{nr}$ in steel B decreases from 1060 °C to 850 °C. This is consistent with the results of Cuddy et al.[89], who found that recrystallization is incomplete at about 1075 °C at pass strains of 0.04~0.13, while the temperature for complete recrystallization can be low as 925 °C when the pass strain is increased to 0.2~0.48.

Such a dramatic decrease in the $T_{nr}$ with increasing pass strain can be due to several contributing factors:

1) Grain refinement. When the pass strain is increased, finer grain sizes are produced by static recrystallization. Such fine structures supply more nucleation sites for subsequent recrystallization and also soften more quickly.

2) Increased dislocation density. When the pass strain is increased, higher dislocation densities are generated, which also promote more rapid recrystallization. When a fixed interpass time is used, this makes it possible for recrystallization to go to completion at lower temperatures.

3) Precipitate coarsening. When the pass strain is increased, the density of dislocations increases, which leads to more rapid coarsening of the precipitates [90]. These coarsened particles lose their effectiveness in retarding recrystallization, and thus allow recrystallization to continue to take place at lower temperatures.

The TEM micrographs shown in Fig. 4.14 show the effect of increasing the pass strain on precipitate coarsening. The upper micrograph was obtained

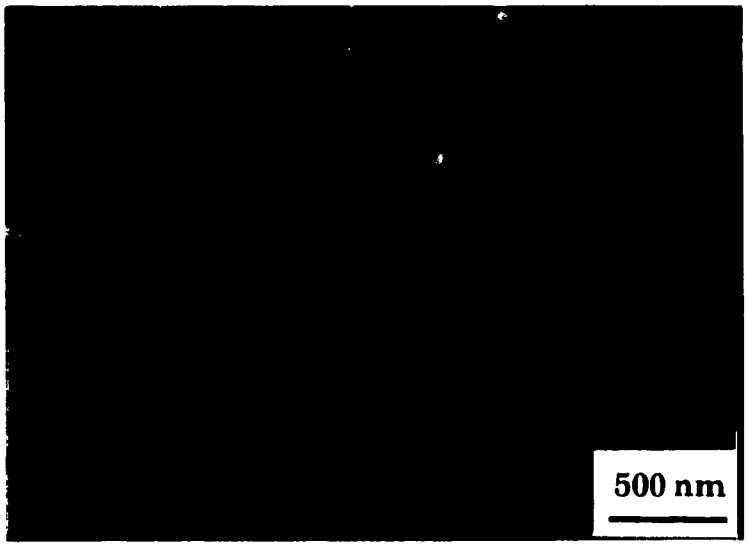


(a) $\varepsilon = 0.3$/pass


(a) $\varepsilon = 0.7$/pass

**Fig. 4.14** Carbon extraction replicas showing the influence of deformation on precipitate size. (a) quenched at 972 °C; (b) quenched at 860 °C.

from a specimen deformed using pass strains of 0.3 and quenched at 972 °C (near the $T_{nr}$ for this strain), while the lower micrograph represents a specimen deformed using pass strains of 0.7 and quenched at 860 °C (near the $T_{nr}$ for the increased strain). The mean particle size in the latter case (about 110 nm) is considerably larger than in the former case (about 25 nm); these large particles are less effective in retarding recrystallization. Similar observations of precipitate coarsening during hot deformation have been reported by Weiss and Jonas [91], and Speer and Hansen [39].

Based on the Dutta and Sellars recrystallization and precipitation models, the $T_{nr}$ can be approximately determined from the point of intersection between the $t_{0.05p}$ (time for 5% precipitation) curve and the $t_{0.95x}$ (time for 95% recrystallization) curve. The $t_{0.05p}$ and $t_{0.95x}$ times were calculated as follows,

$$t_{0.05p}=3\times10^{-6}[Nb]^{-1}\varepsilon^{-1}Z^{-0.5}\times exp\frac{270000}{RT}\,exp\frac{2.5\times10^{10}}{T^3(ln\,ks)^2} \qquad (4.8a)$$

or

$$t_{0.05p}=A\,\varepsilon^{-1} \qquad (4.8b)$$

where

$$A=3\times10^{-6}[Nb]^{-1}Z^{-0.5}\times exp\frac{270000}{RT}\,exp\frac{2.5\times10^{10}}{T^3(ln\,ks)^2} \qquad (4.8c)$$

$$t_{0.05x}=6.75\times10^{-20}d_0^2\,\varepsilon^{-4}\times exp\frac{300000}{RT}\,exp\{(\frac{2.75\times10^5}{T}-185)[Nb]\} \qquad (4.9a)$$

$$t_{0.95x}=Ct_{0.05x} \qquad (4.9b)$$

where $t_{0.05x}$ is the time for 5% recrystallization, Z is the Zener-Hollomon parameter, R is the universal gas constant, and $k_s$ is the supersaturation ratio, which can be determined using equation 4.3. C is a constant and can be derived from the Avrami equation using an exponent n = 2:

$$X = 1 - exp(-\alpha t^n) \tag{4.10a}$$

$$t = -\frac{(ln(1-X))^{\frac{1}{n}}}{\alpha^{\frac{1}{n}}} \tag{4.10b}$$

then
$$C = \frac{t_{0.95x}}{t_{0.05x}} = \left[\frac{ln(1-0.95)}{ln(1-0.05)}\right]^{\frac{1}{n}} \tag{4.10c}$$

$$t_{0.95x} = Ct_{0.05x} = 7.66\, t_{0.05x} \tag{4.11}$$

or
$$t_{0.95x} = B\varepsilon^{-4} \tag{4.12a}$$

where $$B = 7.64 \times 6.75 \times 10^{-20} d_0^2 \times exp\frac{300000}{RT}\, exp\{(\frac{2.75 \times 10^5}{T} - 185)[Nb]\} \tag{4.12b}$$

The dependences of $t_{0.05p}$, $t_{0.05x}$ and $t_{0.95x}$ on strain at a deformation temperature of 960 °C and a strain rate of 2 $s^{-1}$ are illustrated in Fig. 4.15 for steel A.

It can be seen that the $t_{0.05p}$ curve intersects the $t_{0.05x}$ and $t_{0.95x}$ curves at $\varepsilon_1 = 0.27$ and $\varepsilon_2 = 0.43$, respectively. Thus, for values of $\varepsilon < 0.27$, precipitation is initiated prior to recrystallization, and $t_{0.05x}$ and $t_{0.95x}$ are shifted to longer times (as indicated by the broken curves). Between strains of 0.27 and 0.43, $t_{0.05p}$ is larger than $t_{0.05x}$ but smaller than $t_{0.95x}$, which means that recrystallization begins before precipitation, although its completion will be delayed by precipitation, which is initiated later. Furthermore, when $\varepsilon > 0.43$, $t_{0.05p}$ is larger than both $t_{0.05x}$ and $t_{0.95x}$; therefore recrystallization is completed before precipitation can be initiated. This then delays precipitation to longer times because of the decrease in the dislocation density. In other

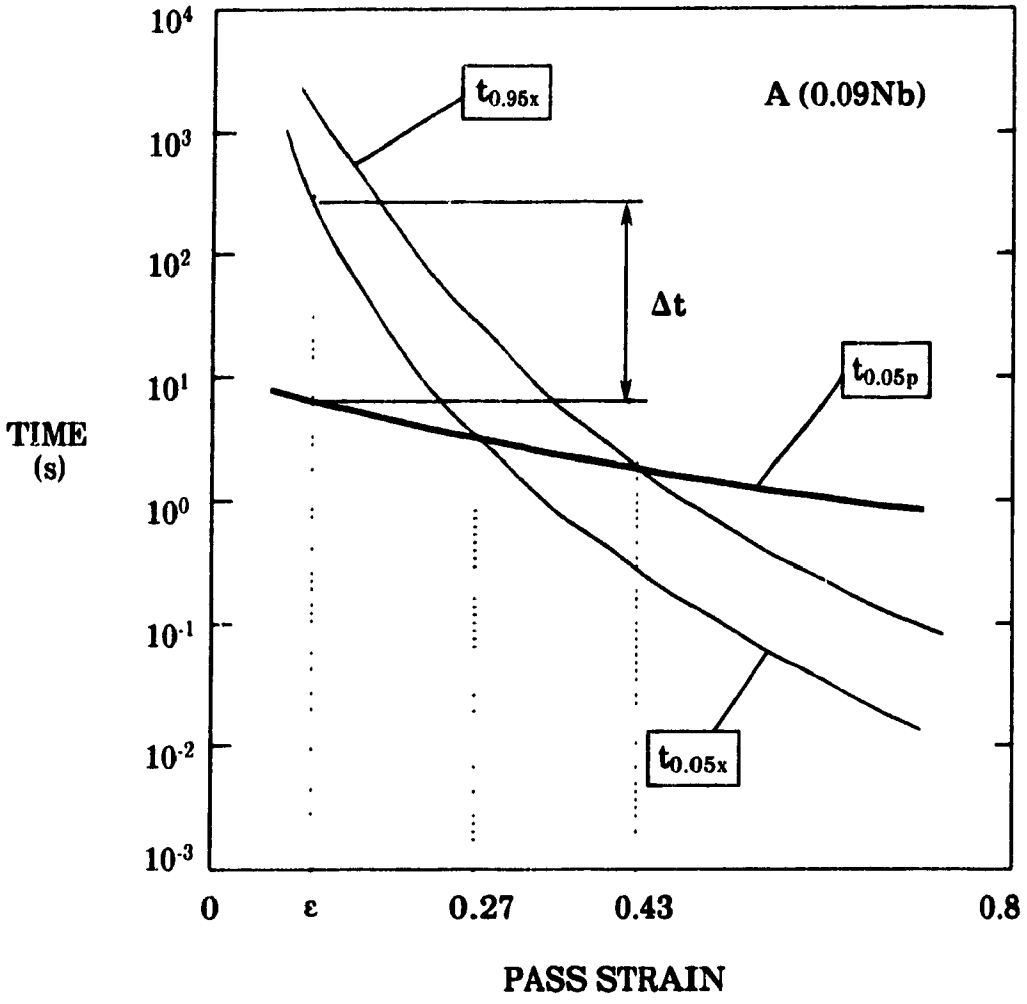


**Fig. 4.15** Influence of strain on $t_{0.05p}$, $t_{0.05x}$ and $t_{0.95x}$ at 960 °C.

words, if $\Delta t > 0$ ($\Delta t = t_{0.05x} - t_{0.05p}$), precipitation is initiated prior to recrystallization; otherwise, recrystallization is initiated before precipitation.

The rates of change of $t_{0.05p}$ and $t_{0.95x}$ with strain were obtained from the first partial derivatives of equations 4.8b and 4.12a:

$$\frac{\partial t_{0.05p}}{\partial \varepsilon} = -A\,\varepsilon^{-2} \qquad (4.13)$$

$$\frac{\partial t_{0.95r}}{\partial \varepsilon} = -4B\varepsilon^{-5} \qquad (4.14)$$

As deformation increases the dislocation density, and dislocations act as nucleation sites for both recrystallization and precipitation, increasing the strain increases the rate of both phenomena. The increases are different, however, for the two mechanisms. From equations 4.13 and 4.14, it can be seen that the recrystallization kinetics are more sensitive to strain than the precipitation kinetics, although the difference diminishes as the strain approaches unity. Thus, the $T_{nr}$ decreases continuously with strain. As an example, the steel A results in Fig. 4.13 show that when the strain is increased from 0.1 to 0.2, the $T_{nr}$ decreases by 57 °C (from 1053 °C to 996 °C). When the strain is increased from 0.2 to 0.4, the $T_{nr}$ decreases by 71 °C (from 996 °C to 925 °C).

The austenite-to-ferrite transformation start temperature ($A_{r3}$) also increases with increasing pass strain (see the lower solid line in Fig. 4.13). This can be attributed to strain induced transformation. Roberts et al.[86, 92, 93] and Kozasu et al.[10] explained this phenomenon in terms of the increase in the total possible nucleation site area per unit volume by means of grain elongation and the generation of transition bands at temperatures below the $T_{nr}$. Roberts et al.[92] also found that the bulges formed at pre-existing grain boundaries are particularly effective nucleation sites for ferrite; the density of these also increases with increasing strain below the $T_{nr}$. In other words, the number of nucleation sites for ferrite increases with increasing strain below the $T_{nr}$.

Fig. 4.16 shows the dependence of the total strain below the $T_{nr}$ on pass strain. It can be seen that the total strain below the $T_{nr}$ increases with pass strain, which leads to the increase in $A_{r3}$. It is worthy of note that the difference between the $T_{nr}$ and $A_{r3}$ decreases with increasing pass strain. When the pass strain is 0.1, the difference is about 297 °C, while the difference is only 50 °C when the pass strain is 0.7. This suggests that when the finishing

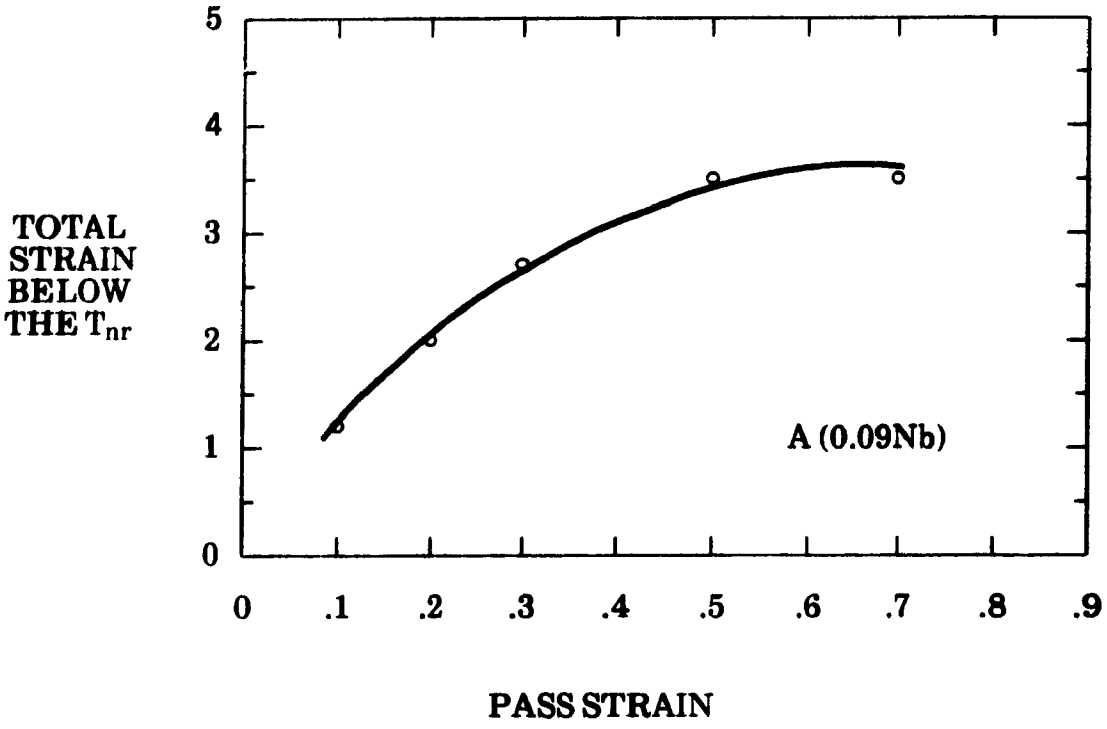


Fig. 4.16 Dependence of the total strain below the $T_{nr}$ on the pass strain (strain rate $\dot{\varepsilon} = 2\ s^{-1}$, interpass time = 30 s).

pass strain is large, the final stages of deformation take place in the $\alpha+\gamma$ two phase region. This will lead to difficulties in predicting the final grain size.

### 4.4.2 EFFECT OF STRAIN RATE

Some mean flow stress vs. 1000/T curves for steel B are presented in Fig. 4.17. For these tests, the pass strain (0.3/pass) and interpass time (30 seconds) were held constant, and only the strain rate was varied from test to test. It can be seen that the mean flow stress increases with increasing strain rate. This is because the amount of restoration caused by dynamic recovery decreases as the strain rate is increased. At lower strain rates, the deformation time is

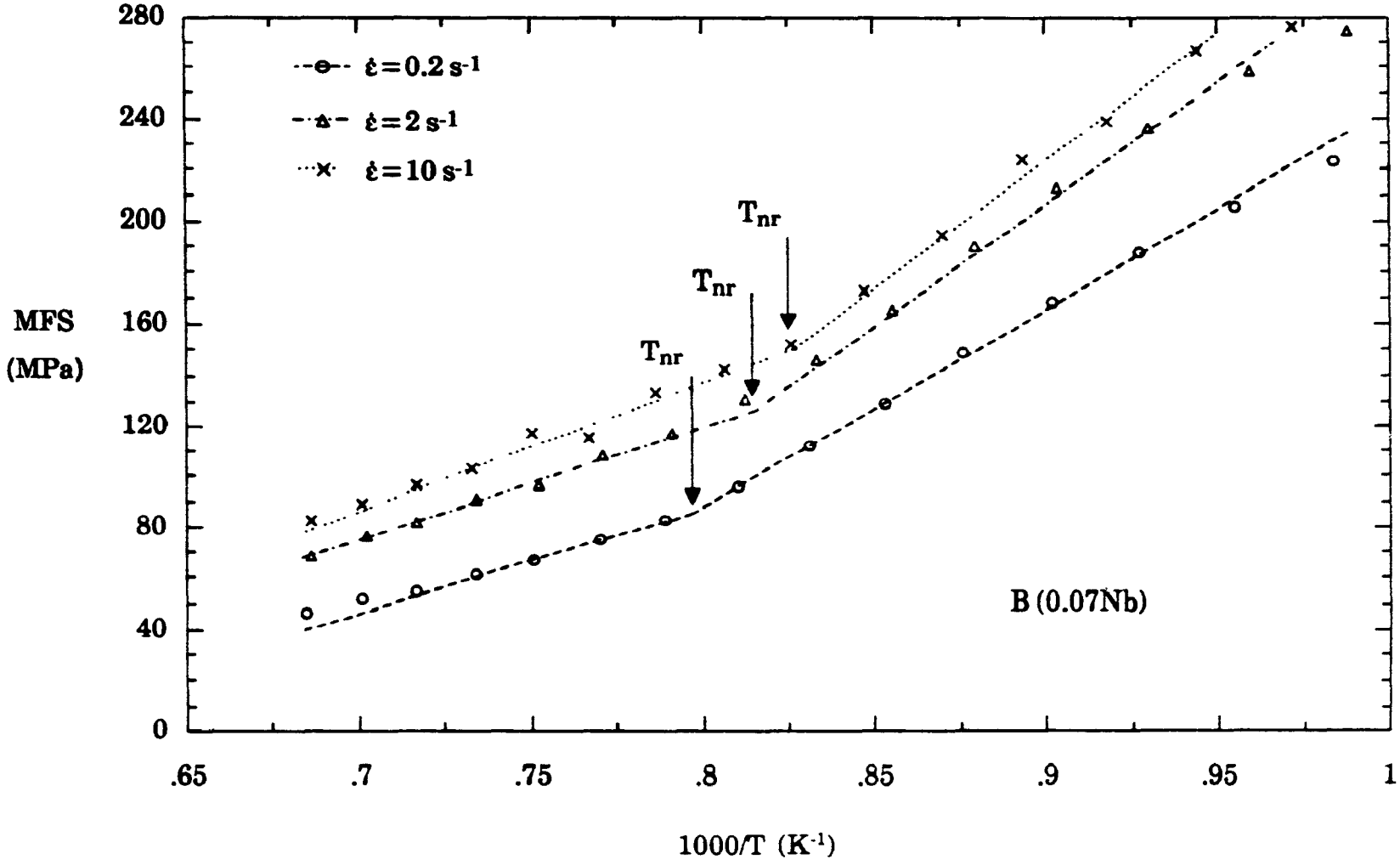


Fig. 4.17 Dependence of the mean flow stress (MFS) on inverse pass temperature for samples deformed according to schedule A; $\varepsilon = 0.3$, $t = 30$ s.

longer, which leads to more restoration. When the strain rate is 0.2 $s^{-1}$, for example, the deformation time is 1.5 seconds for a strain of 0.3. This time is long enough to cause appreciable dynamic restoration, and therefore produces a relatively low mean flow stress. By contrast, a strain rate $\dot{\varepsilon} = 10\ s^{-1}$ leads to a deformation time of 0.03 seconds. This short time will minimize the restoration, and lead to a higher mean flow stress. Such less restored and highly strained austenite supplies more driving force for static recrystallization, which decreases the $T_{nr}$ in turn. The results shown in Fig. 4.18 demonstrate that the $T_{nr}$ decreases with increasing strain rate, and this phenomenon becomes more evident when the strain is large. Nevertheless, it should be noted that when the strain is small, the effect of strain rate on the $T_{nr}$ is weak, and can even be reversed [94]. The reason for the latter phenomenon is not clear, but the following explanation can be suggested.

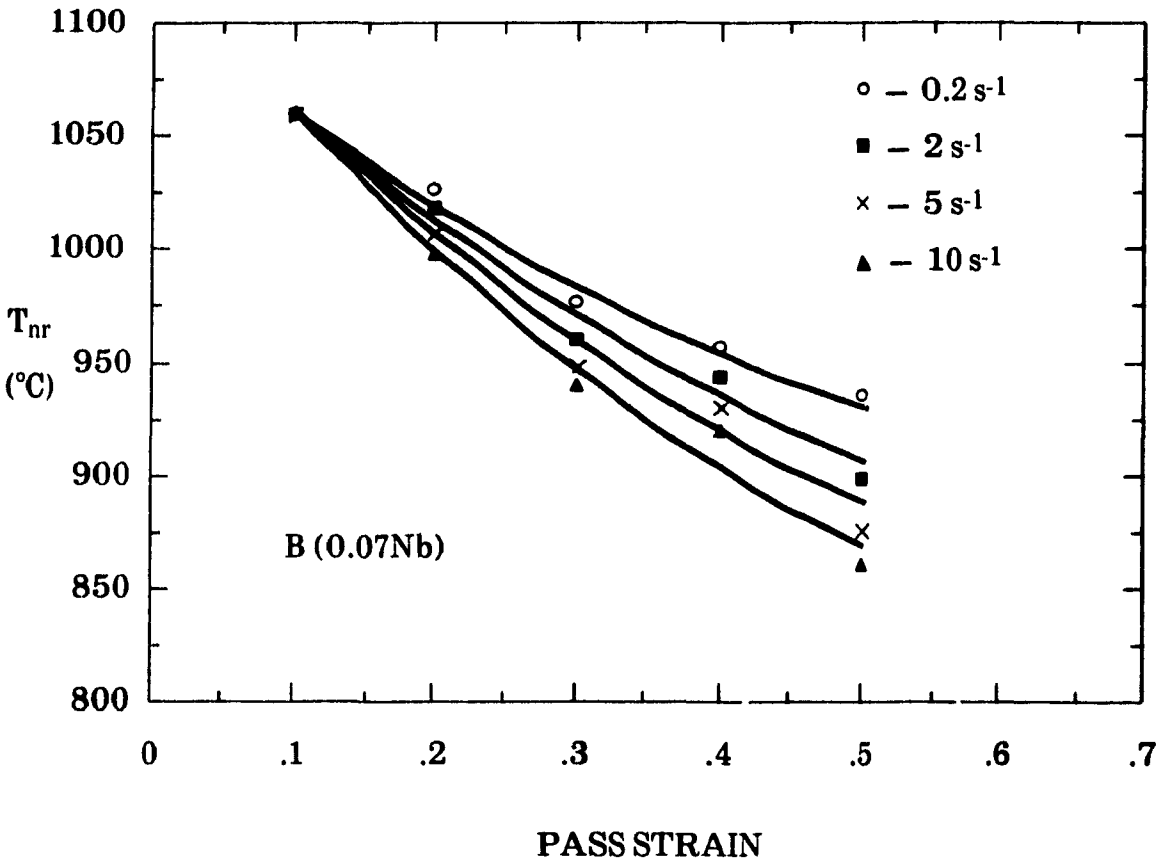


Fig. 4.18 Effect of strain rate on the $T_{nr}$ (interpass time = 30 s).

In general, in the absence of strain induced precipitation, increasing the rate of deformation decreases the incubation time and increases the rate of subsequent recrystallization. This is due to the increase in dislocation density and the decrease in subgrain size that accompanies the strain rate increase, both of which increase the driving force for recrystallization[19]. In the range of temperatures where strain induced precipitation is likely to occur, not only recrystallization but also precipitation are accelerated at high strain rates. There is an interaction between these two processes. When the strain is large, the recrystallization kinetics are accelerated over the precipitation kinetics; this leads to a decrease in the $T_{nr}$. When the strain is small, however, the precipitation kinetics are accelerated over the recrystallization kinetics, thereby increasing the $T_{nr}$.

### 4.4.3 EFFECT OF INTERPASS TIME

A set of mean flow stress vs. 1000/T curves for steel B is presented in Fig. 4.19. For the tests shown here, the pass strain (0.3/pass) and strain rate ($\dot{\varepsilon}=2\ s^{-1}$) were held constant, and the interpass time was changed from test to test (ranging from 5 seconds to 200 seconds). For a selected test, the individual interpass times were identical. It can be seen that at temperatures above the $T_{nr}$, the interpass time does not affect the mean flow stress because full recrystallization takes place, and there is no precipitation strengthening. In this case, the mean flow stress is only a function of temperature.

At temperatures below the $T_{nr}$, precipitation takes place, so that the increase in mean flow stress is attributable, not only to the decreasing temperature, but also to precipitation strengthening. At low temperatures, recrystallization gets sluggish, while precipitation becomes more active. At temperatures close to the nose of the PTT curve, longer interpass times will lead to precipitate coarsening, and thus weaken the effect of precipitation strengthening. This is why the mean flow stress for interpass times of 150 seconds in Fig. 4.19 is lower than that for interpass times of 30 seconds at temperatures below the $T_{nr}$.

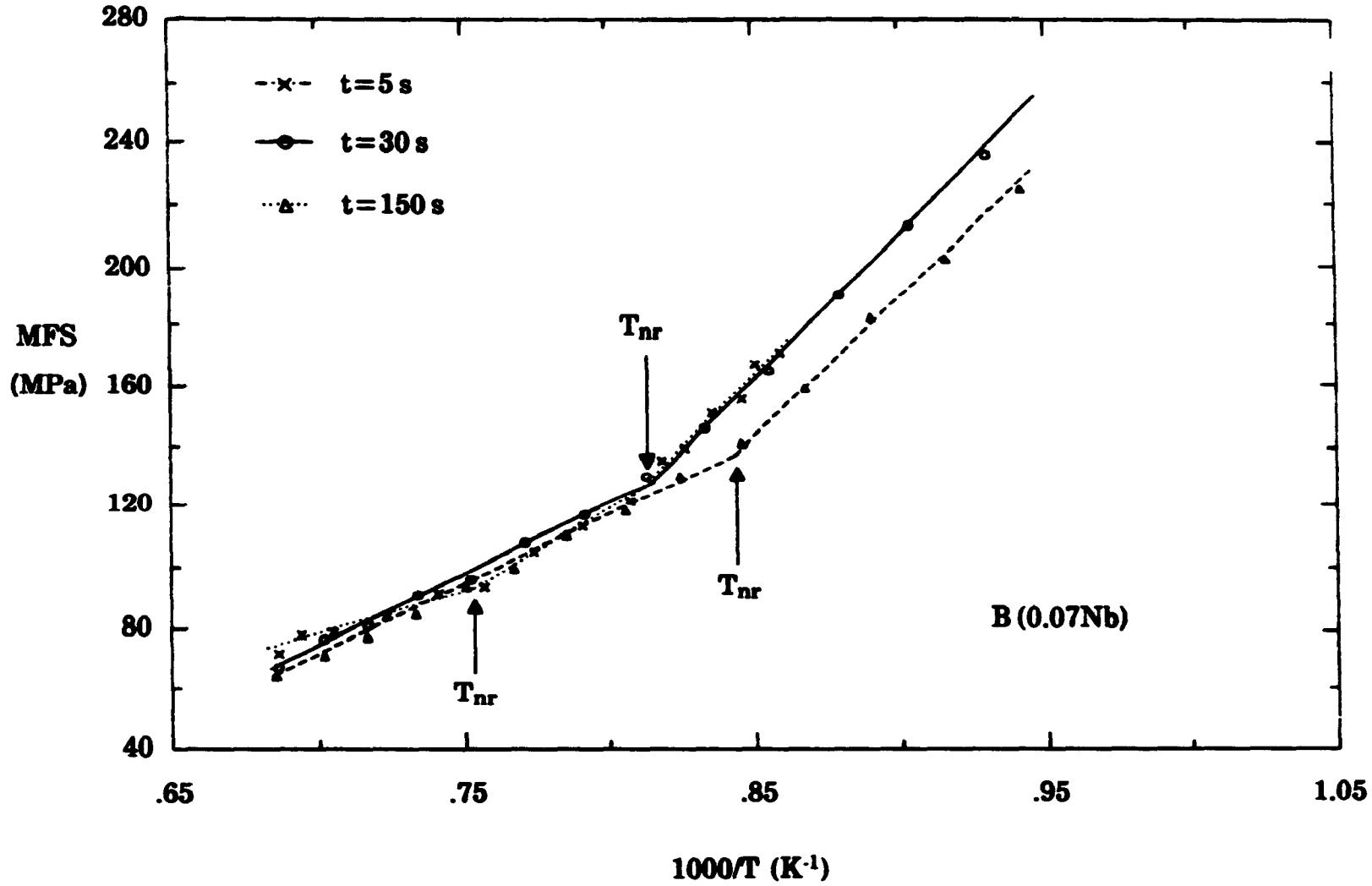


Fig. 4.19 Dependence of the mean flow stress (MFS) on inverse pass temperature for samples deformed according to schedule A; $\dot{\varepsilon}=2\ s^{-1}$, $\varepsilon=0.3$.

The dependence of the $T_{nr}$ on interpass time for steel B is illustrated in Fig. 4.20. It can be seen that the interpass time range from 5 seconds to 200 seconds can be divided into three regions: the short interpass time region ($t<12.5$ seconds), the medium interpass time region ($12.5<t<80$ seconds), and the long interpass time region ($t>80$ seconds). In the short interpass time region (region I), precipitation is unable to take place in the early stages of multipass deformation, so that only solute drag acts to retard recrystallization [95]. In this region, the possibility of recrystallization increases with increasing interpass time, leading to the decrease in the $T_{nr}$. With further increases in the interpass time, if no precipitation takes place, the $T_{nr}$ would decrease continuously along the broken curve. For the present steels, however, when the interpass time increases beyond a critical value (for instance, 12.5 seconds for steel B), precipitation takes place; thus the retardation of recrystallization is mainly attributable to precipitation in this case. When the interpass time is increased further, the volume fraction of precipitate increases. Then the retardation of recrystallization by precipitation becomes stronger, and the $T_{nr}$ shifts to the solid curve. In the third region, the interpass time is quite long (>80 seconds), precipitate coarsening starts, and then the retardation of recrystallization by precipitates becomes weaker. This leads to the $T_{nr}$ decreasing again.

Typical TEM micrographs of steel B samples processed with different interpass times are collected in Fig. 4.21. The quenching temperature was 910 °C for all the samples, but the total times from the solution temperature to the temperature at which quenching was carried out were different because different interpass times were used. The total time was 45 seconds for sample A, 270 seconds for sample B, 720 seconds for sample C, and 1800 seconds for sample D. It can be seen that when the interpass time was increased from 5 seconds to 200 seconds, the mean particle size increased from 15 nm to 135 nm. After the precipitates reached their maximum volume fractions, they coarsened by consuming the smaller ones. The TEM observations are in good agreement with the previous mechanical results, and provide evidence for the explanation presented above.

The interpass time dependence of the $T_{nr}$ in steels A and C is displayed in Fig. 4.22. The steel B results are also presented in this figure for

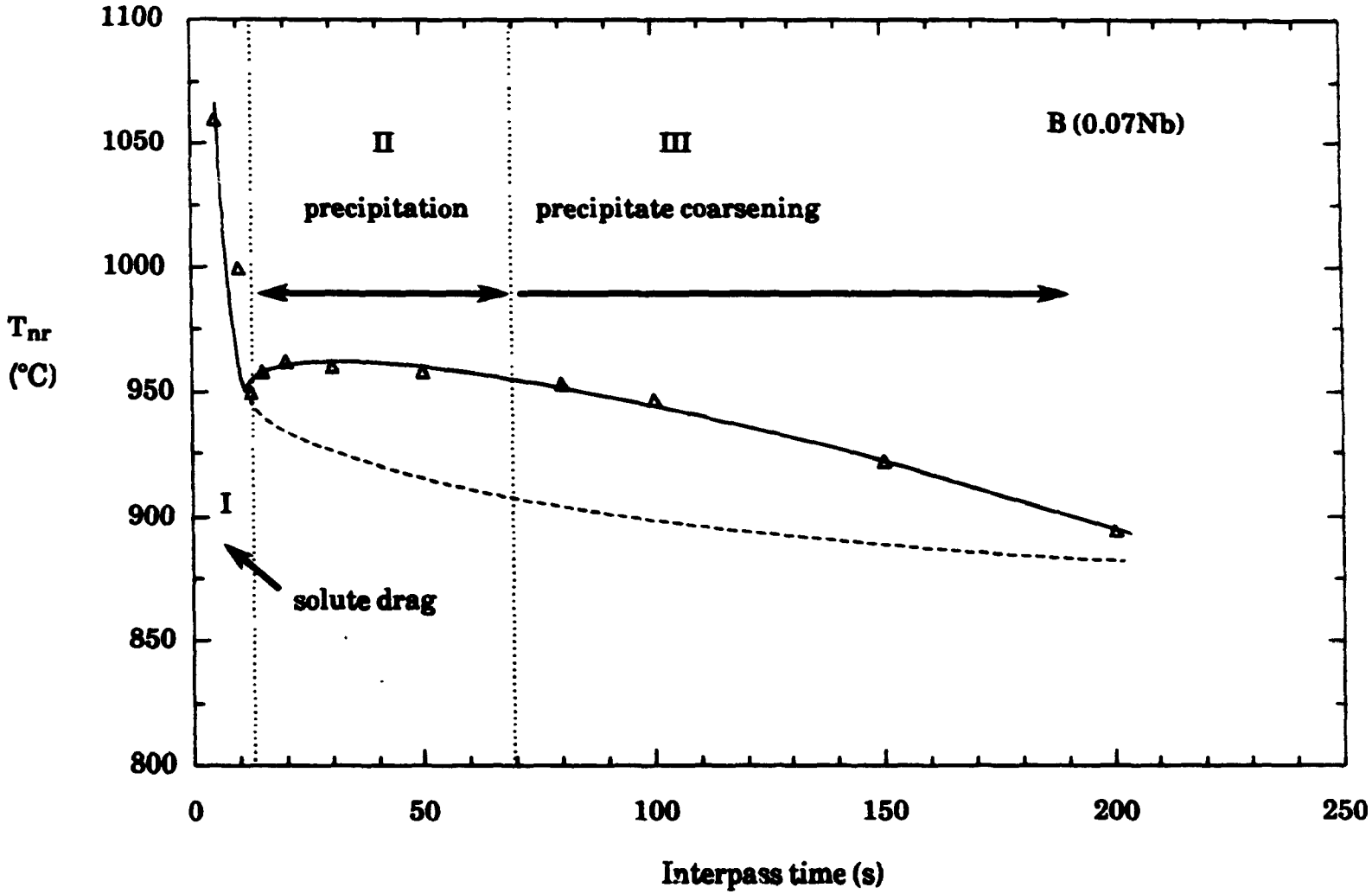


Fig. 4.20 Dependence of the $T_{nr}$ on interpass time.

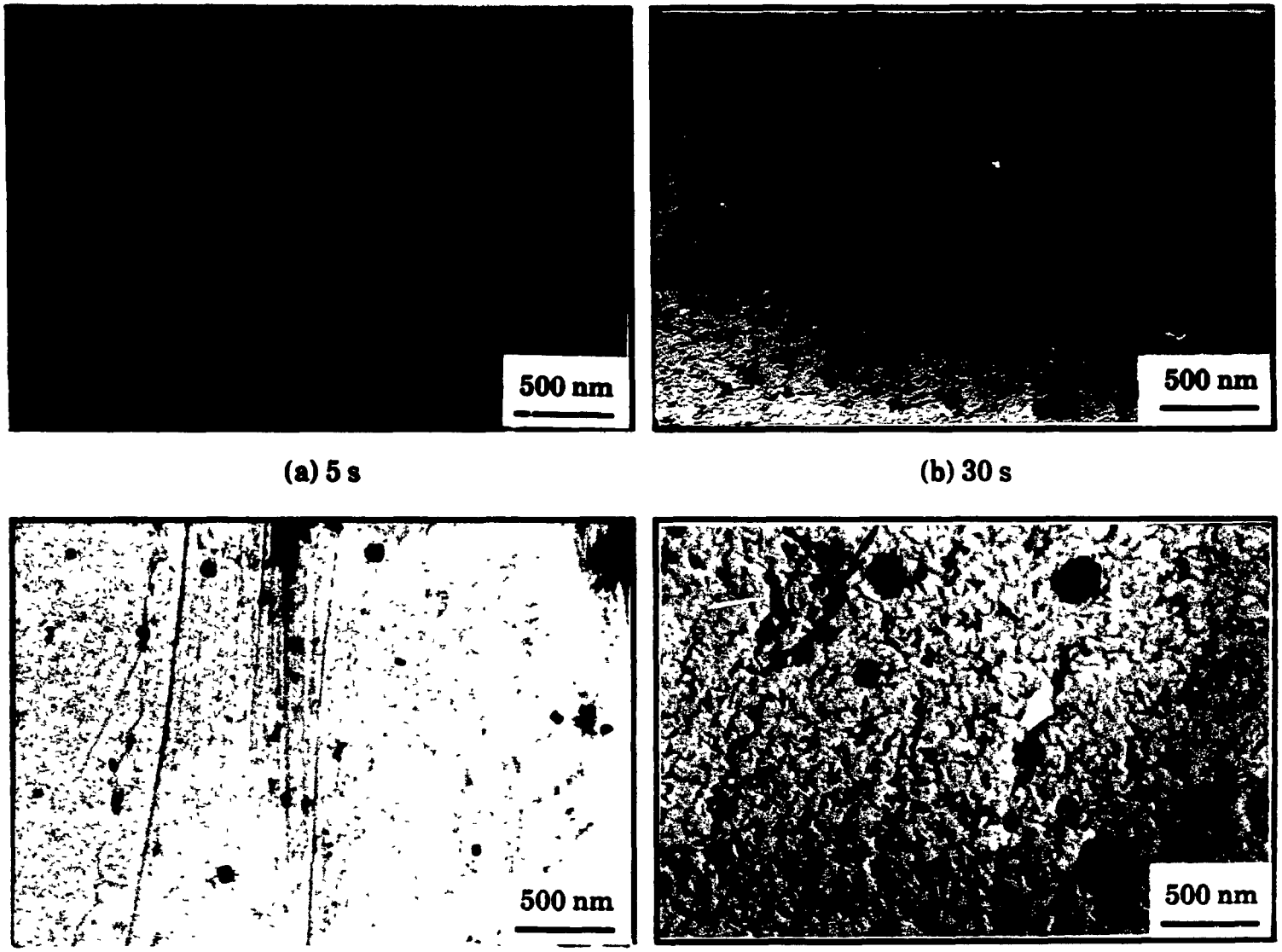


(a) 5 s

(b) 30 s

(c) 80 s

(d) 200 s

Fig. 4.21 Carbon extraction replicas showing the dependence of the morphology of the Nb(C,N) precipitates on interpass time. All of the specimens were quenched at 910 °C.

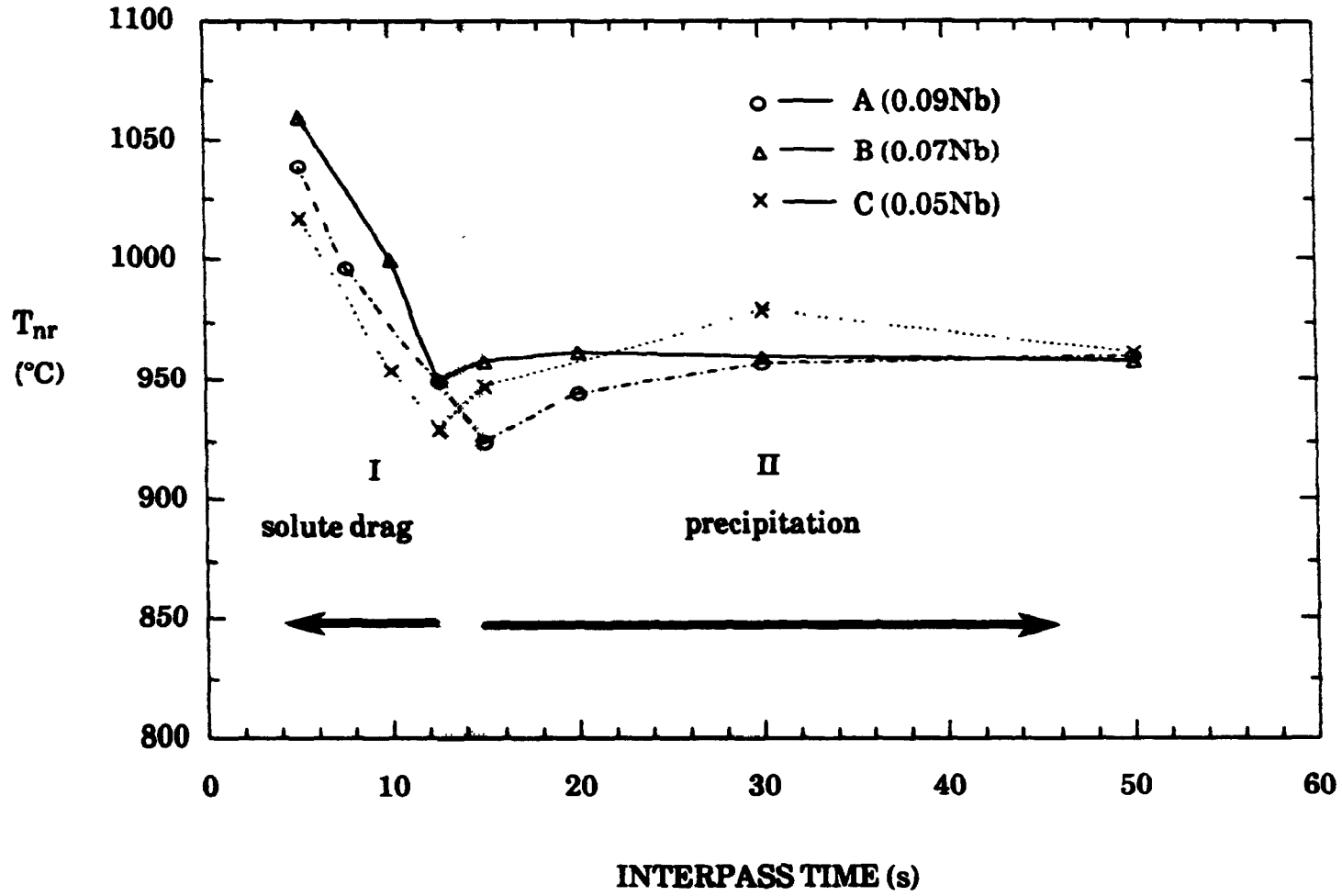


**Fig. 4.22 Dependence of the $T_{nr}$ on interpass time.**

comparison. It can be seen that precipitation takes place earlier in steels B and C. This is because steel C has a higher supersaturation at the deformation temperature, and steel B has the TiN precipitates acting as nucleation sites for Nb(C,N) precipitation. Thus the precipitation kinetics of both steels are accelerated over that of steel A. In the short interpass time region where solute drag controls recrystallization, the order of the $T_{nr}$ for these steels is A, B, C. This is because steel A has the highest concentration of Nb in solution and the solute concentration is lowest in steel C. The presence of Ti in steel B probably led to the precipitation of TiN. These particles can act as nucleation sites for the precipitation of Nb(C,N) [84, 85], and accelerate the kinetics of precipitation in this way. This may be why the steel B $T_{nr}$ is higher than that of steel A in the precipitation region even though the niobium concentration in steel A is higher.

It should be pointed out that the method used in the present study has its limitations. When the mean flow stress vs. 1000/T diagram is being used to determine the $T_{nr}$, it is assumed that no dynamic recrystallization takes place during deformation. In the case of very short interpass times, 2 seconds for instance, static recrystallization cannot be completed even at relatively high temperatures, so that only partial restoration takes place. In this case, the strain is accumulated from pass to pass. Once the accumulated strain is able to initiate dynamic recrystallization during the next pass, the mean flow stress drops to the solid curve shown in Fig. 4.23. This makes it impossible to determine the $T_{nr}$ using the MFS-1000/T diagram.

## 4.5. PREDICTION OF THE $T_{nr}$

Several models have been developed for predicting recrystallization and precipitation start times. Of these, that of Dutta and Sellars (described in equations. 4.8a to 4.9b) is the most convenient for industrial practice because only the deformation parameters are needed for the calculation of the recrystallization start ($t_{0\ 05x}$) and finish ($t_{0\ 95x}$) times and the precipitation start time ($t_{0.05p}$). Plotting RTT (recrystallization-temperature-time) and PTT (precipitation-temperature-time) curves on the same diagram, the $T_{nr}$ for a given deformation condition can then be determined from the point of

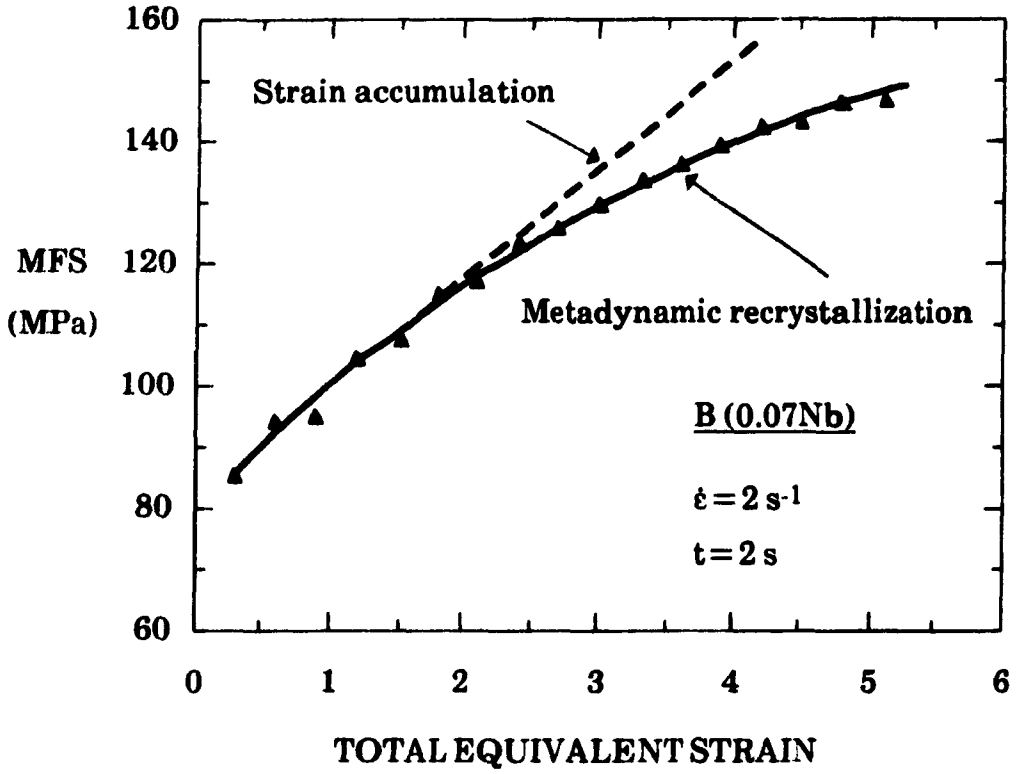


Fig. 4.23 Multipass deformation of steel B with a short interpass time (2 s).

intersection between $t_{0.05p}$ and $t_{0.95x}$. However, the Dutta and Sellars models were derived under isothermal conditions; this can lead to error if these models are applied directly to the prediction of $T_{nr}$ under continuous cooling conditions. Fig. 4.24 shows the measured $T_{nr}$'s and the $T_{nr}$'s predicted using Dutta and Sellars model for steel A. It is obvious that the difference between the measured and predicted $T_{nr}$'s is large when the strain is large. To solve this problem, the additivity rule was used in the present study to calculate the continuous cooling behavior from isothermal data.

### 4.5.1 THE ADDITIVITY RULE

Fig. 4.25 illustrates the concept of the additivity rule. Scheil [96] originally proposed that the reaction starts when the sum of the ratios of reaction time to reaction start time ($\tau_0$) reaches unity.

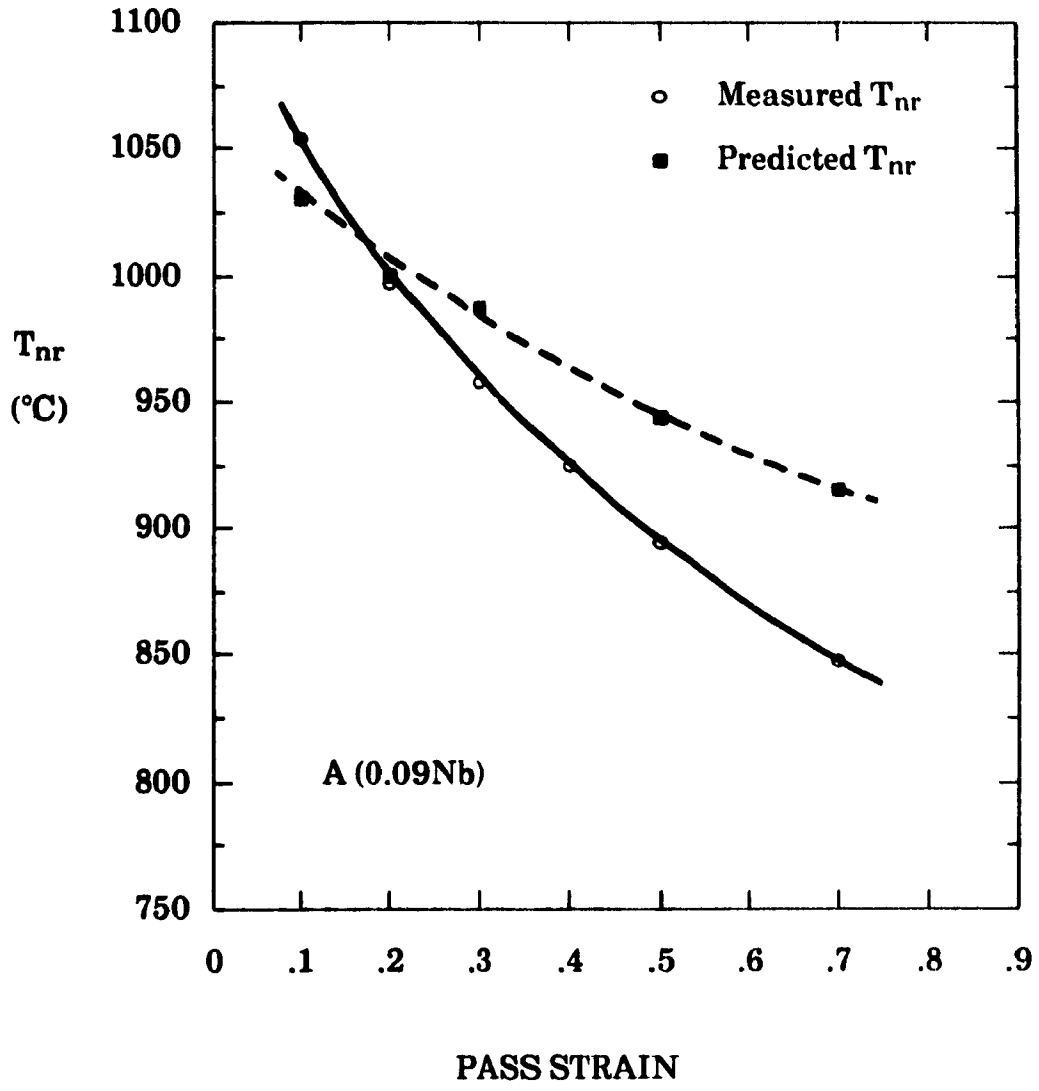


**Fig. 4.24** Dependence of the $T_{nr}$ on pass strain ($\dot{\varepsilon} = 2\ s^{-1}$, $t = 30$ s).

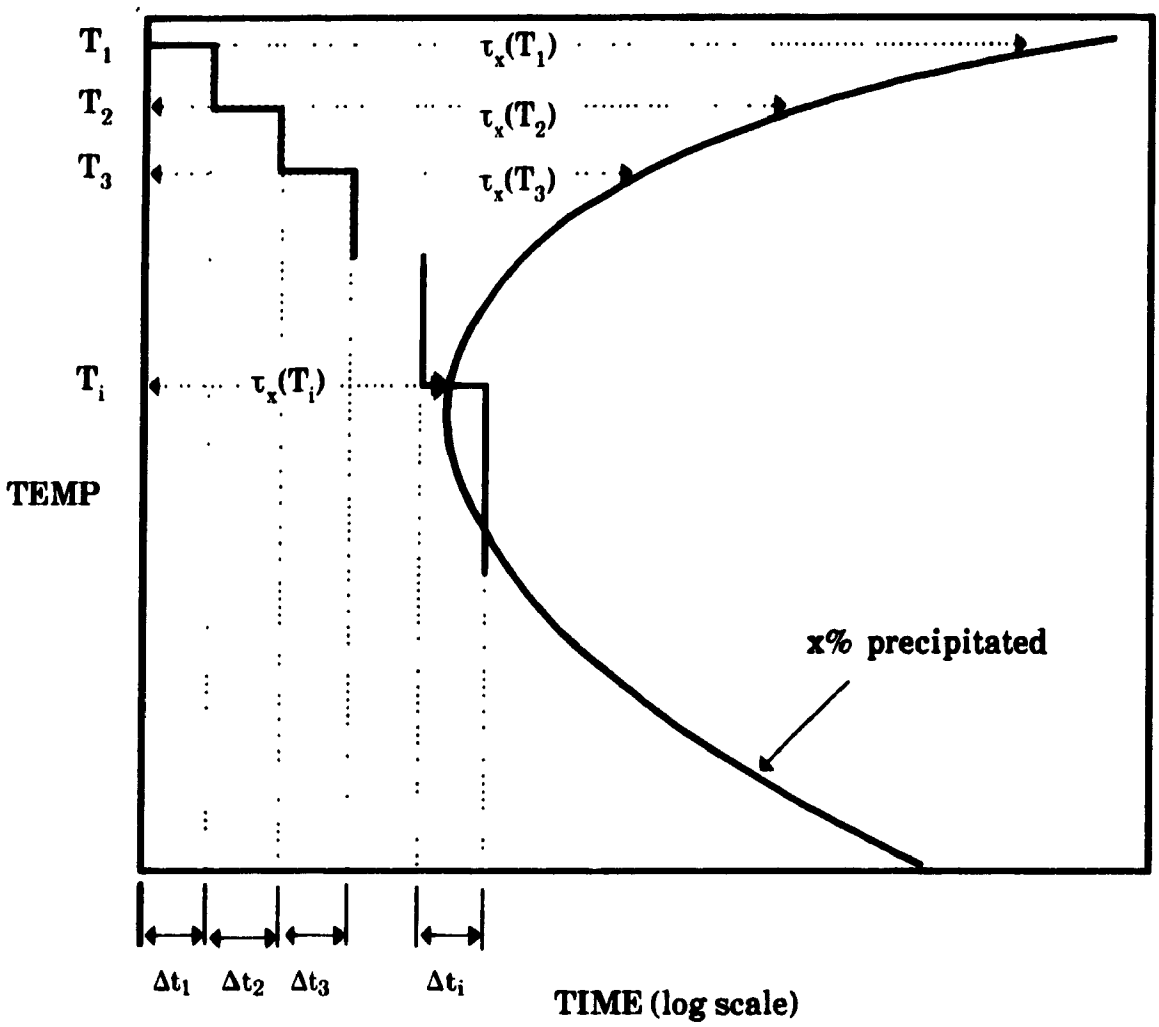


**Fig. 4.25 A diagrammatic representation of the additivity rule concept.**

$$\sum_{i=1}^{n} \frac{\Delta t_i}{\tau_0(T_i)} = 1 \qquad (4.15)$$

This rule has been widely used to predict the start time of phase transformations. Umemoto et al.[97-102] extended this method to predict the time when the reaction reaches x%. The additivity rule, in this case, can be rewritten as:

$$\sum_{i=1}^{n} \frac{\Delta t_i}{\tau_x(T_i)} = \sum_{i=1}^{n} \frac{1}{\tau_x(T_i)} \frac{\Delta t_i}{\Delta T_i} \Delta T_i = 1 \qquad (4.16)$$

where $\tau_x(T_i)$ is the time when the reaction reaches x% at temperature $T_i$, $\Delta t_i$ is the incremental hold time at temperature T and $\Delta t_i/\Delta T_i$ is the inverse of the cooling rate. If the cooling curve is divided into sufficiently small steps, then the equation can be expressed as an integral:

$$\int_{T_e}^{T} \frac{1}{\tau_x(T_i)} \frac{dt}{dT} dT = 1 \qquad (4.17)$$

where $T_e$ is the equilibrium temperature at which the reaction is initiated.

It has been shown that the CCT (continuous-cooling-transformation) behavior predicted from IT (isothermal-transformation) data using the additivity rule was in reasonable agreement with the experimental results when the calculations were carried out for the proeutectoid ferrite, pearlite and bainite transformations [97,99-100]. Park et al.[103] applied the additivity rule successfully to calculate the CCP (continuous-cooling-precipitation) curve using isothermal data (PTT). Since recrystallization is a kind of phase

transformation, it is expected that the CCR (continuous-cooling-recrystallization) behavior can be calculated by the same rule. This calculation was performed in the present study and is described below.

### 4.5.2 CALCULATION OF CCR AND CCP CURVES

To calculate the CCR and CCP curves, the following assumptions were made: i) after each deformation, the occurrence of recrystallization and precipitation can be modeled separately; and ii) at the i-th pass, the deformation temperature can be used in place of $T_e$ in equation 4.17.

The cooling curves were divided into 0.01 °C increments, and $\tau_x$ and $\Delta t_i$ were calculated at each temperature. The recrystallization finish and precipitation start times for each pass were then evaluated from the times when the sum of the ratios of each reaction time ($\Delta t_i$) to $\tau_x$ reaches unity. The programs for calculating the $t_{0.05p}$ and $t_{0.95x}$ times under continuous cooling conditions are listed in Appendix II.

For calculation of the recrystallization finish time ($t_{0.95x}$) at the i-th pass, the recrystallized grain size at the $(i-1)$-th pass was used as the initial grain size of the i-th pass. It can be evaluated using equation 4.6 given in the previous section. The RPTT (recrystallization-precipitation-temperature-time) diagrams obtained in this way for steel A are presented in Fig. 4.26. The broken curves represent $t_{0.95x}$, and the solid ones represent $t_{0.05p}$. The arrows identify the points of intersection of the $t_{0.95x}$ and $t_{0.05p}$ curves. The temperatures that correspond to these points are the predicted $T_{nr}$'s, and the results are presented in Fig. 4.27.

It can be seen that the predicted $T_{nr}$'s are slightly lower than the measured ones. This deviation could result from the way the initial grain size for each pass was calculated. In the literature, the following values of the constant D have been reported: 1.1 [10], 0.66 [57, 104], and 1.86 [105] $\mu m^{0.33}$. In order to improve the accuracy of the predicted $T_{nr}$'s, the values $D = 1.1\ \mu m^{0.33}$ for steel A, and 1.6 $\mu m^{0.33}$ for steels B and C were chosen to evaluate the austenite grain size. The recalculated RPTT diagrams obtained in this way

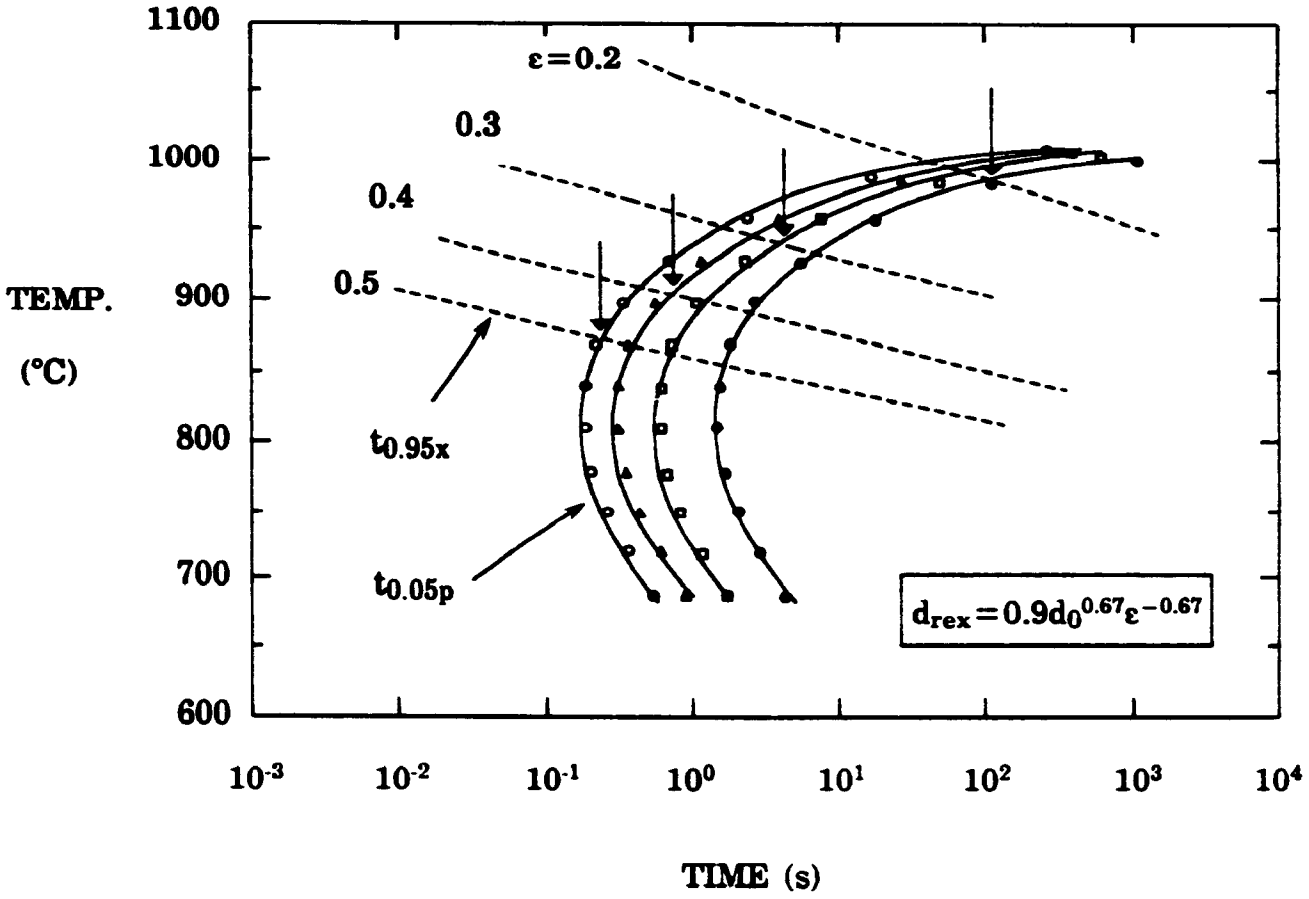


Fig. 4.26 RPTT diagram pertaining to continuous cooling conditions (0.09Nb steel).

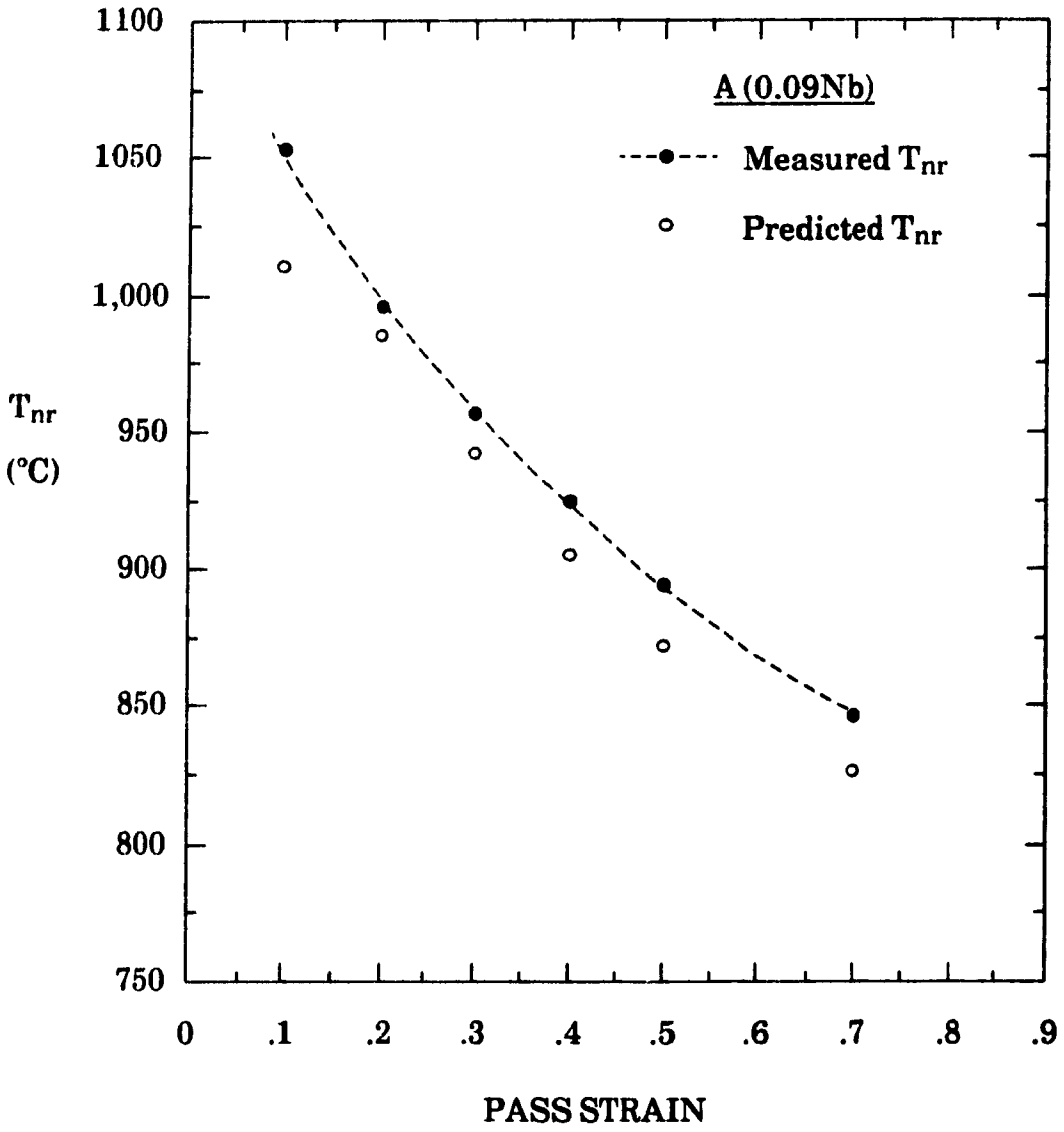


Fig. 4.27 Comparison of the measured and predicted $T_{nr}$'s ($\dot{\varepsilon} = 2\ s^{-1}$, $t = 30$ s).

are presented in Appendix III and the redetermined $T_{nr}$'s are displayed in Fig. 4.28. It is evident that, by correcting for the continuous cooling conditions pertaining to the present experiments, the agreement between the predicted and measured $T_{nr}$'s is improved considerably.

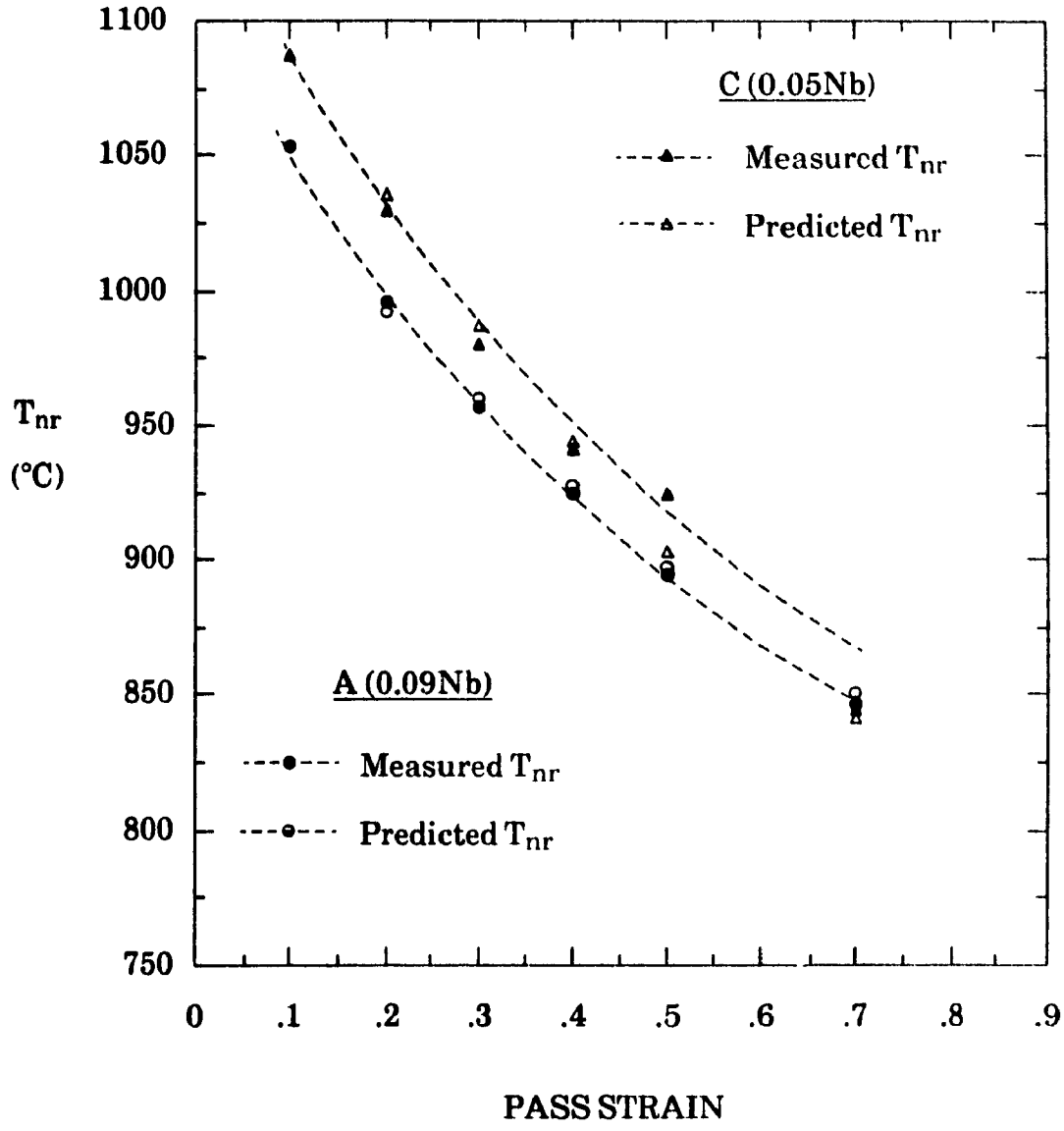


Fig. 4.28 Comparison of the measured and predicted $T_{nr}$'s ($\dot{\varepsilon} = 2\ s^{-1}$, $t = 30$ s).

CHAPTER 5

# DYNAMIC RECRYSTALLIZATION

As described in Chapter 2, dynamic recrystallization, unlike static recrystallization, takes place *during* deformation. Since Rossard and Blain revealed this phenomenon in their work in 1959, many researchers have been attracted by this process. It no longer is only a laboratory curiosity, but can have applications in industrial practice. Jonas et al.[106] have suggested that dynamic recrystallization can take place under some industrial conditions, such as rod and hot strip rolling. Recently, a systematic study of the mechanisms of dynamic recrystallization and of metadynamic recrystallization was carried out by Roucoules[107] in the CSIRA Steel Processing laboratory at McGill. In that work, a Ti-Mo and a Ti-Nb steel were tested. As a complement to that investigation, two higher Nb steels were tested in the present work. The results are presented below.

## 5.1 SINGLE PASS DEFORMATION

As described in Chapter 3, four roughing passes followed by a single large strain pass were used to study the influence of deformation temperature on the dynamic recrystallization of steel A. The flow curves obtained in this way are presented in Fig. 5.1.

To investigate the occurrence of strain accumulation and of dynamic recrystallization, the mean flow stress pertaining to the 5th pass and the mean flow stress over a strain $\varepsilon = 0.3$ of the 5th pass were calculated using the following equations:

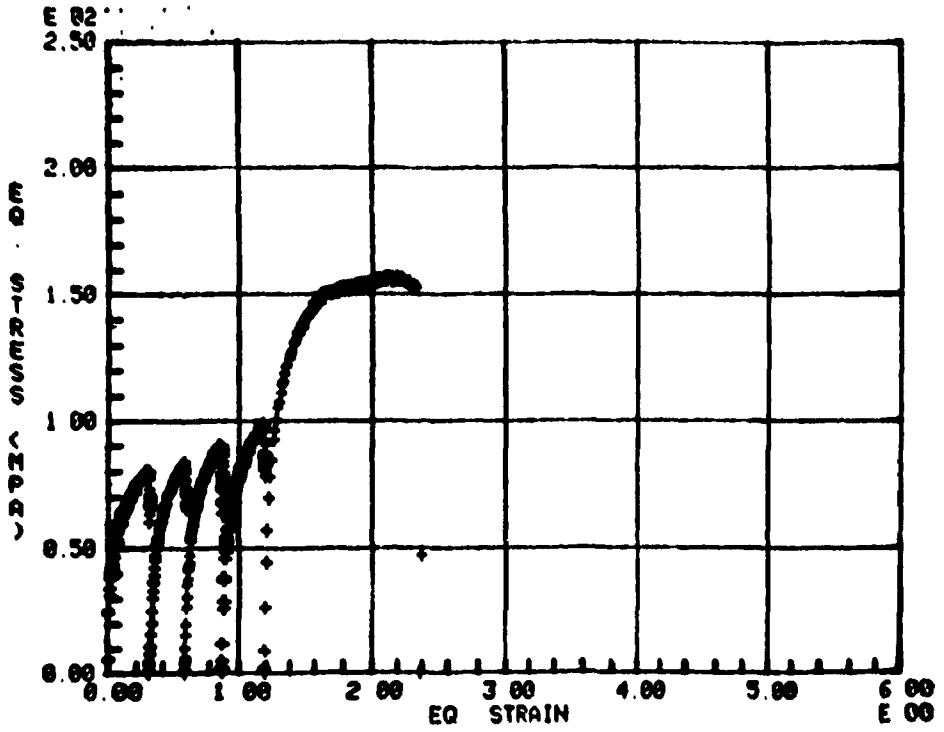


STRESS (MPa)

STRAIN

Fig. 5.1 Stress-strain curves for samples deformed according to Schedule B (5th pass strain = 1.2).

$$\bar{\sigma}_{eq1} = \frac{1}{\varepsilon_b} \int_0^{\varepsilon_b} \sigma_{eq} d\varepsilon_{eq} \qquad (\varepsilon_b = 0.3 \sim 2.4) \tag{5.1}$$

$$\bar{\sigma}_{eq2} = \frac{1}{0.3} \int_0^{0.3} \sigma_{eq} d\varepsilon_{eq} \tag{5.2}$$

Here $\bar{\sigma}_{eq1}$ is the mean flow stress of the 5th pass, and $\bar{\sigma}_{eq2}$ is the mean flow stress over a strain $\varepsilon = 0.3$. The method of calculating the mean flow stresses $\bar{\sigma}_{eq1}$ and $\bar{\sigma}_{eq2}$ is illustrated schematically in Fig. 5.2 and the results are presented in Fig. 5.3. To demonstrate the strain accumulation that takes place during multipass deformation, the mean flow stresses measured in a regular test ($\bar{\sigma}_{eq3}$) are also presented in Fig. 5.3.

The $T_{nr}$ for the regular test was about 960 °C; this means that deformation above this temperature leads to full recrystallization, while below this temperature, recrystallization is no longer complete, so that the strain can accumulate from pass to pass. Fig. 5.3 demonstrates that at temperatures above the $T_{nr}$, the mean flow stresses averaged over a strain $\varepsilon = 0.3$ ($\bar{\sigma}_{eq2}$) are equal to those determined under multipass deformation conditions ($\bar{\sigma}_{eq3}$). Below the $T_{nr}$, however, the mean flow stresses measured under multipass conditions shift to the line with the higher slope because of continued work hardening, while $\bar{\sigma}_{eq2}$ still increases with decreasing temperature at the same rate as at temperatures above the $T_{nr}$ (no strain accumulation).

By contrast, the mean flow stresses associated with the 5th pass ($\bar{\sigma}_{eq1}$) in the case of single pass deformation vary along the broken line. It can be seen that the $\bar{\sigma}_{eq1}$ slope changes at point P. Essentially, if there is no dynamic recrystallization, then $\bar{\sigma}_{eq1}$ is only a function of the strain and deformation temperature, and could vary along the dotted line. However, once dynamic recrystallization is initiated during deformation, the evolution of $\bar{\sigma}_{eq1}$ departs

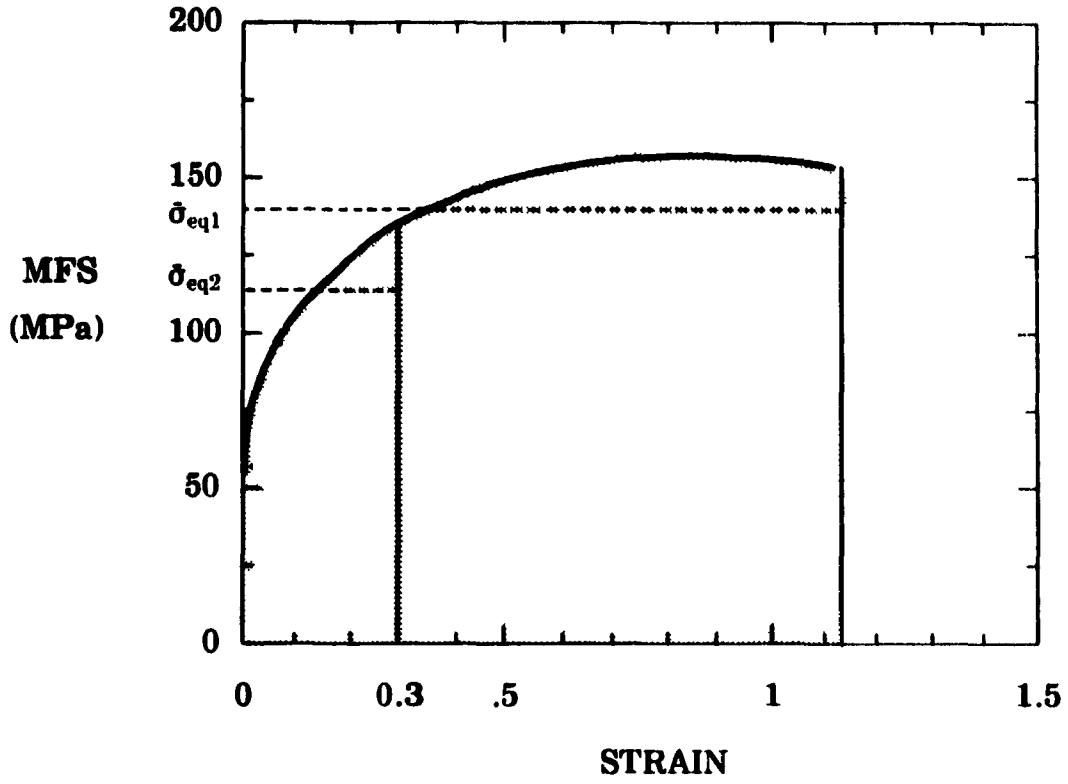


**Fig. 5.2** **A schematic diagram showing the determination of the mean flow stresses $\bar{\sigma}_{eq1}$ and $\bar{\sigma}_{eq2}$ (at $\varepsilon = 0.3$).**

from the dotted line to the broken line. The flow curves in Fig. 5.4 and the microstructures in Fig. 5.5 demonstrate that dynamic recrystallization takes place when the strain reaches 0.9 at a temperature of 1000 °C. The peak strains developed, $\varepsilon_p$, are shown in Table 5.1. It can be seen that the peak strain varies with the deformation temperature. It has been reported in the literature that the peak strains in steels can be represented as follows:

$$\varepsilon_p = A d_0^{1/2} Z^n \tag{5.3}$$

where A is a constant, $d_0$ is the initial grain size and Z is the Zener-Hollomon parameter, which can be represented as,

$$Z=\dot{\varepsilon}\,exp\frac{Q_{def}}{RT} \tag{5.4}$$

The constant A, the exponent n and the activation energy $Q_{def}$ for niobium steels have been reported to be $2.8\times10^{-4}$, 0.17 and 375 kJ/mol, respectively, by Roucoules [107]. The $\varepsilon_p$'s predicted by this equation are also presented in Table 5.1 for comparison with the measured ones.

## 5.2 MULTIPASS DEFORMATION

To demonstrate the influence of the deformation temperature, strain rate, delay time, and initial grain size on strain accumulation and dynamic recrystallization, a series of isothermal tests was carried out using steel B. The deformation temperatures ranged from 910 °C to 970 °C, the strain rates from 0.02 $s^{-1}$ to 5 $s^{-1}$, the delay times from 120 seconds to 1560 seconds, and the grain sizes from 30 μm to 85 μm. The time between passes was 1 second, which is short enough to completely restrain static recrystallization between passes, thus leading to strain accumulation from pass to pass. When the accumulated strain exceeds the critical strain, $\varepsilon_c$, then dynamic recrystallization is initiated, and the envelope of the individual flow curves displays a peak. Typical flow curves generated in this way at temperatures of 970 °C and 910 °C are reproduced in Fig. 5.6.

The accumulated strain under isothermal conditions can be calculated from the following equation:

$$\varepsilon_i^*=\varepsilon_i+\Delta\varepsilon_{i-1} \tag{5.5}$$

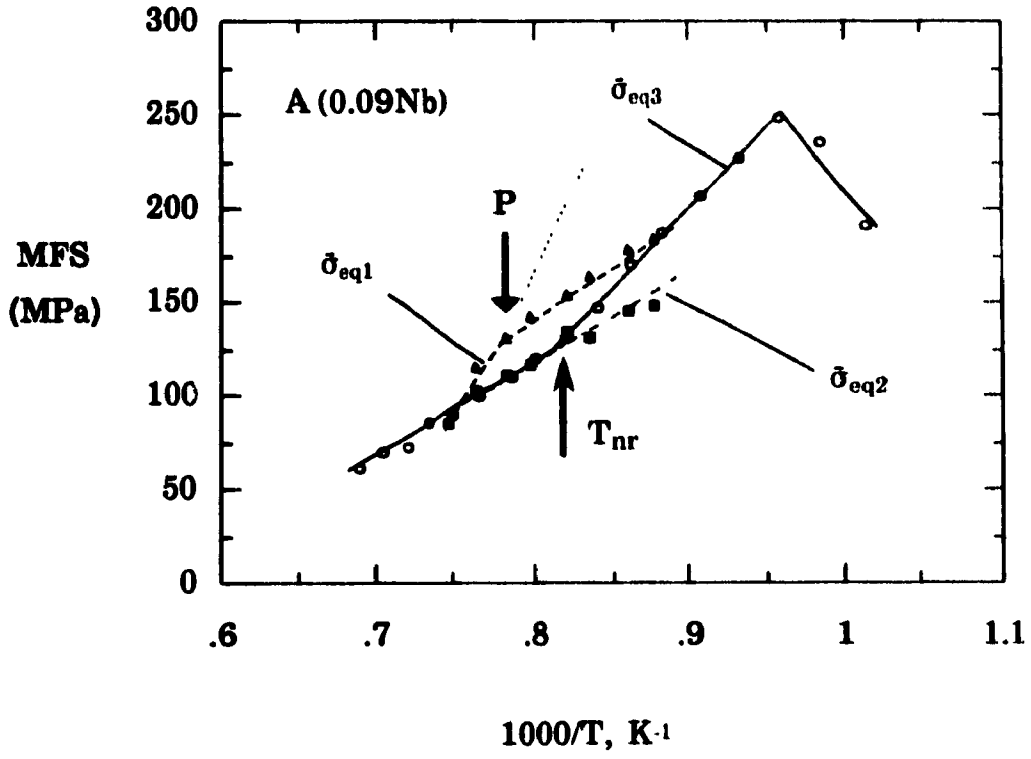


**Fig. 5.3** Dependence of the mean flow stress on inverse absolute pass temperature for samples deformed according to schedule B. Strain of 5th pass = 0.3 ~ 2.4, $\dot{\varepsilon} = 2\ s^{-1}$, interpass time between 4th and 5th pass = 30 s - 240 s.

$\bar{\sigma}_{eq1}$ – mean flow stress of the 5th pass in the case of single pass deformation.

$\bar{\sigma}_{eq2}$ – mean flow stress at $\varepsilon = 0.3$ of the 5th pass in the case of single pass deformation.

$\bar{\sigma}_{eq3}$ – mean flow stress in the case of multipass deformation.

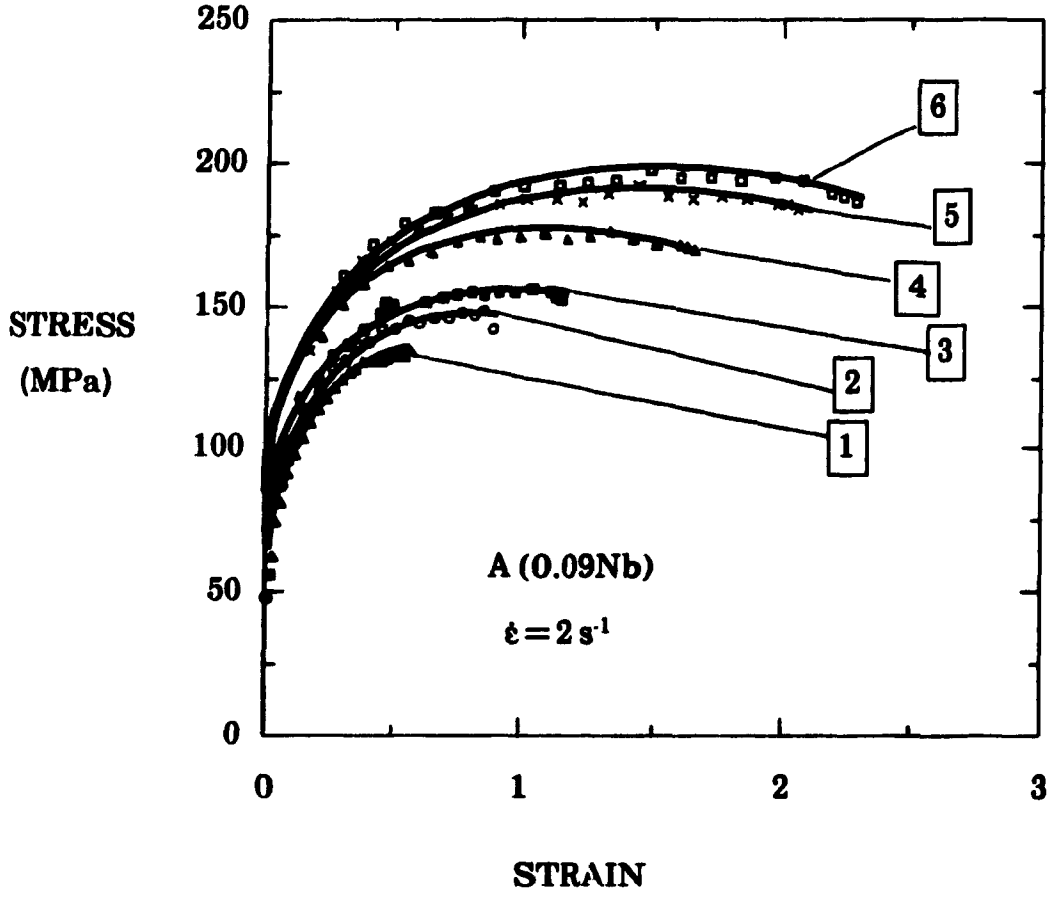


Fig. 5.4 Stress - strain curves of the 5th pass.

1 - strain $\varepsilon = 0.6$, $T_{def} = 1030$ °C; 2 - strain $\varepsilon = 0.9$, $T_{def} = 1000$ °C
3 - strain $\varepsilon = 1.2$, $T_{def} = 970$ °C; 4 - strain $\varepsilon = 1.8$, $T_{def} = 910$ °C
5 - strain $\varepsilon = 2.1$, $T_{def} = 880$ °C; 6 - strain $\varepsilon = 2.4$, $T_{def} = 850$ °C

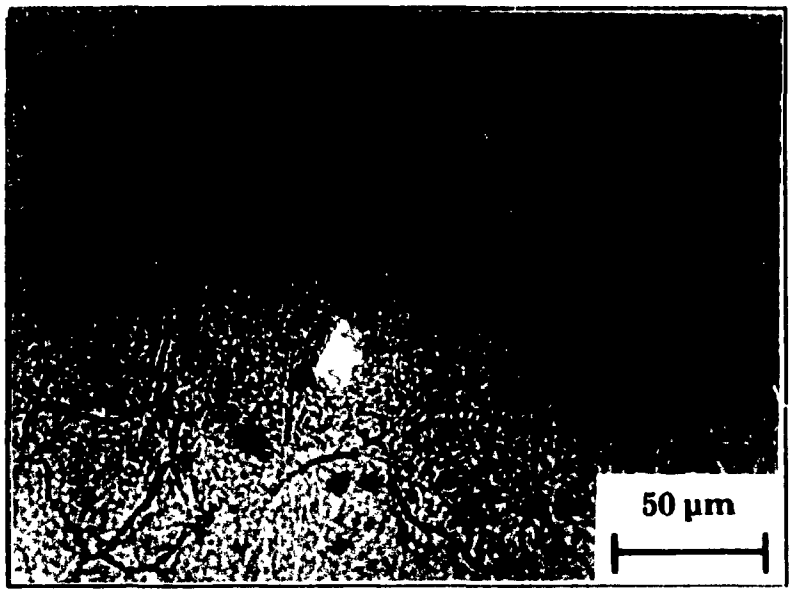


(a) $\varepsilon = 0.3, T_{def} = 1060\,^{\circ}C$ WQ

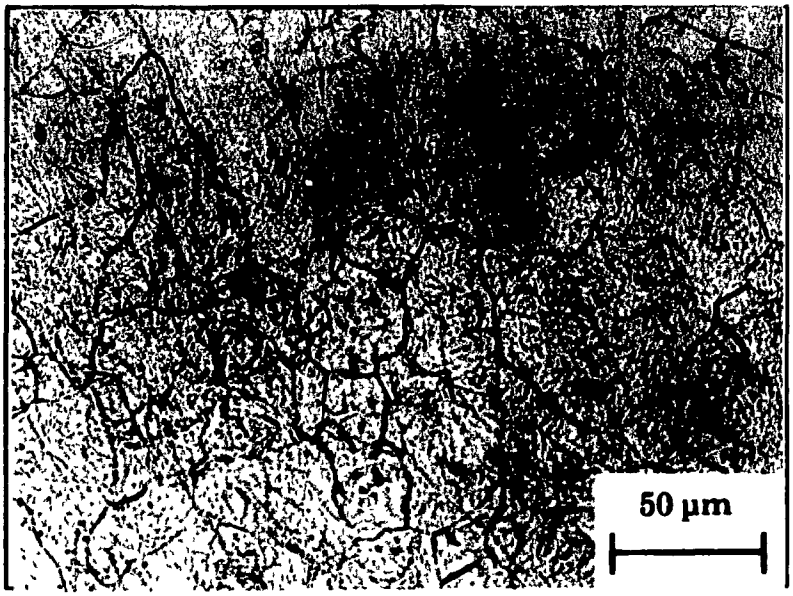


(b) $\varepsilon = 0.6, T_{def} = 1030\,^{\circ}C$ WQ

**Fig. 5.5** Austenite structures produced under different deformation conditions (steel A).

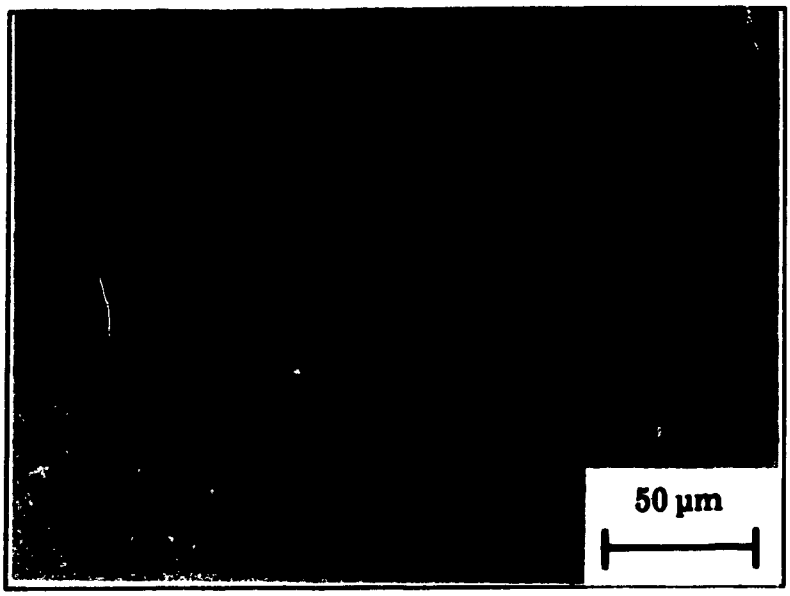


(c) $\varepsilon = 0.9, T_{def} = 1000\ ^{\circ}C$ WQ

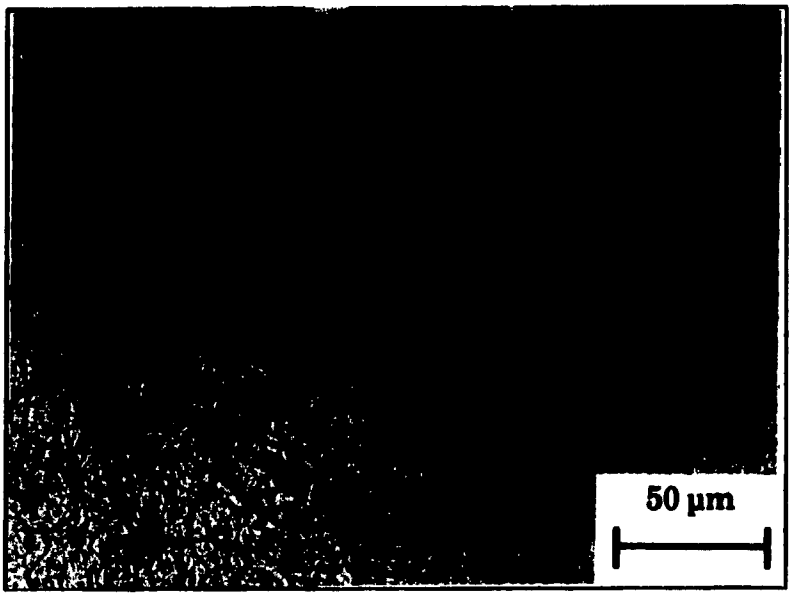


(d) $\varepsilon = 1.2, T_{def} = 970\ ^{\circ}C$ WQ

Fig. 5.5 Austenite structures produced under different deformation conditions (steel A).

Table 5.1 $\varepsilon_p$ under different deformation conditions

| Test No | Deformation temperature °C | Strain of 5th pass | Measured peak strain $\varepsilon_p$ | Predicted peak strain $\varepsilon_p$ |
|---|---|---|---|---|
| 1 | 1060 | 0.3 | - | - |
| 2 | 1030 | 0.6 | - | - |
| 3 | 1000 | 0.9 | - | - |
| 4 | 970 | 1.2 | 0.85 | 0.89 |
| 5 | 940 | 1.5 | 0.91 | 1.00 |
| 6 | 910 | 1.8 | 1.06 | 1.18 |
| 7 | 880 | 2.1 | 1.4 | 1.42 |
| 8 | 850 | 2.4 | 1.50 | 1.71 |

where $\varepsilon_i^*$ stands for the effective strain at pass i. This is the sum of the i-th pass strain ($\varepsilon_i$) and the residual strain retained from the previous (i-1)st pass ($\Delta\varepsilon_{i-1}$). If $X_{i-1}$ is the fraction recrystallized after the (i-1)-th pass, then the effective residual strain can be described as:

$$\Delta\varepsilon_{i-1}=\varepsilon^*_{i-1}F(1-X_{i-1}) \qquad (5.6)$$

Here, F is a constant equal to 0.5 when the fractional softening is greater than 0.1 and 1 when the fractional softening is less than 0.1[108, 109]. Of course, equation 5.6 is only an approximation, as the recrystallized volume fraction is expected to affect the flow stress, rather than the strain. Furthermore, as the stress-strain curve is not linear in this range, fractional softening cannot be simply replaced by a fractional loss of "strain". Ideally, the residual strain can be calculated from the flow curve and the fractional softening. In the case of

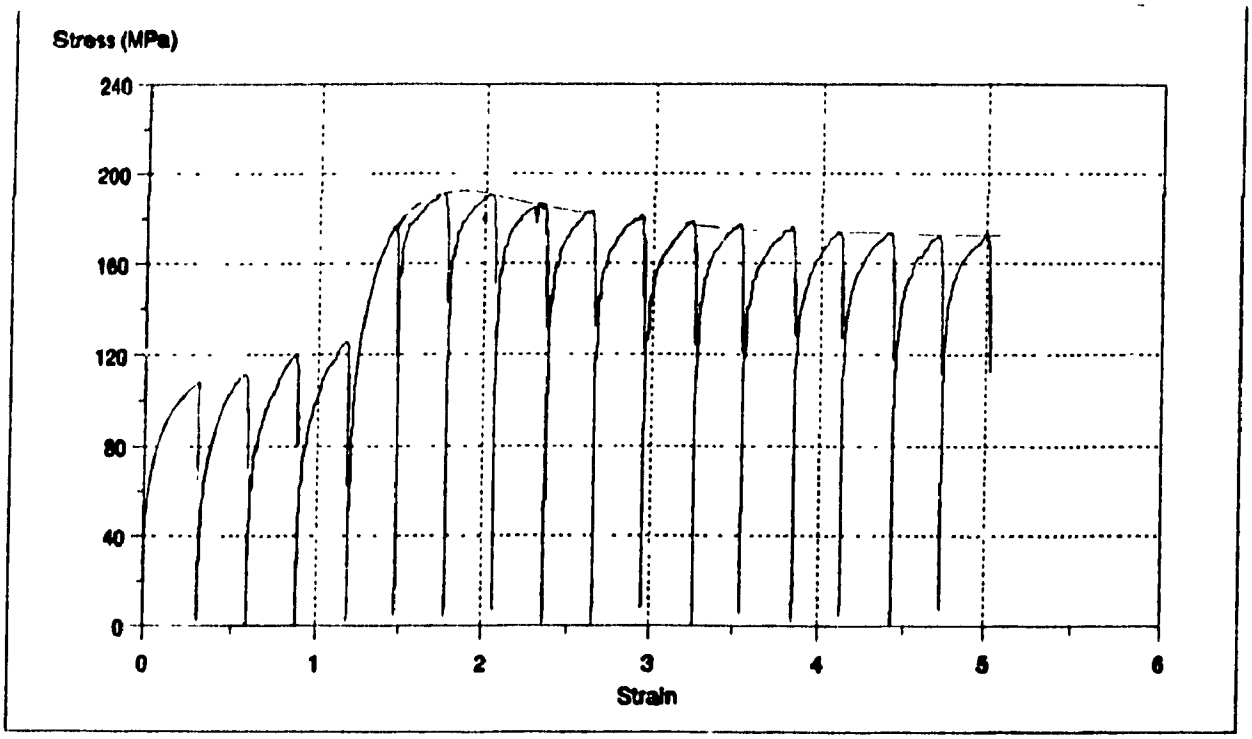


(a)

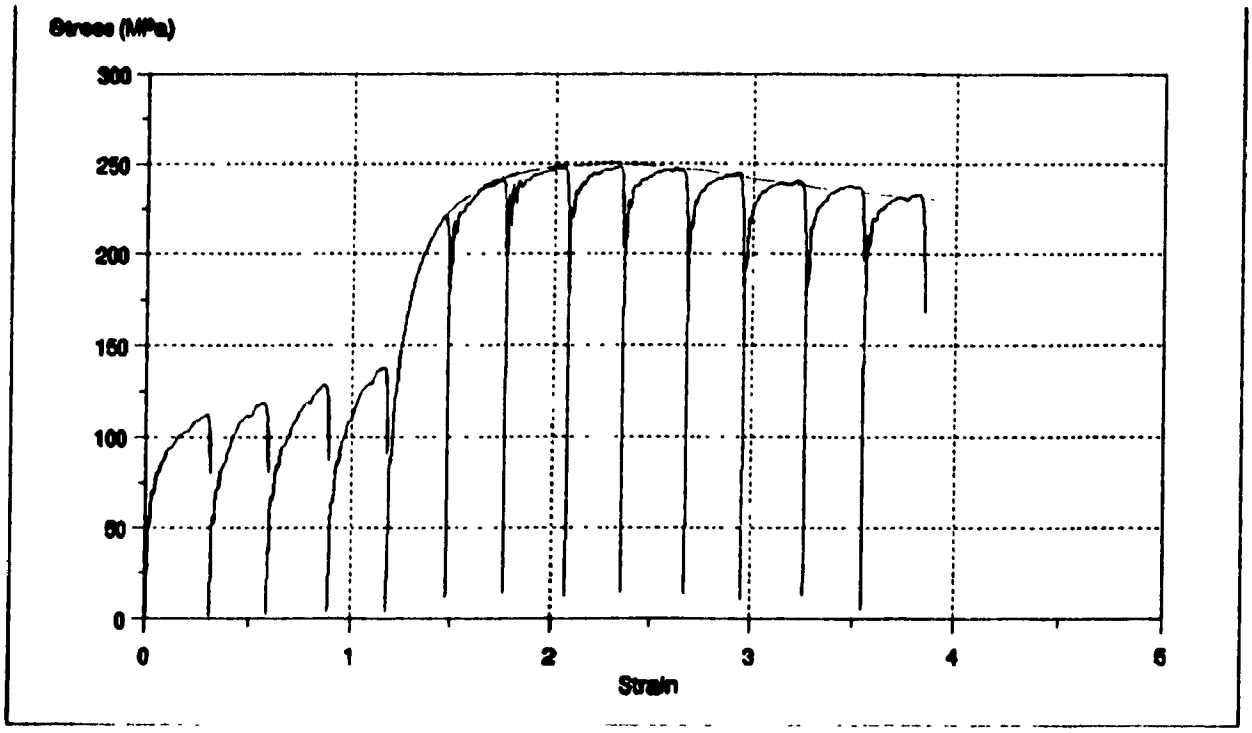


(b)

Fig. 5.6 Stress-strain curves for samples deformed according to schedule C: strain = 0.3/pass, strain rate = 2/s, interpass time = 1 s, isothermal stage is initiated at 5th pass, and at temperatures of (a) 970 °C, and (b) 910 °C.

very short interpass times ($\leq$ 1 second), the fractional softening resulting from static recrystallization between passes is less than 0.1; in this case, the accumulated strain can simply be determined from the sum of the pass strains,

$$\varepsilon_i^* = \sum_{k=1}^{i} \varepsilon_k \tag{5.7}$$

The peak strains and peak stresses were determined by drawing the envelopes of the flow curves, and the effects of the deformation parameters on these quantities are presented in Figs. 5.7~5.10.

It can be seen that both the peak strain and the peak stress decrease with increasing deformation temperature but increase with strain rate. This is well described by equation 5.3. Increasing the deformation temperature or decreasing the strain rate leads to a decrease in the Zener-Hollomon parameter, and thus a decrease in the peak strain. The influence of delay time after roughing on the peak stress and strain is associated with Nb(C,N) precipitation. It is demonstrated in Fig. 5.9 that the peak stress and strain increase with delay time. However, when the delay time exceeds a certain value (for example, 360 seconds), the peak strain decreases with further increase in delay time, while peak stress is not particularly affected.

This phenomenon can be understood in terms of the effect of precipitation on dynamic recrystallization. In the region of testing temperatures where strain induced precipitation occurs, increasing the delay time increases the volume fraction of precipitate, thus enhancing the retarding effect of Nb(C,N) on the subsequent dynamic recrystallization. This can lead to the peak strain increasing with delay time. When the delay time is long enough to cause precipitate coarsening, however, the retarding effect of Nb(C,N) on dynamic recrystallization will be lost. As a result, the peak strain decreases with further increases in delay time.

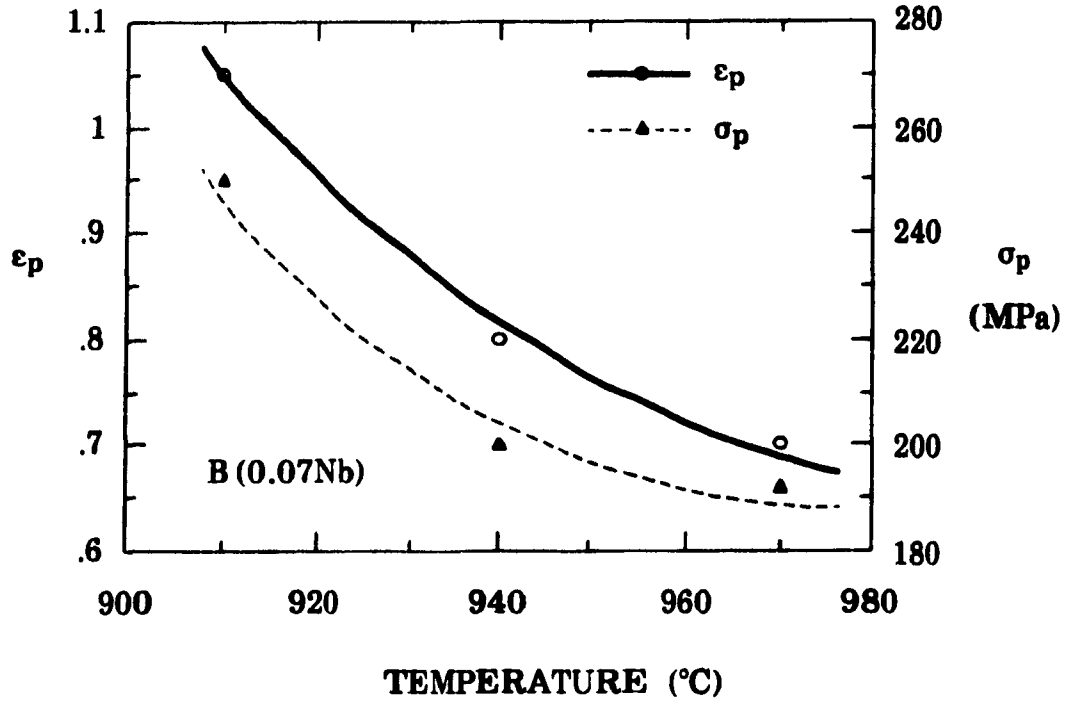


Fig. 5.7 Dependence of the peak strain and stress on deformation temperature (multipass deformation, $\varepsilon_p$ is the accumulated strain); strain rate $\dot{\varepsilon} = 2\,s^{-1}$, strain $\varepsilon = 0.3$/pass, interpass time $t = 1$ s.

The dependence of the peak stress on initial grain size is demonstrated in Fig. 5.10. It can be seen that the peak stress is not particularly sensitive to the initial grain size (grain size after four roughing passes, but before the isothermal stage), but the peak strain increases with grain size. This is because the nucleation sites for dynamic recrystallization are associated with grain boundaries, and therefore with the initial grain size. Smaller initial grain sizes supply more nucleation sites, and lead to lower peak strains.

It must be pointed out that the simulation of flat rolling by torsion testing is not directly applicable to the industrial situation, because of differences in deformation mode. The $\varepsilon_x$ (critical strain for static recrystallization) and $\varepsilon_p$ (peak strain for dynamic recrystallization) determined in torsion have been shown to be higher than those determined in tension or compression[18,110]. Care should therefore be taken before applying the results of the present work to rolling problems.

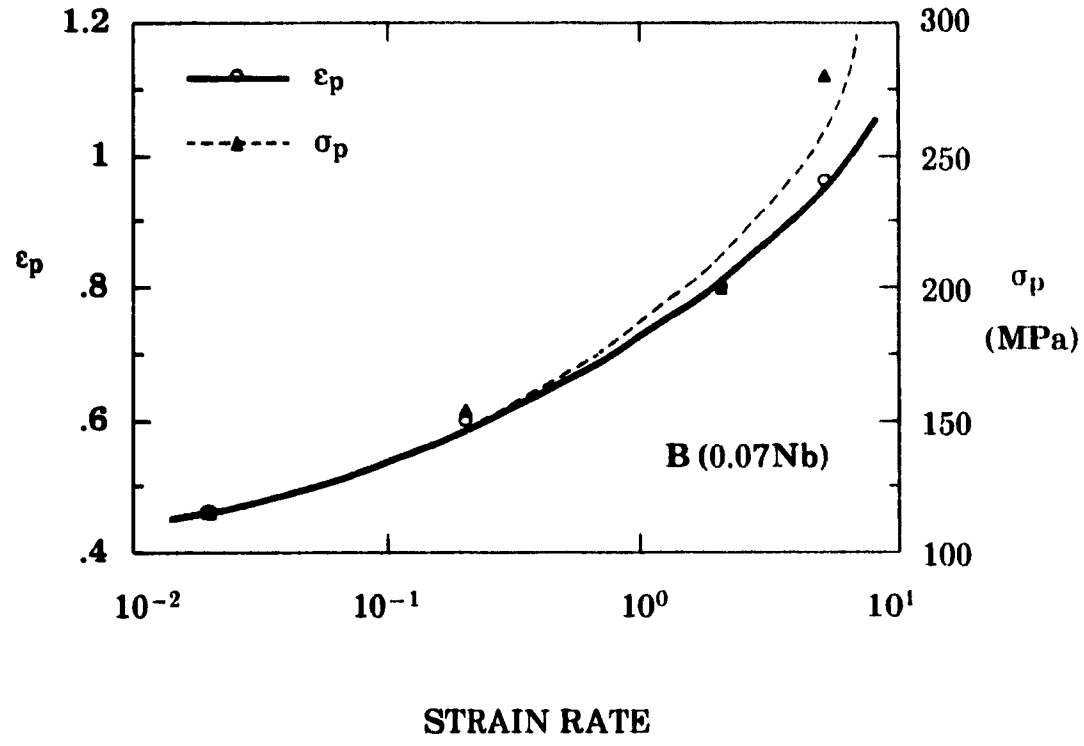


**Fig. 5.8** Dependence of the peak strain and stress on strain rate (multipass deformation, $\varepsilon_p$ is the accumulated strain); strain $\varepsilon = 0.3$/pass, deformation temperature T = 940 °C, interpass time t = 1 s.

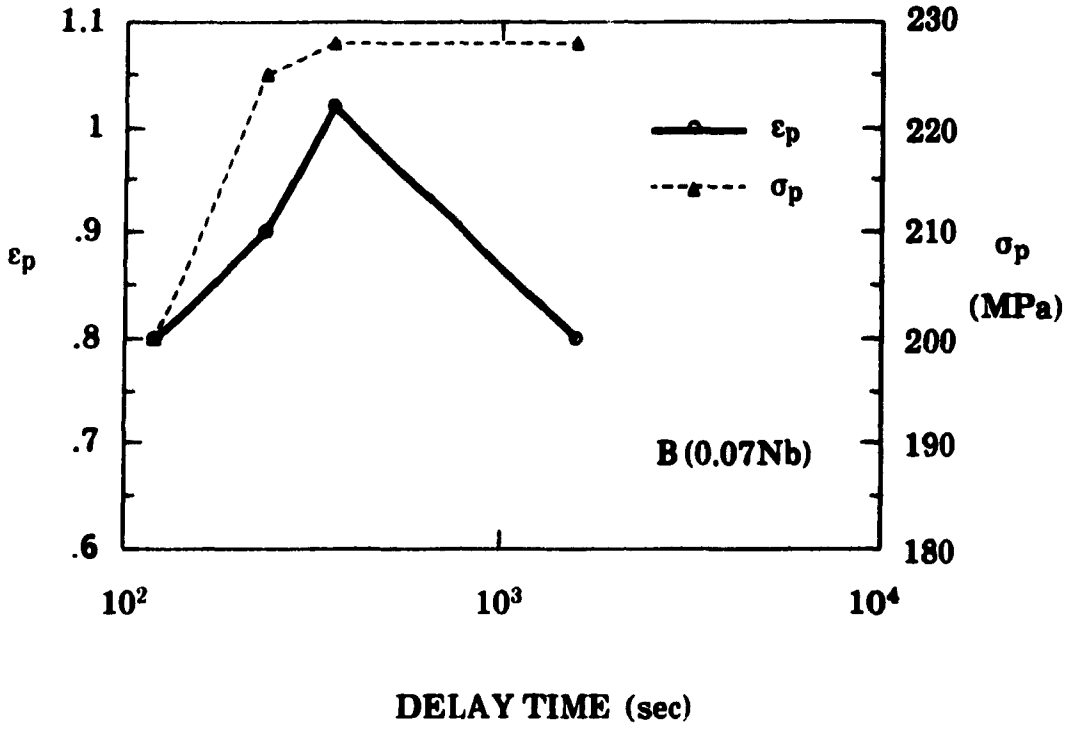


Fig. 5.9 Dependence of the peak strain and stress on delay time after roughing (at isothermal stage, $\varepsilon_p$ is the accumulated strain), strain rate $\dot{\varepsilon} = 2\ s^{-1}$, strain $\varepsilon = 0.3$/pass, deformation temperature $T = 940\ ^\circ C$, interpass time $t = 1$ s.

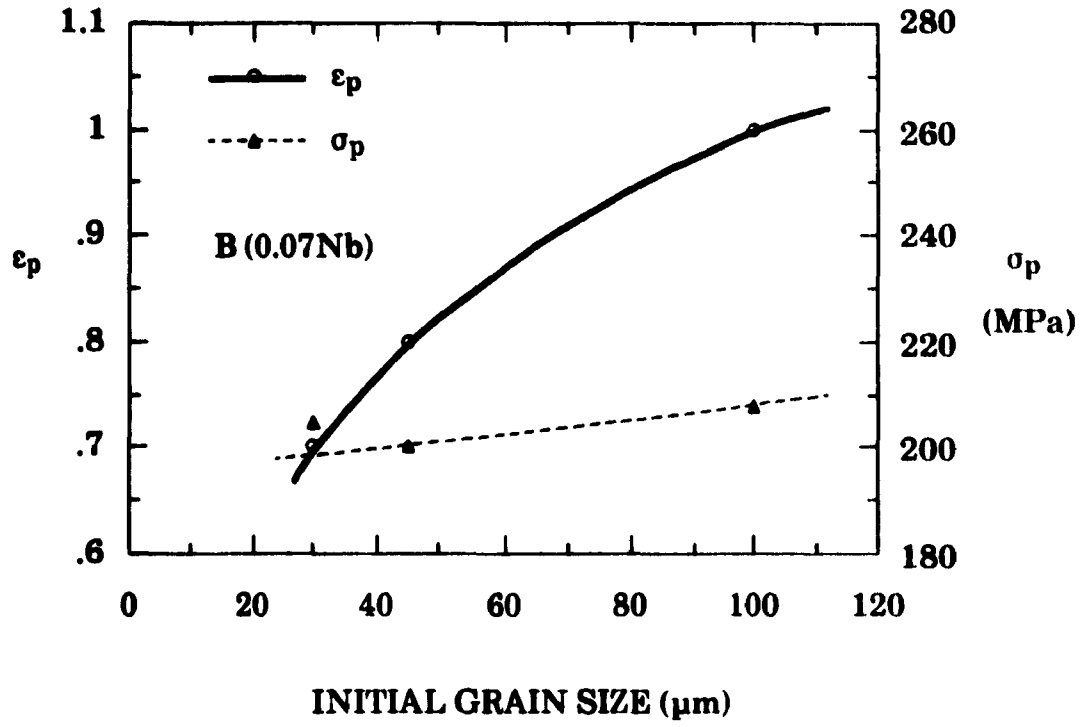


**Fig. 5.10** Dependence of the peak strain and stress on initial grain size (grain size after roughing, but before the isothermal stage). $\varepsilon_p$ is the accumulated strain, strain rate $\dot{\varepsilon} = 2\ s^{-1}$, strain $\varepsilon = 0.3$/pass, interpass time $t = 1$ s.

CHAPTER 6

# CONCLUSIONS

In the present study, the effects on the $T_{nr}$ of reheating temperature, initial austenite grain size and concentration of microalloying elements were investigated. Furthermore, the effects on the $T_{nr}$ of deformation parameters such as the pass strain, strain rate, and interpass time were also examined in detail by means of MFS vs. 1000/T diagrams. Based on the Dutta and Sellars models, CCR (continuous-cooling-recrystallization) and CCP (continuous-cooling-precipitation) curves were calculated by applying the additivity rule to continuous cooling conditions. The $T_{nr}$'s were predicted by plotting RPTT (recrystallization-precipitation-temperature-time) diagrams and determining their points of intersection. The effects of the deformation parameters on the peak strain were also investigated. Based on the results presented in Chapters 4 and 5, the following conclusions are drawn.

1. In microalloyed steels, through the formation of Nb(C,N), Nb is the most effective alloying element for increasing the $T_{nr}$. The addition of Ti to a Nb-bearing steel enhances the retardation of recrystallization. This is because TiN, which precipitates before Nb(C,N), can act as nucleation

sites for subsequent Nb(C,N) precipitation, accelerating the kinetics of Nb(C,N) precipitation in this way. This leads to an increase in the $T_{nr}$.

2. Reheating temperature has a significant influence on the $T_{nr}$ due to the change in the driving force for Nb(C,N) precipitation. For a given steel and given deformation temperature, the supersaturation and the volume fraction of niobium carbonitride available for precipitation both decrease with decreasing reheating temperature; in this way, the retarding effect of Nb(C,N) precipitation on recrystallization becomes weaker as the reheating temperature is decreased.

3. The volume fraction of undissolved precipitates also increases with decreasing reheating temperature. These large particles can act as nucleation sites for recrystallization during subsequent deformation. This also leads to a decrease in the $T_{nr}$.

4. Initial austenite grain size has no effect on the $T_{nr}$ during multipass deformation, because initially dissimilar grain sizes converge to nearly the same grain size after several roughing passes. In this study, it was also observed that coarse-grained structures are refined more quickly than fine-grained structures.

5. Strain is an important factor affecting the $T_{nr}$. This is because the dislocation density increases with the amount of deformation, while dislocations act as nucleation sites for both recrystallization and precipitation. When the strain is increased, recrystallization is accelerated to a greater extent than precipitation; thus, the $T_{nr}$ decreases significantly with increasing strain.

6. In the case of deformation with large pass strains, strain-induced precipitate coarsening takes place at the later stages of multipass deformation. These coarsened precipitates cannot retard recrystallization effectively, which leads to a lowering of the $T_{nr}$.

7. In the range of temperature where strain induced precipitation is likely to occur, both recrystallization and precipitation are accelerated at high

strain rates. When the strain is large, increasing the strain rate accelerates the recrystallization kinetics more than the precipitation kinetics, thereby decreasing the $T_{nr}$.

8. The effect of interpass time on the $T_{nr}$ can be divided into three regions. In the short interpass time region (region I), strain induced precipitation is unable to take place. Therefore, recrystallization is mainly retarded by solute drag, and the $T_{nr}$ decreases with increasing interpass time. As long as precipitation takes place in region II, the volume fraction of precipitate increases with increasing interpass time, and thus the retarding effect of the precipitates is strengthened. Thus, the $T_{nr}$ increases with increasing interpass time. When the interpass time reaches the value at which precipitate coarsening takes place, the $T_{nr}$ decreases with further increases in interpass time.

9. CCR and CCP curves were calculated by applying the additivity rule to the isothermal models of Dutta and Sellars. The $T_{nr}$'s were predicted using RPTT diagrams. The predicted $T_{nr}$'s are in good agreement with the measured ones.

10. In the case of multipass deformation under isothermal conditions, the peak strain decreases with increasing deformation temperature, but increases with increasing strain rate and initial grain size. The influence of delay time after roughing on the peak strain can be divided into two categories. In the case of short delay times, the volume fraction of precipitate increases with increasing delay time, thus, strengthening the retarding effect of the precipitates. This increases the strain required to initiate dynamic recrystallization. In the case of long delay times, precipitates coarsening occurs and weakens the retarding effect of the precipitates. This leads to lower peak strains.

# REFERENCES


1. F.B. Pickering: "Microalloying 75", Union Carbide Corporation, New York, NY, (1977), p. 9.

2. K.J. Irvine: "Strong, Tough Structural Steels", The Iron and Steel Institute, Publication 104, (1967), p. 1.

3. J.N. Cordea: Symposium on Low Alloy High Strength Steels, Nurnberg, RBD, (1970), p. 61.

4. R.W. Vanderbeck: Weld. J., 37, (1958), p. 114.

5. A.J. DeArdo: Proc. Int. Conf. THERMEC-88, ed. I. Tamura, Tokyo, Japan, (1988), p. 20.

6. M. Cohen and S.S. Hansen: "HSLA Steels: Metallurgy and Applications", Proc. Int. Conf. on HSLA Steels'85, eds. J.M. Gray, T. Ko, S. Zhang, B. Wu and X. Xie, ASM, p. 61 (1987).

7. J.J. Irani, D. Burton, and J.D. Jones and A.B Rothwell: in"Strong tough structural steels", The Iron and Steel Institute, London, (1967), p. 110.

8. A.B. Le Bon and L.N. de Saint Martin: "Microalloying 75", ed. M. Korchynski, Union Carbide Corporation, New York, NY, (1977), p. 90.

9. H.J. McQueen and J.J. Jonas: "Treatise on Materials Science and Technology", ed. R.J. Arsenault, Academic Press, New York, NY, 6, (1975), p. 393.

10. I. Kozasu, C. Ouchi, T. Sampei and T. Okita: "Microalloying 75", ed. M. Korchynsky, Union Carbide Corporation, New York, NY, (1977), p. 120.

11. T. Tanaka, T. Enami, M. Kimura, Y. Saito and T. Hatomura: "Thermomechanical Processing of Microalloyed Austenite", eds. A.J. DeArdo, G.A. Ratz and P.J. Wray, AIME, Warrendale Pa., (1982), p. 195.

12. A.N. Mitra, M.D. Maheshwari, T. Mukherjee and J.J. Irani: Proc. Int. Conf. High Strength Low Alloy Steels, eds. D.P. Dunn and T. Chandra, Univ. Wollongong, Wollongong, (1984), p. 38.

13. K. Kuribayashi and R. Horiuchi: Proc. Int. Conf. THERMEC-88, ed. I. Tamura, Tokyo, Japan, (1988), p. 903.

14. S. Yue, R. Barbosa, J.J. Jonas and P.J. Hunt: '30th Mechanical Working and Steel Processing Conference', Iron and Steel Society of AIME, Dearborn, (1988), p. 37.

15. W. Roberts: "HSLA Steels: Technology and Application", ASM, Metals Park, Ohio, (1984), p. 33.

16. F.H. Samuel, S. Yue, J.J. Jonas and K.R. Barnes: ISIJ International, 30, 1990, p. 216.

17. L.N. Pussegoda, S. Yue and J.J. Jonas: Metall. Trans. A, 21A, (1990), p. 153.

18. J.J. Jonas and T. Sakai: in "Deformation, Processing and Structure", 1982 ASM Materials Science Seminar, G. Krauss, ed., ASM, Metals Park, Ohio, (1984), p. 185.

19. C.M. Sellars: "Hot Rolling and Forming Processes", eds. C.M. Sellars and J. Davies, The Metals Society, London, (1980), p. 3.

20. J.J. Jonas and M.J. Luton: "Advances in deformation processing",eds. J.J. Burke and V. Weiss, Plenum Publishing Corporation (1978), p. 128.

21. C. Rossard and P. Blain: Rev. Mét., 55, (1958), p. 573.

22. C. Rossard and P. Blain: Rev. Mét., 56, (1959), p. 286.

23. M.J. Luton and Sellars: Acta Metall., 17, (1969), p. 1033.

24. S. Sakui, T. Sakai and K. Takeishi: Trans. ISIJ, 17, (1977), p. 718.

25. T. Sakai, M.G. Akben, and J.J. Jonas: "Thermomechanical Processing of Microalloyed Austenite", eds. A.J. DeArdo, G.A. Ratz and P.J. Wray, AIME, Warrendale, Pa., (1982), p. 237.

26. C. Ouchi and T. Okita: Tetsu-to-Hagane, 62, (1976), p. 208.

27. W. Roberts, H. Bodén and B. Ahlblom: Metal Science, 13, (1979), p. 195.

28. F.H. Samuel, S. Yue, J.J. Jonas and K.R. Barnes: ISIJ International, 30, (1990), p. 216.

29. L.N. Pussegoda and J.J. Jonas: ISIJ International, 31, (1991), p.278.

30. C. Roucoules, P.D. Hodgson, and S. Yue: Proc. Int. Conf. on Processing, Microstructure and Properties of Microalloyed and Other Modern Low Alloy Steels, ed. A.J. DeArdo, Warrendale Pa., (1991), p.95.

31. W.E. Duckworth, R. Phillips, and J.A. Chapman: J. Iron Steel Inst., 203, (1965), p. 1108.

32. K.J. Irvine, F.B. Pickering, and T. Gladman: J. Iron and Steel Inst., 205, (1967), p. 161.

33. M. Umemoto, H. Ohtsuka, H. Kato and I. Tamura: Proc. Int. Conf. High Strength Low Alloy Steels, eds. D.P. Dunn and T. Chandra, Univ. Wollongong, Wollongong, (1984), p. 107.

34. R.K. Amin and F.B. Pickering: "Thermomechanical Processing of Microalloyed Austenite", eds. A.J. DeArdo, G.A. Ratz and P.J. Wray, AIME, Warrendale, Pa., (1982), p. 377.

35. "Processing and Properties of Low Carbon Steel", J.M. Gray, TMS-AIME, New York, NY, (1973).

36. "Microalloying 75", Proceedings, Union Carbide Corporation, New York, NY, (1977),

37. "The Hot Deformation of Austenite", J.B. Ballance, ed., TMS-AIME, New York, NY, (1977).

38. S. Yamamoto, C. Ouchi, and T. Osuka: "Thermomechanical Processing of Microalloyed Austenite", eds. A.J. DeArdo, G.A. Ratz and P.J. Wray, AIME, Warrendale, Pa., (1982), p. 613.

39. J.G. Speer and S.S. Hansen: Metall. Trans. A, 20A, (1989), p. 25.

40. R. Coladas, J. Masounave, and J.P. Bailon: "The Hot Deformation of Austenite", J.B. Ballance, ed., TMS-AIME, New York, NY, (1977), p. 341.

41. M.G. Akben, I. Weiss, and J.J. Jonas: Acta Metall., 29, (1981), p. 111.

42. H.L. Andrade, M.G. Akben, and J.J. Jonas: Metall. Trans. A, 14A, (1983), p. 1967.

43. J.W. Martin and R.D. Doherty: Stability of Microstructure in Metallic Systems, Cambridge, UK: Cambridge University Press, (1976), p. 40.

44. R.W.K. Honeycombe: The Plastic Deformation of Metals, 2nd Edition, Metals Park, Ohio: ASM, (1984), p. 287.

45. R.W. Cahn: "Recrystallization, Grain Growth and Textures", H. Margolin, Ed., Metals Park, Ohio, ASM, (1966), p. 99.

46. P.A. Beck and P.R. Sperry: "Effect of Recrystallization Texture on Grain Growth", Transactions of the AIME, 185, (1949), p. 240.

47. P.A. Beck and P.R. Sperry: "Strain Induced Boundary Migration in High Purity Aluminum", Journal of Applied Physics, 21, (1950), p. 150.

48. J.E. Bailey and P.B. Hirsch: "The Recrystallization Process in Some Polycrystalline Metals", Proc. of the Royal Society of London, A267, (1962), p. 11.

49. W.C. Leslie: The Physical Metallurgy of Steels, New York, McGraw-Hill Book Company, (1981), p. 43.

50. C. Zener: "Private communication to C.S. Smith", Trans. AIME, (1949), 175, p. 15.

51. T. Gladman: "On The Theory of the Effect of Precipitate Particles on Grain Growth in Metals", Proc. of the Royal Society of London, 294, (1966), p. 298.

52. L.J. Cuddy: "Thermomechanical Processing of Microalloyed Austenite", eds. A.J. DeArdo, G.A. Ratz and P.J. Wray, AIME, Warrendale, Pa., (1982), p. 129.

53. L.J. Cuddy: 1st RISO International Symposium on Metallurgy and Material Science, ed. N. Hansen, A.R. Jones and T. Leffers, Roskilde, Denmark, RISO National Laboratory, (1980), p. 317.

54. S.S. Hansen, J.B. Vander Sande, and Morris Cohen: Metall. Trans. A, 11A, (1980), p. 387.

55. J.J. Jonas: "High Strength Low Alloy Steels", eds. D.P. Dunne and T. Chandra, University of Wollongong, Wollongong, Australia, (1985), p. 80.

56. M.G. Akben, B. Bacroix and J.J. Jonas: Acta Metall. 31, (1983), p. 161.

57. A. le Bon, J. Rofes-Vernis, and C. Rossard: Metal Science, 9, (1975), p. 36.

58. I. Weiss and J.J. Jonas: Metall. Trans., 10A, (1979), p. 831.

59. J.J. Jonas and I. Weiss: Met. Sci., 3, (1979), p. 238.

60. F. Boratto, R. Barbosa, S. Yue, and J.J. Jonas: "Thermec-88", ed. I. Tamura, Tokyo, Japan, (1988), p.383.

61. S. Yue and J.J. Jonas: Materials Forum, 4, (1990), p. 245.

62. S. Koyama, T. Ishii and K. Narita: Jap. Inst. of Metal. J., 35, (1971), p. 698.

63. B. Dutta and C.M. Sellars: Materials Science and Technology, 3, (1987), p.197.

64. L.J. Cuddy: Metall. Trans. A, 12A, (1981), p. 1313.

65. C.M. Sellars and J.A. Whiteman: Met. Sci., 14, (1979), p. 187.

66. K. Esaka, J. Wakita, M. Takahashi, O. Kawano and S. Harada: *Seitetsu-Kenkyu*, (1986), No. 32, p. 92.

67. P. Choquet, P. Fabregue, J. Giusti and B. Chamont: Proc. Int. Symp. on Mathematical Modelling of Hot Rolling of Steel, ed. S. Yue, CIM, Hamilton, (1990), p. 34.

68. O. Kwon, K.B. Kang, K.J. Lee, J.K. Lee, K.S. Lee and R.W. Chang: The Structure/Property Prediction and Control Model for Plain Carbon Steels, RIST, Korea, (1988).

69. P.D. Hodgson and R.K. Gibbs: Proc. Int. Symp. on Mathematical Modelling of Hot Rolling of Steel, ed. S. Yue, CIM, Hamilton, (1990), p. 76.

70. W. Roberts, A. Sandberg, T. Siwecki and T. Warlefors: Int. Conf. on Technology and Applications of HSLA Steels, ASM, Philadephia, (1983), p. 67.

71. H. Yada and T. Senuma: J. Jpn. Soc. Technol. Plast., 27, (1986), p. 34.

72. O. Kwon and A.J. DeArdo: Acta Metall., 39, (1990), p. 529.

73. W.J. Liu: Ph.D. Thesis, McGill University, Montreal, 1989.

74. W.P. Sun: Ph.D. Thesis, McGill University, Montreal, 1991.

75. S.H. Park: Ph.D. Thesis, McGill University, Montreal, 1991.

76. S.L. Semiatin, G.D. Lahoti, and J.J. Jonas: Mechanical Testing, 8, ASM Metals Handbook, 9th Edition, ASM, Metals Park, Ohio, (1985), p. 154.

77. D.S. Fields and W.A. Backofen: Proc. ASTM. 57, (1957), p. 1259.

78. J. Wadsworth, J.H. Woodhead, and S.R. Keown: Metal Science, 10 (1976), p. 342.

79. E. Valdes and C.M. Sellars: Materials Science and Technology, 7, (1991), p. 622.

80. M.J. Luton, R. Dorvel, and R.A. Petkovic: Metall. Trans. A, 11A, (1980), p.411.

81. L.M. Brown and W.M. Stobbs: Phil. Mag. 23, (1971), p.1201.

82. P.F. Chapman and W.M. Stobbs: Phil. Mag. 19, (1969), p.1015.

83. T.C. Rollason and J.W. Martin: J. Mat. Sci. 5, (1970), p.127.

84. S.V. Subramanian, F. Boratto, J.J. Jonas and C.M. Sellars: "Microalloyed Bar and Forging Steels", ed. M. Finn, Hamilton, Ontario, Canada, (1990), p. 120.

85. H.L. Zou and J.S. Kirkaldy: Metall. Trans. A, 22A, (1991), p.1151.

86. W. Roberts: Scandinavian Journal of Metallurgy 9, (1980), p. 13.

87. R. Priestner, C.C. Earley, and J.H. Rendall: J. Iron Steel Inst., (1968), p. 1252.

88. F.N. Rhines, R.A. Ellis, Jr. and A.B. Gokhale: Scripta Metallurgica, 15, (1981), p. 783.

89. L.J. Cuddy, J.J. Bauwin, and J.C. Raley: Metall. Trans. A, 11A, (1980), p. 381.

90. W.P. Sun, M. Militzer, and J.J. Jonas: Metall. Trans. *A*, 23A, (1992), p. 3013.

91. I. Weiss and J.J. Jonas: Metall. Trans. *A*, 11A, (1980), p. 40.

92. W. Roberts, H. Lidefelt and A. Sandbery: "Hot Working and Forming Processes", eds. C.M. Sellars and G.J. Davies, The Metals Society, London, (1979), p. 38.

93. W.L. Roberts: "Flat Processing of Steel", Marcel Dekker, Inc., New York and Basel.

94. D.Q. Bai, S. Yue, W.P. Sun and J.J. Jonas: Proc. Int. Conf. on Processing, Microstructure and Properties of Microalloyed and Other Modern Low Alloy Steels, ed. A.J. DeArdo, Warrendale Pa., (1991), p.165.

95. W.P. Sun, M. Militzer, D.Q. Bai, and J.J. Jonas: "Recrystallization'92", Materials Science Forum, 113-115, (1992), p. 533.

96. E. Scheil: Arch. Eisenhüttenwes., 12, (1935), p. 565.

97. M. Umemoto, K. Horiuchi, and I. Tamura: Trans. Iron Steel Inst. Jpn., 22, 1982, p. 854.

98. M. Umemoto, N. Nishioka, and I. Tamura: Trans. Iron Steel Inst. Jpn., 22, (1982), p. 629.

99. M. Umemoto, K. Horiuchi, and I. Tamura: Trans. Iron Steel Inst. Jpn., 23, (1983), p. 690.

100. M. Umemoto, N. Nishioka, and I. Tamura: Proc. 3rd Int. Cong. on Heat Treatment of Materials, TMS, Shanghai, (1983), p. 5.35.

101. M. Umemoto, Z.H. Gao, and I. Tamura: Mater. Sci. Technol., 3, (1987), p. 249.

102. H. Ohtsuka, M. Umemoto, and I. Tamura: Tetsu-to-Hagané, 73, (1987), p. 144.

103. S.H. Park, S. Yue, and J.J. Jonas: Metall. Trans. A, 23A, (1992), p.1641.

104. A.B. Le Bon : Mém. Sci. Rev. Métall., 57, (1973), p. 577.

105. H. Weiss et al.: J. Iron Steel Inst., 211, (1973), p. 653.

106. J.J. Jonas: "Recrystallization'90", ed. T. Chandra, The Minerals, Metals and Materials Society, (1990), p. 27.

107. C. Roucoules: Ph.D. Thesis, McGill University, Montreal, 1992.

108. P. Choquet, A.B. Le Bon and C. Perdrix: "Strength of Metals and Alloys", eds. H.J. McQueen, J.P. Bailon, J.I. Dickson, J.J. Jonas and M.G. Akben, Pergamon Press, Oxford, (1985), p. 1025.

109. G.L. Wang: Ph.D. Thesis, McGill University, Montreal, 1990.

110 J.J. Jonas and C.M. Sellars: ISS 10th Process Technology Conference, Toronto, Ontario, Canada, (1992), p. 67.

# APPENDIX I

## CALCULATION OF AUSTENITE COMPOSITIONS AT GIVEN SOLUTION TEMPERATURES

Following Wadsworth et al.[78], the austenite compositions at given temperatures can be calculated as follows:

If at a given temperature an amount $x$ wt. % of $AB_n$ exists in an alloy containing amounts $A_T$ and $B_T$ wt. % of elements $A$ and $B$, then

$$[A]+px=A_T \tag{I.1}$$

$$[B]+qx=B_T \tag{I.2}$$

Here $p$ and $q$ are the mass fractions of $A$ and $B$ in $AB_n$, respectively, and can be readily found from the atomic weights $a_A$ and $a_B$ of elements $A$ and $B$.

$$p=\frac{a_A}{a_A+na_B} \tag{I.3}$$

$$q=\frac{na_B}{a_A+na_B} \tag{I.4}$$

At a given temperature, the solubility product is constant,

$$k=[A][B]^n \tag{I.5}$$

$[A]$ in equation (I.1) can be replaced by $k/[B]^n$ giving

$$\frac{k}{[B]^n} + px = A_T \qquad \text{(I.6)}$$

Eliminating $x$ from equations (I.2) and (I.6) gives the following general expression:

$$p[B]^{n+1} - (pB_T - qA_T)[B]^n - qk = 0 \qquad \text{(I.7)}$$

$(pB_T - qA_T)$ is a constant for a given alloy and can be replaced by $r$; then

$$p[B]^{n+1} - r[B]^n - qk = 0 \qquad \text{(4.1)}$$

Equation (4.1) is soluble when $n = 1$, and once $[B]$ has been found, $[A]$ can be derived from equation (I.5):

$$[A] = \frac{k}{[B]^n} \qquad \text{(4.2)}$$

For a given alloy ($p$, $q$, $A_T$ and $B_T$ fixed) at a given temperature ($k$ fixed), the values of $[A]$ and $[B]$ can be determined. Table 4.2 shows the austenite compositions calculated using Wadsworth's equations for the present steels tested at selected temperatures. In the present case, $[A]$ and $[B]$ in Wadsworth's equations were replaced by $[Nb]$ and $[C + 12/14\,N]$, respectively.

# APPENDIX II

## COMPUTER PROGRAM FOR CALCULATING THE PRECIPITATION START TIME (PS) AND RECRYSTALLIZATION FINISH TIME (RF)

```
***CALCULATION OF PS DURING CONTINUOUS COOLING***
      IMPLICIT DOUBLE PRECISION (A-Z)

      A=3.0D0*10.0D0**(-6.0D0)
      B=2.5D0*10.0D0**10.0D0
      C=4.127D0*10.0**(-3.0D0)
      Q=2.7D0*10.0D0**5.0D0
      R=8.31D0
      NB=0.09D0
      EPS=0.3D0
      STRT=2.0D0

      DO 300 K1=1, 17
      TEMP0=1453.0D0-(K1-1.0D0)*30.0D0

      SUM=0.0D0
      TIMC=0.0D0

      DO 100 K2=1, 5000
      DTIME=0.01D0
      TIMC=TIMC+DTIME
      TEMP0=TEMP0-0.01D0

      X1=A*NB**(-1.0D0)*EPS**(-1.0D0)
      Z=STRT*DEXP(4.0D0*10.0D0**5.0D0/R/TEMP0)
```

```
      X2=Z**(-0.5D0)
      X3=DEXP(Q/R/TEMP0)
      KS=C/10.0D0**(2.26D0-6770D0/TEMP0)
      X4=TEMP0**3.0D0*(DLOG(KS))**2.0D0
      X5=DEXP(B/X4)
      CPS=X1*X2*X3*X5

      SFRCTN=DTIME/CPS
      SUM=SUM+SFRCTN

      IF(SUM.GE.1.0D0) GOTO 200
100   CONTINUE
200   TEME=TEMP0-273.0D0
      TIME=DLOG(TIMC)

      PRINT*, TIME, TEME
300   CONTINUE
      STOP
      END



***CALCULATION OF RF DURING CONTINUOUS COOLING***
      IMPLICIT DOUBLE PRECISION (A-Z)

      A=51.57D0*10.0D0**(-20.0D0)
      B=3.0D0*10.0D0**5.0D0
      C=2.75D0*10.0D0**5.0D0
      R=8.31D0
      NB=0.09D0
      TEMP0=1453.0D0
      EPS=0.3D0
      GAMAD=339.23D0

      DO 300 K1=1,14
```

```
      TEMP0=1453.0D0-(K1-1.0D0)*30.0D0
      GAMAD=0.9D0*GAMAD**0.67D0*EPS**(-0.67D0)

      SUM=0.0D0
      TIMC=0.0D0

      DO 100 K2=1, 5000
      DTIME=0.01D0
      TIMC=TIMC+DTIME
      TEMP0=TEMP0-0.01D0

      X1=A*GAMAD**2.0D0*EPS**(-4.0D0)
      X2=DEXP(B/R/TEMP0)
      X3=DEXP((C/TEMP0-185.0D0)*NB)
      CRF=X1*X2*X3

      SFRCTN=DTIME/CRF
      SUM=SUM+SFRCTN

      IF (SUM.GE.1.0D0) GOTO 200
100   CONTINUE
200   TEME=TEMP0-273.0D0
      TIME=DLOG(TIMC)

      PRINT*, TIME, TEME
300   CONTINUE
      STOP
      END
```

# APPENDIX III

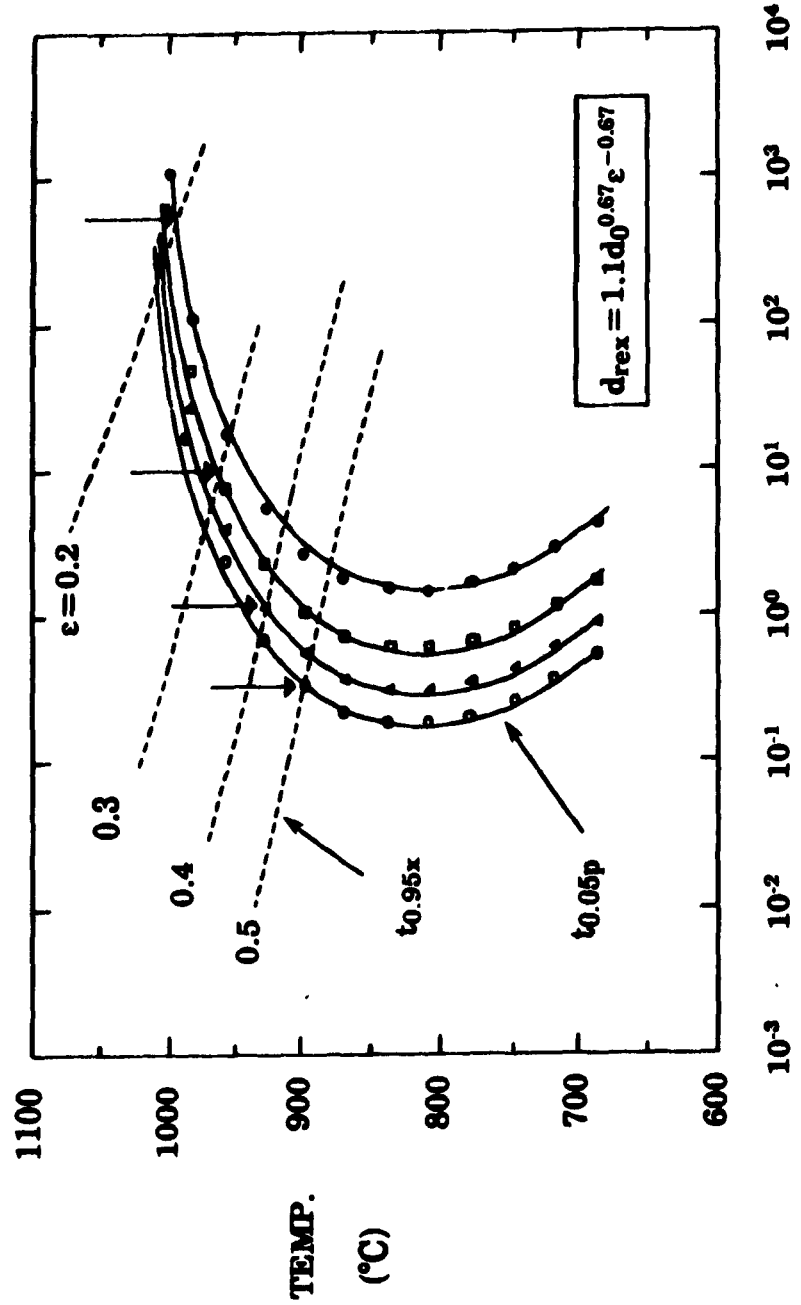


Fig. III.1 RPTT diagram pertaining to continuous cooling conditions (0.09Nb steel).

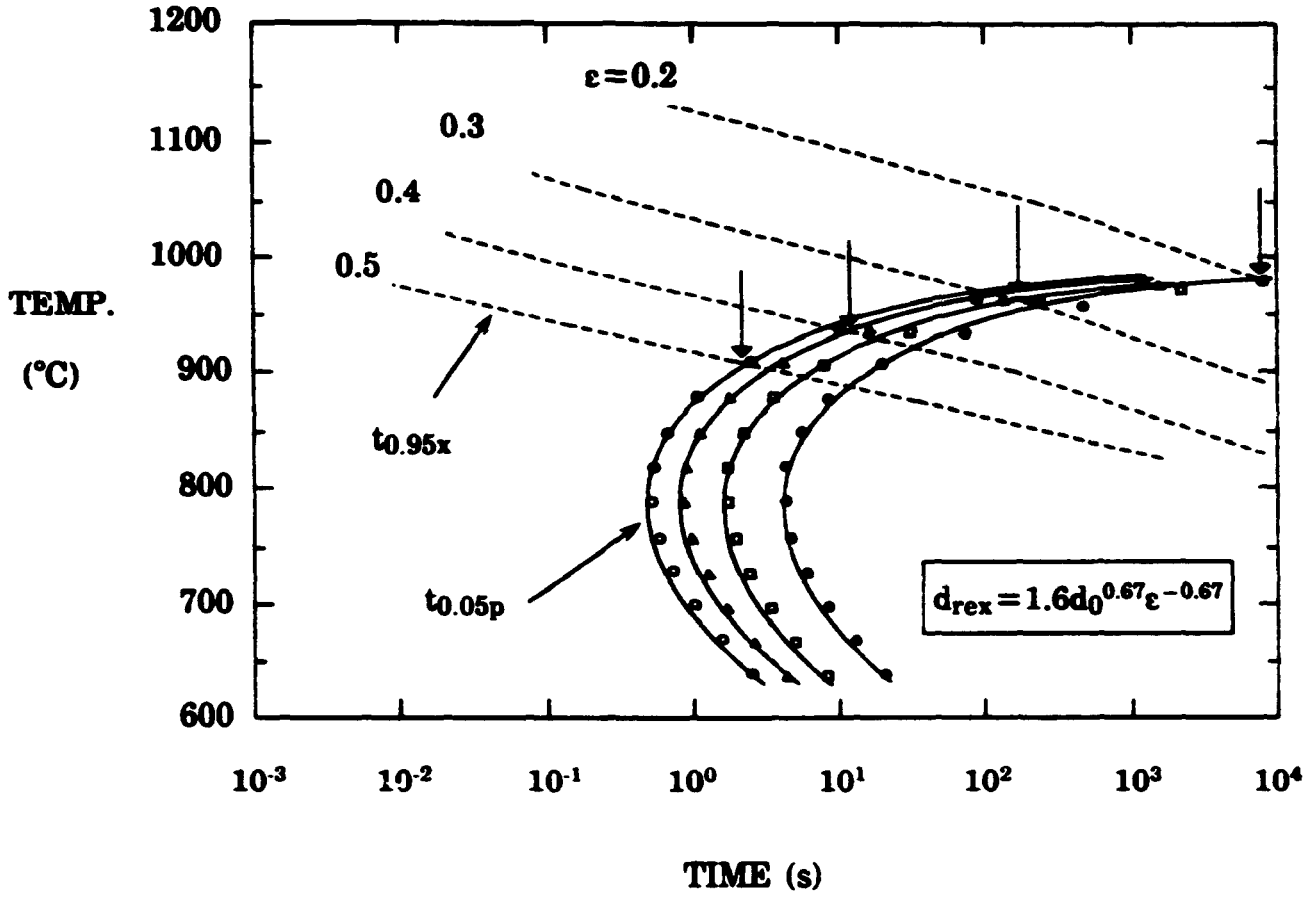


**Fig. III.2 RPTT diagram pertaining to continuous cooling conditions (0.07Nb steel).**

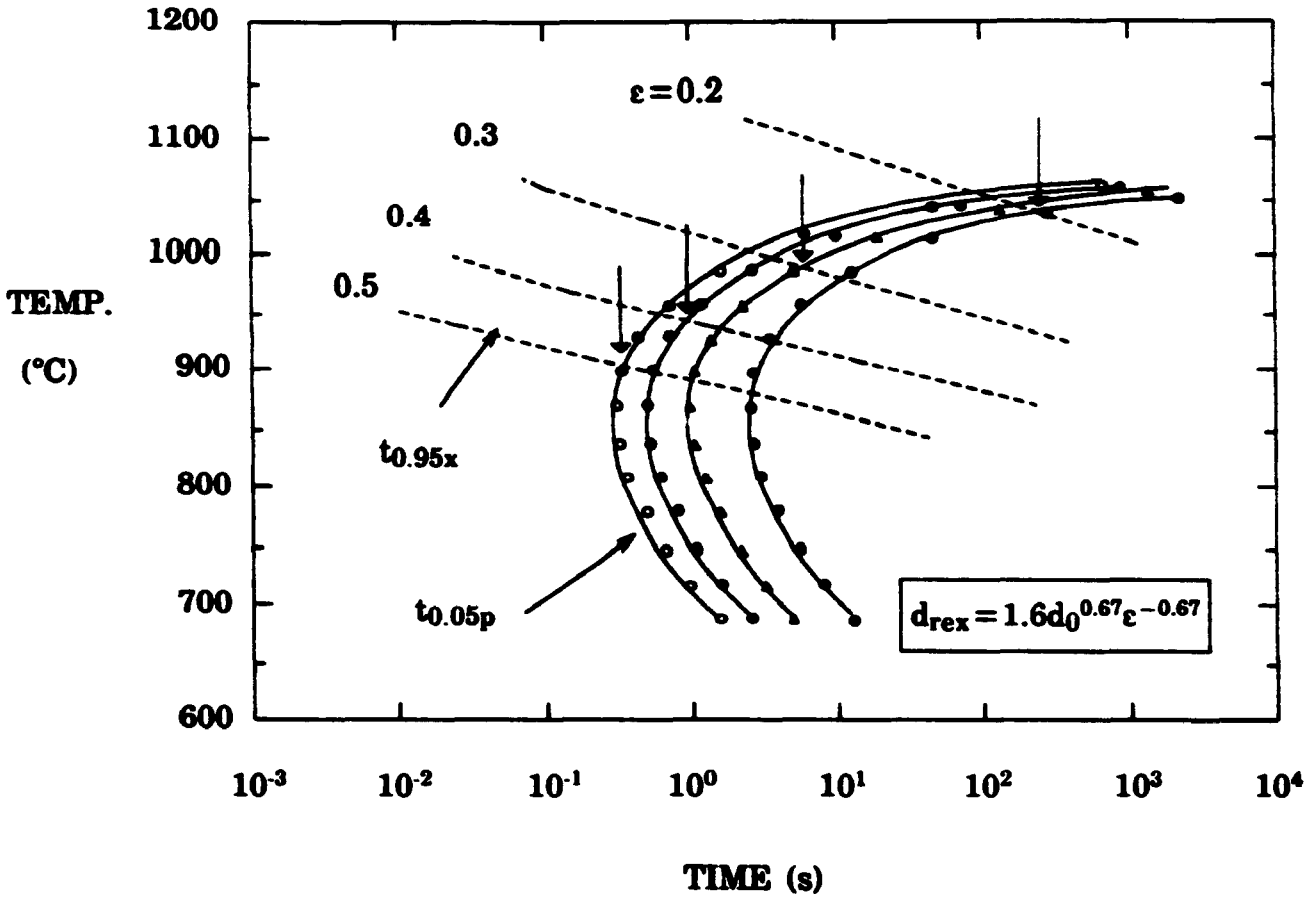


**Fig. III.3 RPTT diagram pertaining to continuous cooling conditions (0.05Nb steel).**